INSTITUTO POTOSINO DE INVESTIGACIÓN CIENTÍFICA Y TECNOLÓGICA, A.C.

POSGRADO EN CIENCIAS AMBIENTALES

Application of seaweed, natural biopolymers, and carbon-based materials as a wastewater treatment of water-soluble hydrocarbons

Tesis que presenta

Carlos Enrique Flores Chaparro

Para obtener el grado de

Doctor en Ciencias Ambientales

Director de la Tesis:
Dr. José René Rangel Méndez

San Luis Potosí, S.L.P., Julio de 2018

IPICYT

Constancia de aprobación de la tesis

La tesis ***"Application of seaweed, natural biopolymers and carbon-based materials as a wastewater treatment of water-soluble hydrocarbons"*** presentada para obtener el Grado de Doctor en Ciencias Ambientales, fue elaborada por **Carlos Enrique Flores Chaparro** y aprobada el trece de julio del dos mil dieciocho por los suscritos, designados por el Colegio de Profesores de la División de Ciencias Ambientales del Instituto Potosino de Investigación Científica y Tecnológica, A.C.

Dr. José René Rangel Méndez
Director de la tesis

Dr. Luis Felipe Cházaro Ruiz
Miembro del Comité Tutoral

Dra. María Catalina Alfaro de la Torre
Miembro del Comité Tutoral

Dr. Miguel Ángel Huerta Díaz
Miembro del Comité Tutoral

Créditos Institucionales

Esta tesis fue elaborada en la División de Ciencias Ambientales del Instituto Potosino de Investigación Científica y Tecnológica, A.C., bajo la dirección del Dr. José René Rangel Méndez.

Durante la realización del trabajo el autor recibió una beca académica del Consejo Nacional de Ciencia y Tecnología (424187) y del Instituto Potosino de Investigación Científica y Tecnológica, A. C.

La investigación desarrollada en esta tesis fue financiada a través del programa de Proyectos de Desarrollo Científico para Atender Problemas Nacionales (PDCPN−01−247032).

El autor agradece el apoyo otorgado por la División de Ciencias Ambientales del Instituto Potosino de Investigación Científica y Tecnológica, A.C., para la presentación del trabajo en conferencias nacionales e internacionales.

IPICYT

Instituto Potosino de Investigación Científica y Tecnológica, A.C.

Acta de Examen de Grado

El Secretario Académico del Instituto Potosino de Investigación Científica y Tecnológica, A.C., certifica que en el Acta 012 del Libro Primero de Actas de Exámenes de Grado del Programa de Doctorado en Ciencias Ambientales está asentado lo siguiente:

En la ciudad de San Luis Potosí a los 13 días del mes de julio del año 2018, se reunió a las 16:00 horas en las instalaciones del Instituto Potosino de Investigación Científica y Tecnológica, A.C., el Jurado integrado por:

Dr. Ma. Catalina Alfaro de la Torre	**Presidente**	**UASLP**
Dr. Luis Felipe Cházaro Ruiz	**Secretario**	**IPICYT**
Dr. Cesar Nieto Delgado	**Sinodal**	**IPICYT**
Dr. José René Rangel Méndez	**Sinodal**	**IPICYT**

a fin de efectuar el examen, que para obtener el Grado de:

DOCTOR EN CIENCIAS AMBIENTALES

sustentó el C.

Carlos Enrique Flores Chaparro

sobre la Tesis intitulada:

Application of seaweed, natural biopolymers and carbon-based materials as a wastewater treatment of water-soluble hydrocarbons

que se desarrolló bajo la dirección de

Dr. José René Rangel Méndez

El Jurado, después de deliberar, determinó

APROBARLO

Dándose por terminado el acto a las 19:15 horas, procediendo a la firma del Acta los integrantes del Jurado. Dando fe el Secretario Académico del Instituto.

A petición del interesado y para los fines que al mismo convengan, se extiende el presente documento en la ciudad de San Luis Potosí, S.L.P., México, a los 13 días del mes de julio de 2018.

Dr. Horacio Flores Zúñiga
Secretario Académico

Mtra. Ivonne Lizette Cuevas Vélez
Jefa del Departamento del Posgrado

INSTITUTO POTOSINO DE INVESTIGACIÓN CIENTÍFICA Y TECNOLÓGICA, A.C.
IPICYT
SECRETARIA ACADEMICA

Dedicatorias

Dedico esta tesis a mis padres y mis hermanas por su comprensión y apoyo constante.

A todos aquellos profesores que legaron importantes enseñanzas dentro y fuera de la academia. También a aquellos maestros de vida me enseñaron a empatar el desarrollo profesional y humano. Su presencia ha marcado mi existencia. Todos ellos ejemplo de humildad, honestidad, respeto, dedicación y perseverancia.

Agradecimientos

Agradezco al Dr. José René Rangel Méndez por enseñar con su ejemplo la pasión y entrega necesarias para desarrollar un trabajo competitivo. Aprecio su sinceridad para señalar los problemas, sabiduría para encontrar soluciones y su humildad para seguir aprendiendo junto a su equipo de trabajo.

A la Dra. Catalina Alfaro de la Torre (FCQ/UASLP) por sus valiosos comentarios y su gran humildad para motivarme a seguir avanzando. Valoro mucho su colaboración durante el desarrollo de este proyecto.

Al Dr. Luis Felipe Cházaro Ruíz por su importante contribución durante el desarrollo del proyecto. Reconozco su trato amable y su gran aportación para la escritura de los manuscritos.

Al Dr. Miguel Ángel Huerta Díaz por formar parte del equipo de trabajo a pesar de las limitaciones logísticas. Por su invaluable contribución y comentarios durante los avances de investigación.

Al Dr. Robert Hurt por darme la oportunidad de colaborar en su laboratorio (Environmental and Health Nanoscience, en Brown University, EUA), y permitirme conocer su destacada trayectoria.

Gracias al Dr. Kosterlitz (Premio Nobel de Física 2016) por permitirme observar como disfrutaba de impartir clases y compartir su ciencia a alumnos de licenciatura en la universidad de Brown.

Agradezco a los técnicos de División por su entrega diaria y paciencia conmigo.

Contents

List of Tables

CHAPTER 1

CHAPTER 2

CHAPTER 3

CHAPTER 4

CHAPTER 5

CHAPTER 6

List of figures

CHAPTER 1

CHAPTER 2

CHAPTER 3

CHAPTER 4

CHAPTER 5

CHAPTER 6

Glossary

UNESCO. The United Nations Educational, Scientific and Cultural Organization (UNESCO) is a specialized agency of the United Nations (UN) based in Paris..

BTEX. Acronym BTEX stands for Benzene, Toluene, Ethylbenzene, and Xylene (volatile organic compounds).

EBCT. Empty Bed Contact Time. The time takes to the influent go through the bed [min].

V_B. Breakthrough volume at a concentration of 0.02 [mL].

V_C. Breakthrough volume at a selected or establish concentration [mL].

H_{MTZ}. Height MTZ. The rate of removal of de adsorbate by the biosorbent in the bed [cm].

Fractional capacity (φ). The fractional capacity of the column in the adsorption zone at breakpoint to continue to remove solute from a solution.

R_{MTZ}. The rate of movement of the Mass Transfer Zones (MTZ). The affinity of the adsorbate by the adsorbent. Related to the kinetic rate [cm/min].

$S_{T0.02}$. Specific throughput. Volume treated per mass adsorbent at a Ct/C0 = 0.02 [mL/g].

S_{Tobj}. Volume treated per mass adsorbent at the concentrations defined by US-EPA [mL/g].

Resumen

Macroalgas marinas, polímeros naturales y óxido de grafeno como materiales adsorbentes para la remoción de hidrocarburos solubles

Actualmente la liberación de hidrocarburos (HC) al medio acuático (> 6000 toneladas en 2016), es uno de los problemas emergentes de mayor impacto al ambiente. Una de las principales fuentes de emisión son los derrames de HC por actividades de la industria petroquímica. De acuerdo a estudios, los HC más solubles son los más tóxicos para organismos acuáticos. Las principales estrategias de respuesta contemplan el uso de tecnologías de adsorción. En años recientes, las investigaciones se han orientado a la búsqueda de materiales alternativos que permitan la remoción de contaminantes con capacidades de remoción similares a los adsorbentes comerciales.

En este trabajo se evaluó la capacidad de biosorción de tres especies de macroalgas (pardas, verdes y rojas), a diferentes fuerzas iónicas. En los estudios de caracterización se detectó la presencia de los principales compuestos químicos presentes en la pared celular de los biomateriales. El incremento de la fuerza iónica a un valor hasta un valor de 0.5 M, no tiene un efecto detectable en la carga superficial de los biosorbentes, sin embargo la concentración de los grupos funcionales ácidos se mantuvo constante. La capacidad de adsorción de HC es mayor en biomasa del alga parda (*M. pyrifera*), donde el principal mecanismo se debe a la partición en la fase lipídica y compuestos de carbono no hidrolizable. La capacidad de adsorción de benceno por *M. pyrifera* disminuye a I > 0.45 M por la competencia de moléculas de agua por sitios activos en los biomateriales. Adicionalmente, mediante el uso de diseño de experimentos, se sintetizaron compositos a partir de la biomasa de *M. pyrifera*, quitosano (CS) y pectina. Los biomateriales fueron analizados en experimentos en lote y en continuo donde se demostró su factibilidad como biosorbentes para la remoción de los contaminantes de estudio.

Por último, el óxido de grafeno (OG) es un alótropo de carbono con potencial aplicación en la remoción de contaminantes orgánicos en solución acuosa. Actualmente, su aplicación se ha visto limitada debido a su aglomeración y baja área específica (S_{BET}). Ante esta problemática, la síntesis de sólidos laminares pilareados representa una alternativa al incrementar el área de adsorción y los sitios activos disponibles. El propósito principal de este estudio fue determinar el efecto de la co-precipitación de quitosano entre los espacios interlaminares del óxido de grafeno, y su afinidad por los principales hidrocarburos (HC) solubles en agua (benceno, tolueno y naftaleno). La proporción CS/OG = 0.1 empleando quitosano de bajo peso molecular, registró el mayor incremento del S_{BET} (47 m^2/g). Con el fin de elucidar los mecanismos de adsorción involucrados, se evaluó la afinidad por los HC de estudio a diferentes condiciones de pH, temperatura y presencia de materia orgánica.

PALABRAS CLAVE: algas marinas, biosorción, compositos, hidrocarburos, óxido de grafeno.

Abstract

Application of seaweed, natural biopolymers, and carbon-based materials as a wastewater treatment of water-soluble hydrocarbons

Nowadays the recovery of low-molecular aromatic hydrocarbons (HC) released into natural bodies of water continues to be a challenging task. These contaminants cause severe consequences to the environment and the human health. The oil spill cleanup strategies are primarily designed to deal with HC heavy fractions accumulated in the water surface. Unfortunately, insufficient information is available regarding the treatment of dissolved fractions.

Biosorption on macroalgae (Ma) biomass seems to be a potential alternative to overcome disadvantages associated with expensive costs and complexity of activated carbon production. Three representative samples of brown, green and red macroalgae seaweeds (*Macrocystis pyrifera*, *Ulva expansa* and *Acanthophora spicifera*, respectively) were evaluated to remove benzene and toluene from water, which is the most soluble hydrocarbons. To accomplish this objective, the influence of temperature and ionic strength on biosorption rate were also determined. Raw biomasses were characterized by different physical and chemical techniques to assess their potential as biosorbents and the mechanisms involved. Despite these advantageous properties of seaweed biomass, the physical characteristics (small particle size, low strength, and density) of such biomaterials are not viable for continuous process operation and make biomass challenging to apply. Therefore, the development of innovative low-cost techniques of immobilized biosorbents with particular attention to increasing their effectiveness in the biosorption process is mandatory. The objective of this research was to explore the performance of different biosorbent aggregates through different proportions of brown seaweed-chitosan-pectin on biosorption capacity of the three main soluble hydrocarbons (benzene, toluene, and naphthalene) in water. The biocomposite synthesis was optimized by application of the factorial design and response surface methodology. Moreover, a detailed chemical and physical characterization analysis, by textural properties, potentiometric titrations, elemental content, chemical stability, KBr-FT-IR, and TGA analysis, were performed to explain the adsorption mechanisms. Also, an optimized Ma-Pe-Ch biocomposite was used for BTEX and naphthalene removal in a fixed-bed column under different experimental conditions.

Finally, alternative methods to functionalized graphene oxide with a water-dispersible material are needed to create GO composites for adsorption applications. By introducing molecules or other carbon-based components between GO sheets (pillared agents), an increase in the surface area of the material could be observed. The synthesis of different CS-GO composites achieved an optimized surface area of 47 m^2/g (ratio CS/GO = 0.1). Various characterization techniques verified the presence of chitosan molecules between the GO sheets, creating grooves and high energetic adsorption sites. The hydrophobic effect and π-π interactions of the GO structures also with the chitosan (-OH) functional groups determined the favorable adsorption capacity in comparison with the un-modified GO.

KEYWORDS: Adsorption, biosorption, composites, graphene oxide, seaweed

GENERAL BACKGROUND

According to reports, the annual world production of liquid petroleum products such as gasoline, kerosene and heating oils is more than 3 billion metric tons, so we can infer that the use and processing of these hydrocarbons have a reasonable probability of producing major environmental issues. Thus, not only great oil spill accidents could be sources of these pollutants.

Although these pollutants share the same source, it is a fact that not all of them behave in the same way. Some molecules tend to partition from water to air, and others form water to solids; some have moderate toxicity, and others are known to possess a carcinogenic nature. In general, hydrocarbons (HC) could be classified into two main types: (a) BTEX, and (b) PAHs. Recently reviews of the toxicological properties of this pollutant have been presented [1,2]. The presence of HC in water could cause severe eco-toxicological effects to the environment and human health. To attend this problem, many revisions concerning produced HC water technologies are available [3,4]. Adsorption technologies possess remarkable advantages due to competitive treatment costs, high efficiency, and selectivity. Nowadays, the process of passive HC binding by using dead biomass is growing attention as an alternative to traditional adsorbents due to the remarkable surface area, high sorption capacity and surface reactivity. In this case, the process is called biosorption, and the biological components are called biosorbents. The main advantages of biosorption are that the precursors are available in large quantities with quite a little processing for treatment processes, generating low-cost alternatives for the removal of organic pollutants [5–8]. Dead plant biomass is composed mainly of cellulose and hemicellulose, for that reason, are the central studied biomass in biosorption studies. The reviews of Abdolali, et al. and Huber et al. present the complete revisions in the research field [9,10].

One of the main areas in biosorption research is the granulation of the precursor materials. This step is necessary for subsequent scale-up evaluations. The most-effective way to manufacture composites based in biosorbents is through the use of

entrapment, encapsulation and bonding methodologies. Moreover, the removal of hydrocarbons by composites is only available for dyes and metals [156–158].
On the other hand, the study of fixed-bed columns packed is mandatory to scale-up biosorption applications. The packed bed should be constituted with porous particles, which allows the diffusion of the pollutants, and the mechanical strength to resist the pressure drop in the bed.

As mentioned above, the synthesis of composites with natural polymers, represent a valuable tool to improve a wide-range performance or obtain a synergetic effect in the final material. Further changes of the precursors include the use of crosslinkers to enhance the mechanical properties of the composites. Additionally, the manufacture of composites would not involve hazardous reaction steps or secondary effects on the environment. For that reason, the formation of composites with carbon-based materials, and extensively with graphene oxide (GO) has registered a relevant increase on environmental studies. [11]. The addition of chitosan between the graphene oxide sheets could increase its surface area and hydrophobicity, making the final material suitable for sorption processes.

Regarding the pillared effect of chitosan on graphene sheets, just a couple of studies present the surface area ($m^2\ g^{-1}$) value, probably because of the negligible surface area of the final composite. For that reason, further characterization of GO-CS composites as adsorbent is needed to elucidate a possible pillared effect.

MOTIVATION OF THIS RESEARCH

Nowadays the recovery of low-molecular aromatic hydrocarbons (HC) released into natural bodies of water continues to be a challenging task. These contaminants bring severe consequences to the environment and the human health. The oil spill cleanup strategies are primarily designed to deal with the heavy fractions accumulated in the water surface. Unfortunately, insufficient information is available regarding the treatment of dissolved fractions. Harmful pollutants as aromatic hydrocarbons, such as benzene, toluene, benzene, ethylbenzene, and xylene (the BTEX group); polycyclic aromatic hydrocarbons (PAH), such as naphthalene are considered as priority pollutants and must be removed from water bodies.

Biosorption on macroalgae (Ma) biomass seems to be a potential alternative to overcome disadvantages associated with expensive costs and complexity of activated carbon production. Three seaweeds of a representative sample of brown, green and red macroalgae were evaluated to remove aromatic hydrocarbons from water, which is the most soluble hydrocarbons. Additionally, low-cost techniques for biomass granulation must be evaluated to improve the physical and effectiveness characteristics of such biomaterials for a continuous process application. Thus, chitosan and pectin were employed in conjunction with the algae biomass for the synthesis of a biocomposite for the removal of the pollutants above.

Finally, the improvement of a carbon-based nanomaterial with a natural polymer like chitosan may enhance the affinity towards the same aromatic pollutants. The diffusion of a polycationic polymer like chitosan may function as a pillaring agent, resulting in an increment on the surface area and subsequent affinity for the pollutants under study.

STRUCTURE OF THE THESIS

The present thesis dissertation is structured in the following sections:

Chapter 1 includes a general review regarding the available technologies for the removal of water-soluble hydrocarbons in aquatic media with an emphasis in adsorption technologies. At the end of the chapter, the general and specific objectives are presented.

Chapter 2 summarizes the physicochemical characterization of three-seaweed biomass under study and evaluates the biosorption capacity of benzene and toluene at different pH, temperature, and ionic strength conditions. According to the results, the primary presence of lignin, alginic acids, and lignocellulose fractions, increased the affinity of the biomass for the pollutants under study. Brown biomass registered the highest removal capacities for benzene and toluene, respectively. It was found that the hydrocarbons biosorption affinity was not affected up to an ionic strength of 0.6 M, due to the biosorbents pore occlusion by water clusters. For benzene and toluene nonpolar solutes, the biosorption mechanism is an addition of simultaneous interactions between the sorbents and the chemical constituents of the cell wall, presumably by London (dispersion) forces onto –OH and –NH active sites from polysaccharides and proteins and hydrophobic interactions from lignin and lipid fractions.

Chapter 3 contains the synthesis of macroalgae, chitosan and pectin composites to optimize the uptake of benzene on the modified adsorbent. The biocomposite synthesis was optimized by application of the factorial design and response surface methodology. Moreover, a through chemical and physical characterization analysis, by textural properties, potentiometric titrations, elemental content, chemical stability, KBr-FT-IR and TGA analysis, were performed to explain the adsorption mechanisms. Batch systems analyzed the effect of pH, ionic strength, and dissolved organic matter in the biosorption mechanism.

Chapter 4 is aimed to employ pillared graphene oxide produced by using chitosan at a ratio of CS/GO = 0.1 corresponding to a surface area of 47 m^2 g^{-1}. Evidence of pillared effect is characterized through various physicochemical tests. An enhance of the adsorption affinity for benzene, toluene, and naphthalene was registered. Adsorption kinetics and isotherms were performed and fitted by rate and adsorption models. Low diffusivity constant values (*k1*) were observed. These results show the feasibility of chitosan as a precursor in the development of a surface area of CS-GO composites for the removal of soluble hydrocarbons in water.

Chapter 5 presents the final experimental section where the previously synthesized biocomposite was employed for dynamic experiments. The results showed an evident selectivity for the aromatic molecules is based on their hydrophobicity degree; the removal efficiency increased with a lower influent flux. The experimental results stated the feasibility of macro-algae based composites for continuous processes.

Chapter 6 discusses the primary results in the previous 2-5 chapters followed by a summarized of the main conclusions in **Chapter 7** in addition to the future work and perspectives. Finally, a list of scientific products and scientific congress is also presented

.

CHAPTER 1

INTRODUCTION

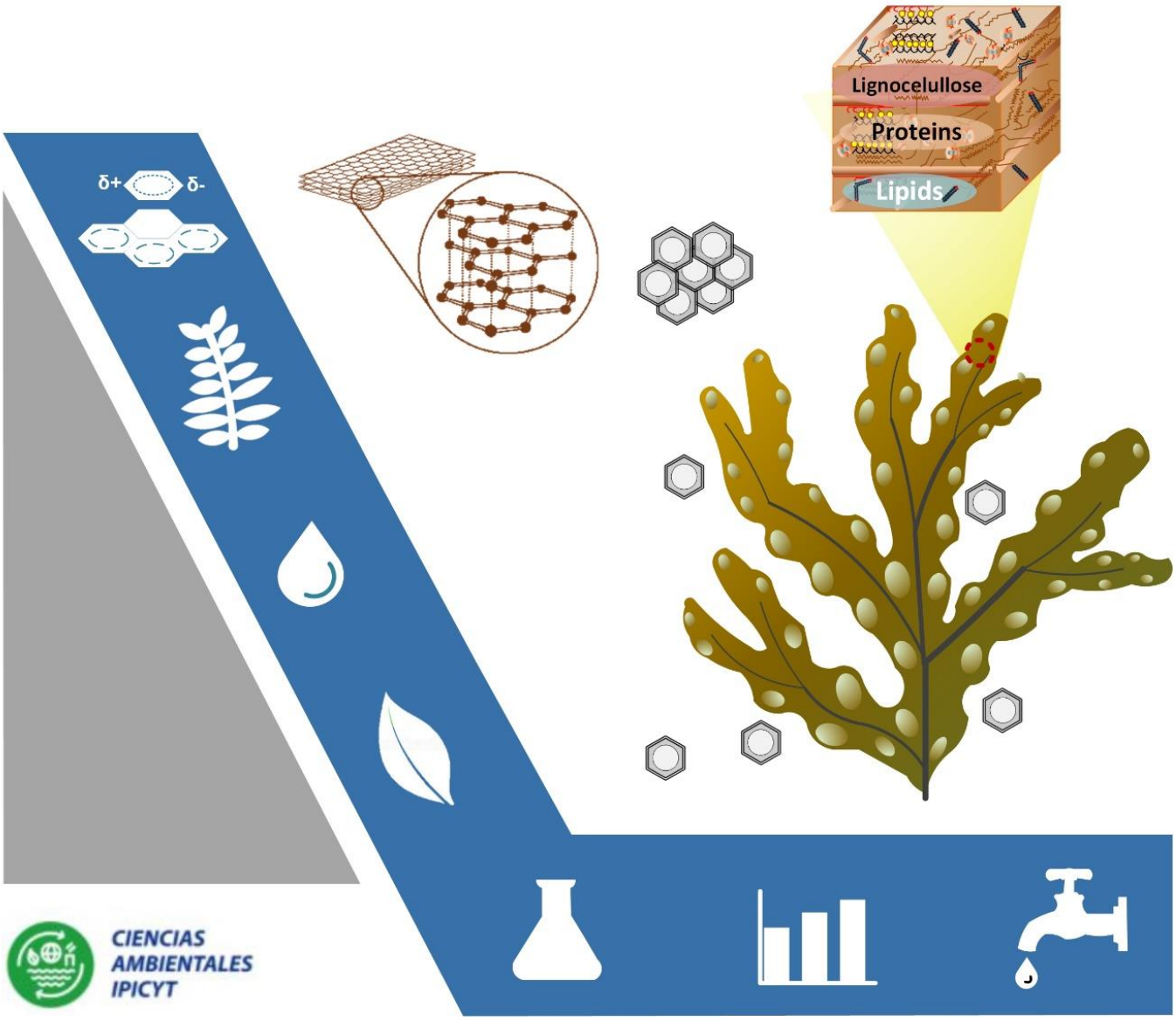

CHAPTER 1

1.1 Water pollution control: An approach to the contamination by organic compounds

The society is facing a global water quality challenge. Water pollution concerns have risen in the international agenda because it is intrinsically associated with environmental, social and economic problems. Sustainable development goals (SDGs) proposed by the United Nations (UN) establish the necessity of reliable supplies of clean water, calling for advances to all countries by 2030 [12]. As a result, governments and international organizations intensify water policies to reduce health hazards and improve wastewater management. The most recent water assessment report by the United Nations Educational, Scientific, and Cultural Organization (UNESCO) addressed in 2016 that an estimated 90% of sewage in developed nations is discharged without previous treatment to water bodies [13]. Also, 300-400 megatonnes of industrial wastewater are released into the environment [13]. Point and non-point sources include several contaminants in wastewater (e.g., pathogens, nutrients, suspended solids, inorganic pollutants, among others), with organic pollutants playing a significant role [14]. The presence of organic compounds is crucial because interacts with biologic systems with high bioaccumulation, carcinogenic, teratogenic and mutagenic potential [15]. Many kinds of toxic organic compounds include dyes, phenols, pesticides, polycyclic hydrocarbons (PAHs), phenols, polychlorinated biphenyls (PCBs), halogenated aromatic hydrocarbons, crude oil, surfactants, and so forth. In addition to these, hydrocarbons and other compounds (e.g., alcohols, aldehydes, ketones, pharmaceutical or BTEX) also discharge in the wastewater. These pollutants remain either in solvated, colloidal or suspended form [16]. Due to this, organic molecules could be transported long distances to different bodies of water [17], and are even detected in the effluent of wastewater treatment plants [18]. With a growing demand for energy and supplies, the petrochemical industry is considered one of the most profitable activities, but at the same time, one of the primary organic wastewater producers [19]. The challenges associated with increasing onshore and offshore oil production from newly explored or deeper reservoirs correlate with the number of incidents and accidental oil spill risks [20]. In 2014, the reported oil spills >1 barrel resulted in the

release of an estimated total of 6,667 tons [21]. Minor spills account for 90 % of hydrocarbon discharges up to a quantity of two million tonnes [20]. Most of the crude oil range in its relative constitution from 55 % to 97 % of hydrocarbons [22]. The hydrocarbons present in oily effluents could be found in four categories according to its physical form in water [23]:

1. Free (floating) fraction: It rises quickly to the surface of water because of the high molecular weight of the components (D_p > 150 µm).
2. Dispersed fraction: It is an array of fine droplets stabilized by their electrical charges without surfactants (*Dp:* 20 - 150 µm).
3. Emulsified fraction: This fraction has a similar distribution as dispersed oil, but the stability is enhanced by the interaction with emulsifiers present in the oil/water interface (D_p < 20 µm).
4. Dissolved fraction: Truly dissolved HC or dispersed in extremely fine droplets (D_p < 5 µm).

Low molecular aromatic compounds like BTEX and a sort of PAHs, are of present significant solubility and bioavailability than other oil hydrocarbon contents, and for this reason, are classified as priority pollutants [24]. BTEX and PAHs are compounds built on benzene ring which molecular structures contempt all carbon atoms in a plane with and have an almost linear relation between molecular weight and the aqueous solubility [7].

1.1.1 BTEX

The BTEX compounds (benzene, toluene, ethylbenzene and the three-xylene isomers) are common water pollutants. BTEX are volatile, monoaromatic compounds that are widely used in industry as solvents and starting materials for numerous chemical synthesis and processes [25]. Several pathways of BTEX contaminants are continuously introduced in the environment because of the disposal of industrial effluents, and accidental events such as oil spills or pipeline leakages in distribution networks [26,27]. The presence of BTEX in the environment is higher than their poly-aromatic counterparts because of their high solubility rates

(Table 1.1), which could be noticed by the octanol-water partitioning coefficient as an indicator of the hydrophobicity of an organic molecule [28]. On the specific case of BTEX and hydrocarbons compounds, the hydrophobicity has a linear relation with the molecular weight and indirect relationship with solubility.

Once these compounds are released into a water column, they undergo elaborate physical, chemical and biological transformations including spreading, drifting, dispersion and weathering), due to the relatively high water solubility and low K_{ow} (Table 1.1). This hydrophilic character allows higher transportation and exposition for marine and freshwater environments, producing adverse effects to organisms and human health (i.e., chronic effects on kidneys, heart, lung and nervous system) [29]. For this reason, BTEX compounds are classified as priority pollutants (Table 1.2) [30].

Table 1.1 Physicochemical properties of BTEX molecules.

Compound	Mole weight (g $mole^{-1}$)	Density (g cm^{-3})	Boiling point (°C)	Water solubility (mg L^{-1})	Molecular diameter ($Å^2$)	Log K_{ow}
Benzene	78.1	878	80.1	1800	30.5	2.1
Toluene	92.1	865	110.6	515	34.4	2.7
o-Xylene	106.2	880	144.5	178	36.8	3.1
m-Xylene	106.2	864	139.1	161	37.9	3.2
p-Xylene	106.2	861	138.3	165	37.5	3.2
Ethylbenzene	106.2	867	136.2	170	38.0	3.2

Water pollution with aromatic compounds and oil droplets includes reservoirs, surface and underground water bodies of fresh or saline water (Table 1.3) [31–33]. The predicted median lethal concentrations for marine organisms are 48, 19 and 2.14 mg L^{-1} for benzene, toluene, and naphthalene, respectively [34]. For that reason, the cost-effective technology for the removal of these pollutants is mandatory.

Table 1.2 Acceptable limits for BTEX in water according to various regulatory institutions (all values are in µg/L).

	WHO DWG[1]	US NPDWS[2]	NOM-127-SSA[3]	BNEC[4]
Benzene	10	5	10	5
Toluene	700	1000	700	2
Ethylbenzene	300	700	300	90
Xylene	500	10,000	500	300

[1] *World Health Organization Drinking Water Guidelines* [30].
[2] *United States National Primary Water Standards (US EPA, 2003)* [24].
[3] *Mexican normative (NOM-127-SSA-1996)* [35].
[4] *Brazilian National Environment Council* [26].

Table 1.3 Reported concentrations of benzene, toluene, ethylbenzene, and xylene. All the values are in ppb or µg/L*.

	Benzene	Toluene	Ethylbenzene	Xylenes
Surface water	< 0.1 – 2.1	< 1 – 15	< 0.1- 1.8	< 0.1 – 1.2
Contaminated surface water	Up to 100	NA	Up to 15	Up to 32
Groundwater	< 0.1 – 1.8	< 1 -100	< 0.1 – 1.1	< 0.1 – 0.5
Contaminated groundwater	Up to 330	Up to 3500	Up to 2000	Up to 1340
Drinking water	< 0.1 – 5	< 1 – 27	< 1 – 10	< 0.1 – 12

*All the data reported in Table 3 was found in a previous report [36], and collated from ATSDR 2000, 2007a, 2007b and 2007c; IPCS 1985, 1993, 1996 and 1997; NTP 2005; WHO 2008; and NHMRC 2004.

1.1.2 PAH's

Water pollution by organic compounds has bio-accumulative, persistent, carcinogenic, mutagenic and detrimental effects on aquatic organisms, flora, fauna as well as human health. Polycyclic aromatic hydrocarbons (PAHs), possess two or more fused benzene rings and represent a relevant environmental concern because of the documented carcinogenicity and the widespread occurrence of several bodies of water [16]. A total of 100 polycyclic molecules are identified by the U.S. Environmental Protection Agency (EPA), and 40 have been listed as prioritized

pollutants [24]. Therefore, their distributions in the environment and potential human health risks have become the focus of much attention. The introduction of PAHs into the aquatic media varies from natural and anthropogenic processes. Anthropogenic sources include automobile exhaust and incomplete combustion of coking coal, domestic heating emissions from coal, oil, gas, and wood, refuse incineration and biomass burning [5]. Additionally, crude oil contains high levels of PAHs, but the relative concentration of each compound depends mostly on the type and origin of oil. Crude oil contains around 0.2 to 7% PAHs, with configurations ranging from to two to six rings; PAHs content increase with the specific gravity of the oil [37]. In general, PAHs have low solubility in water (low K_{ow} = 3-8), high melting and boiling points, and low vapor pressures. Naphthalene is the PAH with the higher solubility rate (31.5 mg/L), therefore, is commonly reported in the dissolved aromatic fractions of oil spills, unusually, in deep water sources. For example, the Deepwater Horizon oil spill in 2011, reported the presence of naphthalene as the third principal component in the dissolved fraction in four sample stations [38]. PAHs affect the productivity and growth of benthic organisms that are generally the main altered organisms by oil pollution in water [39].

1.1.3 Removal of hydrocarbons from aqueous media with an emphasis in the adsorption process

The primary objective of all the wastewater treatment processes is to reduce the wastewater pollution according to the permissible quality standards. The quality standards of treated water are usually designed according to the reuse of the treated water or discharging into water stream [13]. Wastewater treatment process has to consider many factors such as the reliability and efficiency of the process, external equipment, quality of treated water, scale-up conditions, construction space for treatment facilities, waste disposal standards, implementation, and maintenance. Physical, chemical, and biological processes are widely used for the wastewater treatment process of hydrocarbon in aqueous media [23,39–41]. These methodologies are employed in two crucial treatment stages. The first stage consists

of mechanical and physicochemical treatment followed by a second, advanced treatment to polish the physicochemical characteristics of the effluent.

1.1.3.1 First treatment step

A first step is essential because allows the maintenance and well operation of the advanced stages. In this part of the treatment process, the primary target is the considerable reduction of various components like suspended solids (SS), immiscible liquids (emulsions), solids particles (colloids) [18]. In the refinery industry, this is mechanically achieved by gravity in API separators or separation tanks [42]. The mechanical step is followed by the physicochemical steps (Fig.1.1), in which the presence of heavy metals is decreased with small sizes of particulate solids through agglomeration, sedimentation or flotation [43].

1.1.3.2 Advanced treatment step

In this second stage, the main purpose in the second stage is to diminish the concentration to the target limits for discharge of reuse. Physical, chemical, and biological processes are available for this treatment process (Table 1.4) [44]. Biological methodologies include a wide variety of active metabolic biomass including fungi, bacteria, yeast, and algae [45–47]. Anaerobic and anaerobic systems were tested were addressed with the aim to transform or degrade an extensive list of recalcitrant contaminants [48]. The significant drawbacks of these technologies include the uncertainty of reproducibility at al full scale due to the dependence of the process in many variables (e.g., the chemical properties and the homogeneity of conditions of the consortia. Fluidized bioreactors (FBR) have been shown to be useful for toxic pollutants degradation regarding their higher biomass concentration and mass transfer [49].

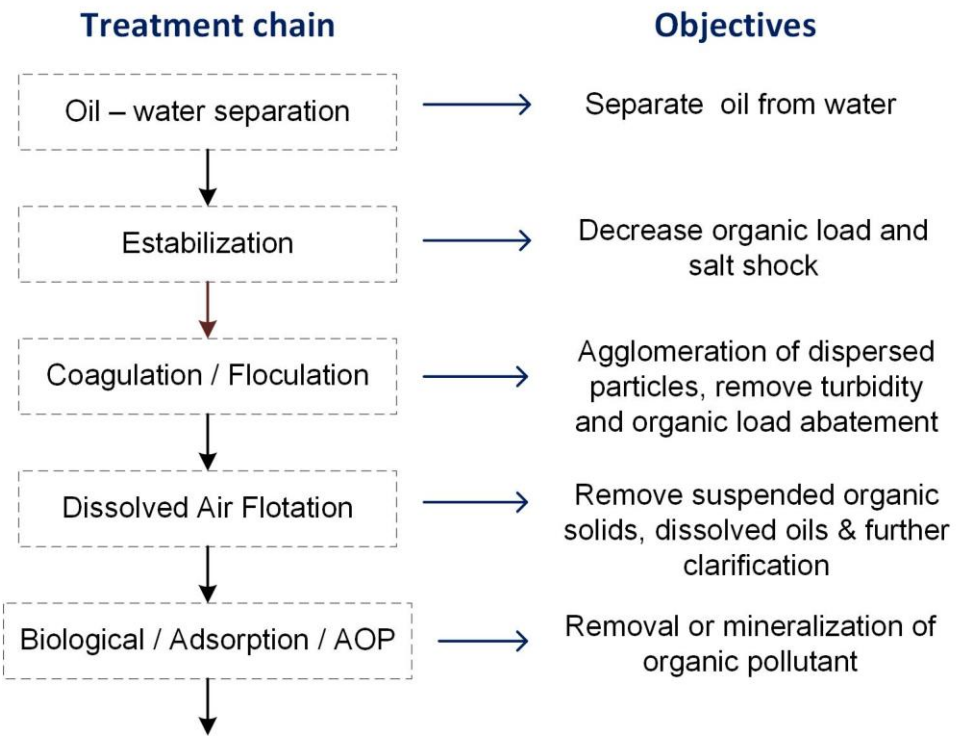

Fig. 1.1 Schematic diagram of a generic sequence for treating hydrocarbon wastewater effluent

Chemical methodologies consist of the use of one or more chemical reactions for water treatment. The most listed procedures include ozonation, precipitation, ion exchange, electrocoagulation, among others. Physical treatment processes are based on the physicochemical characteristics of the pollutants and are generally cheapest forms of treatment. The main types include coagulation, filtration, reverse osmosis and sorption technologies [50].

As indicated in Table 1.4, different methodologies have been evaluated having a varying degree of success. However, sensible disadvantages including high-energy requirements, long periods of treatment, and expensive equipment. Sorption including different adsorbent media such as carbonaceous materials, natural products, and wastes have proven to be an efficient, rapid and feasible alternative for hydrocarbons removal and decolorization of wastewater [51,52].

Table 1.4 Advantages and drawbacks for the removal of hydrocarbons in water. Adapted from Gupta et al., (2018) [53].

Methods	Advantages	Disadvantages
Physical		
Adsorption on activated carbon	High removal efficiency	Regeneration of support, cost-effective
Adsorption on bagasse	Utilization of waste to treat another waste	Post-treatment disposal
Adsorption on peat	Effective adsorbent, no activation required	Lower surface area than activated carbon
Adsorption on fly ash	Simple and effective adsorption, no activation required, inexpensive	Regeneration of support is difficult, highly toxic
Membrane filtration	Effective removal of a wide range of colorants at low volumes	Required high dissolved oxygen, ineffective for light-resistant colorants
Biosorption	Low-cost, High surface active sites	Low surface area and mechanical properties
Chemical		
Ozonation	Effective for azo dye removal	Unsuitable for disperse dyes, releases aromatic amines
Sodium hypochlorite	Low-temperature requirement	Cost-intensive process
Coagulation and precipitation	Short detention time, low capital costs, good removal efficiencies	The high cost of chemicals for pH adjustment, problems of dewatering and sludge handling
Biological		
Aerobic process	Color removal along with biological oxygen demand (BOD) and chemical oxygen demand (COD) removal	Long retention time, low efficiency for removal of recalcitrant pollutants
Anaerobic process	Resistant to a wide variety of complex colorants, produced biogas used for steam generation	Long acclimatization phase
Emerging technologies		
Advanced oxidation processes	High mineralization, effective pretreatment in integrated systems,	High consumption of oxidants

	biodegradability, and removal of toxics	
Electrochemical oxidation	Decolorization of an extensive range of wastes, no alternation in volume	Sludge disposal problem and the requirement of low pH values
Sonication	Highly effective for integrated systems	Relatively new method, awaiting full-scale application
Enzymatic treatment	Effective for specific compounds, unaffected by shock loadings, required shorter contact times	Cost of enzymes, enzyme stability, product inhibition
Redox mediators	Easily available, enhancement of the process by increasing electron transfer efficiency	The mediator may give antagonistic effect and depend on the biological activity of the system
Engineered wetland systems	Cost-effective technology, applicable for vast volumes of wastewater	High installation cost, requires expertise, and difficult to manage during monsoon

1.1.4 Sorbent media

Adsorbents are available as irregular granules, extruded pellets, or formed spheres, depending on the employed production technology. However, could be either of natural origin [8]. Typical adsorbents include carbon-based adsorbents minerals, zeolites, oxides or biopolymers. Polymeric adsorbents are made by copolymerization reactions, showing adsorption properties similar to activated carbon [54], but production costs hinder their widespread application. Zeolites and oxides possess a predominantly hydrophilic character with a naturally negative charge and are widely used in detergent manufacture, petroleum industry and adsorbents for carbon dioxide and hydrogen sulfide wastewater [55,56]. A growing interest in the literature is characterized by the use of natural material occurring in nature because of their high availability of precursors, surface active sites and low cost in comparison with carbon-based adsorbents.

1.1.5 Carbon-based materials

Most of the sorbents used nowadays included engineered adsorbents, known as activated carbons (ACs), manufactured by pyrolysis of carbonaceous materials (e.g., coal, wood, and fruit bones, and shells) followed by physical or chemical treatments to increase the surface area and active sites of the material [57]. Activated carbons usually have a remarkable porous internal structure with a different range of pore diameters. The porosity range includes macro- (> 50 nm), meso- (2- 50 nm) and micro- (< 2 nm) which in conjunction could bring values of surface area up to 2500 m^2 g^{-1} [58]. For this reason, the number of available sites for pollutant interaction is superior to most of the adsorbents. The precise textural characteristics of the final produced activated carbon depends on the precursor, the activation process and any following chemical modification [59].

The chemical structure of activated carbon makes it an efficient material for the removal of organic compounds due to the aromatic assembly of graphitic sheets with aromatic functionalities. Adsorption of organic compounds in the liquid phase is complicated because the orientation of the molecules is something to be considered [60]. Even the solvation phenomenon of aromatics is an actual research topic. Based on the literature, benzene molecule generates Van der Waals interactions and, in minor proportion hydrogen bonds, with water [61]. Adsorption mechanisms include π-π interactions between the adsorbate and the surface of AC. However, hydrogen bonding and Van der Waals interactions could happen with specific functional groups of the pollutants [62]. Different variables affecting adsorption on AC were reported as pH, ionic concentration, temperature, the competition of other species, which would have different effects regarding the nature of the organic adsorbate [62].

1.1.6 Graphene oxide

Besides adsorbents, graphene, as a relatively new type of carbon nanomaterial, has opened an extensive interest in different research fields due to its notable properties such as high transport of charge carriers, mechanical elasticity, thermal and

chemical stability [63]. Related to adsorption, graphene has a large specific surface area (2630 m^2 g^{-1}), but could only offer van der Waals force to bind the adsorbents because of the only presence of sp^2 carbon on the sheet surface [64]. The adsorption capacity of graphene could be enhanced by including functional groups or other components (pillared agents). Graphene oxide, which is one of the graphene derivatives, is characterized by having oxygen groups on the sheet surface in the form of epoxy, hydroxyl, and carboxyl groups [65]. These oxygen groups are capable of binding metal ions and positively charged organic compounds by coordination and electrostatic interaction [66]. However, its negative surface charge exhibits a low affinity for anionic dyes due to electrostatic repulsion. Moreover, graphene and its by-products tend to stack together due to strong van der Waals interactions [67]. Furthermore, when these 2D sheets are made into powders by dehydration, a considerable part of the surface area would be lost. Thus, how to overcome this issue should be considered when developing graphene-based adsorbents [68].

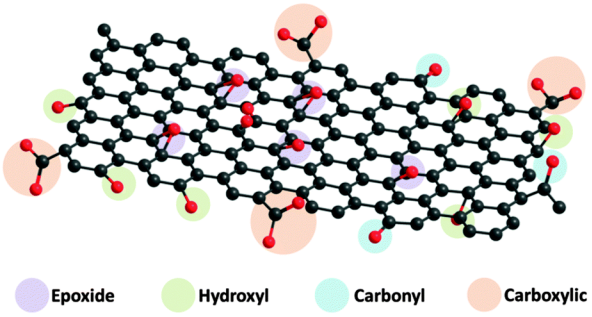

Fig. 1.2 Chemical structure of GO

1.1.7 Ion-exchange resins

Significant use of synthetic resins as sorbents for the removal of organic compound in water is available in the literature [69]. Advantages associated with the use of these materials included regeneration in-situ, regeneration with nonaqueous solvents or solutions of bases, acids or salts. Both the nonaqueous solvents and the resins could be regenerated with adsorptive characteristics similar to carbon-based materials. The resins are constituted mainly by polystyrene-divinylbenzene

copolymers or polymethacrylates cross-linked with a non-aromatic material [70]. The pore size distribution is controlled in this highly porous material. An important characteristic is the absence of ionic functional groups in the structure which makes feasible to remove hydrophobic compounds through van der Waals interactions [70]. The polymeric adsorbent has been successfully applied in the concentration of molecules for following analytical techniques. Adsorption of hydrocarbons includes phenol, carboxylic acids, alkyl benzene sulfonates, among others [71].

1.1.8 Inorganic materials and minerals

The main commercial inorganic adsorbents in use include silica gel, activated alumina, and zeolites. Silica gel is (SG) divided into three classes based on their density: (a) regular, (b) intermediate and (c) low density. Regular density SG possess a high surface area (around 750 $m^2 g^{-1}$). Intermediate and low-density silica gels possess lower surface areas (100 – 300 $m^2 g^{-1}$). It is a widely used adsorbent employed in the industry. A recent report of mesoporous silica with large specific areas (up to 2370 $m^2 g^{-1}$) reviewed the results on the removal of numerous organic pollutants [72].

Activated alumina contains several forms of moderately hydroxylated alumina oxide, Al_2O_3. In general, this adsorbent is prepared by heating the precursor hydrous alumina to remove hydroxyl groups, and the result is a porous structure. The final surface area range for 200 to 300 $m^2 g^{-1}$ and is extensively applied for the uptake of organic pollutants like gasoline, kerosene, and aromatic hydrocarbons [52].

Zeolites are mainly microporous adsorbents that occur naturally in the environment and are synthesized for a particular target of pollutants showing ion exchange properties. Natural zeolites generally show low surface area, but some synthetic zeolites could be as high as 700 mg g^{-1}. Zeolites are commonly used to remove organo-chlorinated pesticides due to the low cost and regeneration ability [55,73].

1.1.9 Biosorbents

Biosorption can also be an attractive alternative for hydrocarbon removal from dilute industrial wastewater [74]. It implies the use of inactive or dead biomass and their derivatives. Many studies have been carried out for the capacities of adsorption of organic molecules on various types of biomass. Biosorption processes constitute a remarkable alternative because it was reported in the last years that this technology could be from 20 to 36 % less expensive in comparison with conventional systems respectively [75]. Biosorption involves the passive binding to metabolic inactive materials [76,77]. Another field of research consists in the immobilization of biomass in a matrix or easily recoverable support. The most common immobilization agents or matrices include alginate, polyacrylamide, polysulphone, silica-gel, cellulose, and chitosan [78].

The advantages of inactive metabolic biomass include an easier store for extended time periods, and it is not subject to hydrocarbon toxicity limitations. Administration of nutrients is not required, and the loaded biomass could be reused [79]. However, in most of the reports, the use of non-living biomass in powdered form has some drawbacks as difficult separation of the sorption system, mass loss after regeneration, reduced mechanical strength and operation difficulties in continuous operations. However, these issues could be overcome by using the appropriate immobilization method [80].

1.1.10 Seaweed biomass

The seaweed or macroalgae are considered photosynthetic organisms with chlorophyll A and accessory pigments. They could be founded in marine or freshwater. The cell structure possesses cellulose [72] typically. The morphology could be unicellular (microalgae) or multicellular (macroalgae). One of the standard classification was made by color, and are classified into three main groups: green, brown and red. The seaweed biomass is suitable for its application as a biosorbent due to their widespread distribution and easy access [81,82].

Algae are known as a rich source of bioactive compounds, and the properties of these compounds are used in various sectors of the industry including chemical, pharmaceutical, human food, and fertilizers [83]. In 2008, aquaculture of macroalgae reached cultivation of 15.8 tons (by weight) and USD 7.4 billion value. The value of cultivated seaweed increased from the US $ 1,768 million in 2001 to US$ 4,143 in 2010 with brown and red types as the main cultivated types [83]

1.1.11 Chitin and chitosan

Among the available biosorbents, chitosan (CS), the linear cationic aminopolysaccharide composed of α-D-glucosamine, is a partially acetylated glucosamine biosorbent and extracted by a deacetylation procedure from chitin, the most abundant biopolymer after cellulose. Chitosan contains 2-acetamido-2-deoxy-β-D-glucopyranose and 2-amino-deoxy- β-D-glucopyranose residues.

In recent years, the application of chitosan for the removal of hydrocarbons in water has been increasing exponentially due to remarkable properties as nontoxic, hydrophilic, antibacterial activity and ability to crosslink other precursors for the synthesis of composites [84]. The amine and two hydroxyl groups act as adsorption sites and junction sites, especially the amine groups that are strongly reactive. However, the applications of chitosan are limited for adsorption applications for its solubility in acidic media [85].

1.1.12 Microorganisms and fungi biomass

Crini and Aksu [78,79] have revised the application of biosorption using yeasts, fungi, and bacteria for the removal of organic pollutants. Recently, the biosorption of pollutants by bacteria and fungi have been growing, especially metals removal, due to their remarkable performance, low cost, and broad availability. A high amount of chelating active site are the main features of this biomass.

1.1.13 Lignocellulosic materials

Probably any imaginable plant-based material could be studied relative to its potential use as an adsorbent of organic compounds. Lignocellulosic biomass is mainly constituted by cellulose, hemicellulose, and lignin in conjunction with other molecules like acetyl groups, minerals and phenolic functional groups [86].

However, a sum of several conditions must establish full filled for selecting an available material, (a) there must be broad availability of the precursor with easy access for harvesting. (b) The precursor should resolve an environmental issue (e.g., the approach of industrial byproducts or the presence of alien species the ecosystem), and finally, it has to register a noticeable affinity for the target pollutants in comparison with carbon-based materials. Several reviews are present in the literature regarding the evaluation of lignocellulosic precursors often called in the literature as low-cost adsorbents [7,8,87–89]. The adsorption mechanisms are well correlated to the content of hydrophobic structures like lignin, cellulose, and hemicellulose. Hydrogen bonding, electrostatic and van der Waals forces were reported in a lesser degree depending on the particular functional groups of the pollutant under study [90].

1.1.14 Synthesis of composites

The aim of the synthesis of composites consists of overcoming some limits for extensive application in comparison with the separate adsorbents. The development of composites produces adsorbents with an improvement in the process separation and concentration of the adsorbents. Many inorganic and organic polymers and fibers have been employed such as lignocellulose extracts, polyethylene, and hydrogels, among others [91,92]. The main synthesized composites regarding the removal of hydrocarbons are briefly discussed in the following sections.

1.1.15 Polymeric composites based on natural fibers

Natural fibers are naturally occurring polymers in our environment, which appear in grasses, leaves or stalks of plants. They are also referred to as lignocellulosic fibers since lignin (5 - 20 %) and cellulose (60 - 80 %) are the main components. There are six main types of fibers including bast fiber, leaf fibers, fruit fibers, grass fibers, straw fibers and other types (wood and roots). The research work of Tsai [93] shows that the mechanical properties of chitosan solutions such as viscosity, and turbidity increase with a higher presence of pectin contained as a reinforcement.

1.1.16 Cellulosic-based composites

Cellulose, the most abundant natural polymer in nature is a homopolymer consisting of β-1,4-glycosidic linked D-glucopyranose units. The basic unit of cellulose is cellobiose (Fig. 1.3). Every glucose unit consists of three hydroxyl groups positioned at the C_2, C_3 and C_6 carbons [94]. The substitution of the primary position at C_6 is more thermodynamically stable than for the secondary positions at C_2 and C_3. The least favored reaction for the hydroxyl group is a reaction at C_3, due to more steric favored C_2 [95].

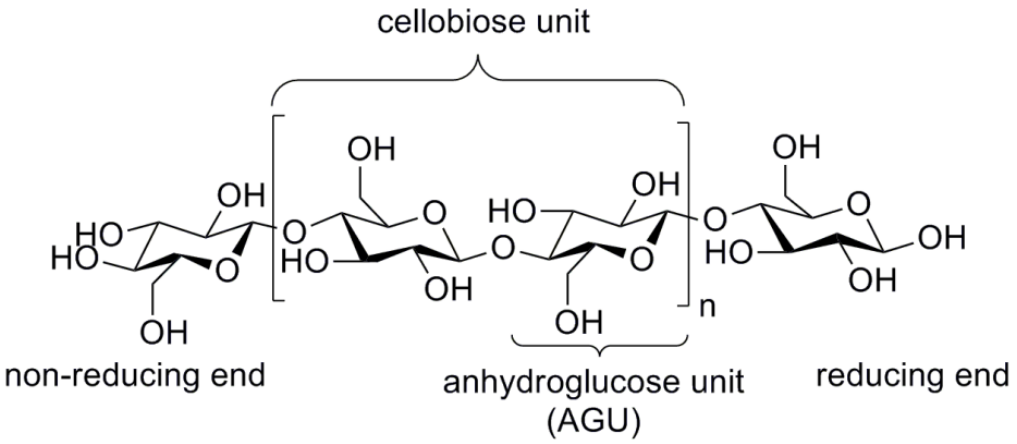

Fig. 1.3 The cellulose polymer with the basic unit of cellobiose

The cellulose molecule has been extensively employed with several precursors in the removal of organic dyes in water such as sodium montmorillonite, FeO_3, hydrogels, graphene oxide, quaternary ammonium salts, chitosan, bentonite, titanium oxide, silica, among others. Unfortunately, no data was founded for the removal of soluble hydrocarbons in water.

1.1.17 Graphene-based polymer composites

Many GO-based composites have been employed for the removal of anionic and cationic dyes and many organic compounds. Some reports include composites with metal oxides, carbon derivatives or polymers synthesized by solvothermal reactions [96], microwave-assisted route [97], one step sonochemical route [98], coprecipitation [99] and ultrasonication route [100], among others. The recovery of adsorbent after use has always been a challenge. A probably way to overcome this is by the synthesis of magnetically active graphene-based composites [101]. The recent increment of research into graphene-based hybrid materials is due to their higher surface area and porosity.

1.1.18 Pillaring of Graphene Oxide

In the past few years, graphene oxide has gained considerable attention due to the potential capability for use as adsorbents related to its theoretical surface area (2630 $m^2\ g^{-1}$) [102]. Nevertheless, the main inconvenient GO is the agglomeration during storage or application, which results in the reduction of the adsorption capacity in batch systems. To solve this issue, physical [103] or chemical modifications [104,105] of GO sheets have been proposed (Fig. 1.4), but continuous efforts are still necessary to improve the surface area of GO sheets. Also, limited works have published about dealing with adsorption of organic pollutants or toxic metals [106,107].

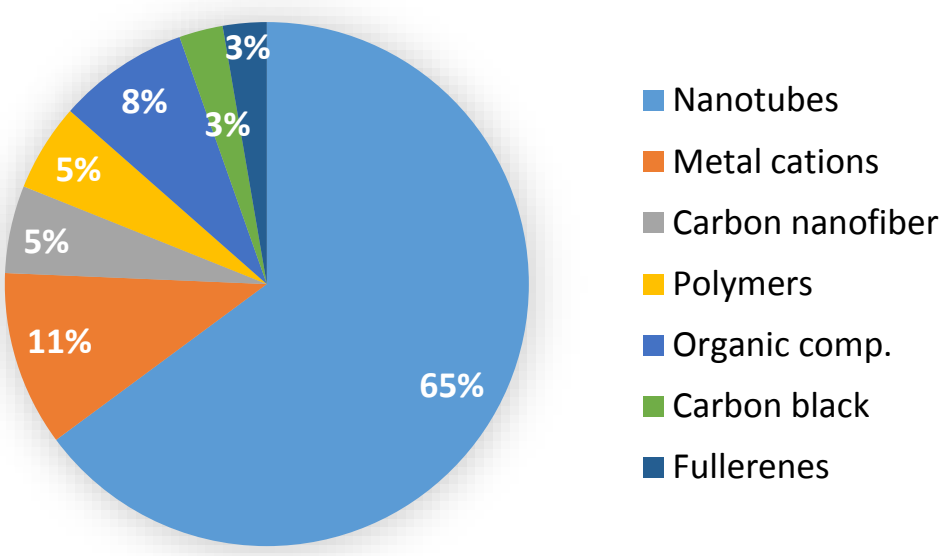

Fig. 1.4 Pillared precursors reviewed in *Isi Web of Knowledge* database (December 2017).

1.2 GENERAL REVIEW

1.2.1 Biosorption of hydrocarbons by seaweed biomass

1.2.1.1 Surface properties and potential uses

Macroalgae as a biosorbent have appeared as a potential alternative in comparison with commercial products for the removal of metals and organics [88]. Natural precursors like seaweed are considered safer, cheaper and efficient. The biosorption main characteristic features in the literature are related to rapid, reversible, economical, and eco-friendly processes. Macroalgae-based biosorbents offer several advantages as (a) diverse of functional groups in the surface, (b) generally uniform distribution of binding sites on the surface, (c) requires minimal preparation processes, (d) any or considerable less chemical modifications, (e) high availability all the year, (f) remarkable removal capacity and biodegradability. Numerous reviews recompiled successful application of this biosorbent for the removal of organic pollutants and hydrocarbons in water [7,87]

1.2.1.2 Characterization of biosorbents

The chemical, structural, and elemental composition of any adsorbents plays undoubtedly crucial role and has paramount significance in the adsorption process. Characterization analysis is pretty similar to carbon-based materials [62], but additional tests should be considered for a complete chemical characterization like the content of lignocellulosic fractions, sulphated polysaccharides and fiber content [79]. The following sections give a review in the characterization of three macroalgae biosorbents of interest.

1.2.1.2.1 Physicochemical properties of seaweed

Algal divisions according to which have cell walls include red, green and brown seaweed [108]. The cell walls are a complex network of biopolymers which consist in a skeleton of crystalline and fibrous parts (e.g., cellulose, hemicellulose) and an embedding matrix of specific polysaccharides, proteoglycans and others molecular components for each division [109]. The red algae possess sulphated galactans like carrageenan and share xylan or mannan fibrils with green algae which also encompass mixed-linkage glucans or ulvans [110]. Sulfated fucans and alginates enclose the main parts contained in brown algae [111]. Detailed analysis of cell-wall (Fig 1.5, Table 1.5) components is an actual research topic [47,112]. A comparative table for the physicochemical constitution of three macroalgae of interest is presented in Table 1.6.

Table 1.5 Main types of macroalgae and chemical constitution of the cell wall.

Division	Example	Common name	Cell wall constitution
Chlorophyta	*U. expansa*	Green	Principally cellulose, glycosides, xylenes, and mannan
Phaeophyta	*Macrocystis pyrifera*	Brown	Cellulose, acidic alginate, mucopolysaccharides (fucoidan)
Rhodophyta	*Acanthophora spicifera*	Red	Cellulose, xylenes, sulfated polysaccharides (galactans)

a) **(b)** **(c)**

Fig. 1.5 Schematic representation: (a) *Macrocystis pyrifera*, (b) *Acanthrophora spicifera* y (c) *Ulva expansa*.

Table 1.6 Review of the chemical composition of three representative types of seaweed. Data compiled from previous reports [76,113–116].

	Macrocystis pyrifera	*Acanthophora spicifera*	*Ulva expansa*
Organic matter (%)	84.4	NR	NR
Ash content (%)	41.6	30	32.2
Total carbohydrates (%)	22.3	30	17.1
Proteins (%)	0.2	7.49	8.8
Alginates (%)	10-40	NR	NR
Lipids (%)	7 g/kg	2.7	5.1
Water content (%)	84.7	NR	86.1
Surface area (m^2/g)	0.2	NR	NR

ND =Not determined

The presence of *Macrocystis pyrifera* is recognized in all the continents, but in the particular case of Mexico, it could be founded in the entire Pacific coast. Raw biomass is industrially employed for the production of fertilizers and alginic acid products [76]. In the case of *Acantrophora spicifera*, this red seaweed is widely distributed in tropical and subtropical oceans [117]. Finally, the green macroalgae *U. expansa*, also known as *U. fasciata*, have a worldwide distribution with a primary presence on the Pacific coast. Nowadays in many regions of the world control plans

are focused on avoiding the spread of these three types of seaweed because they are considered alien species in many ecosystems [118].

1.2.1.3 Modification of sorbent media

Marine macroalgae contain a noticeable amount of light-metal ions and salts pass to the liquid medium after the use of this biomass [79]. This chemical species are not toxic but inevitable become dissolved in the aqueous solutions during the biosorption process. The molecules include carbohydrates, proteins, and pigments. It is common to observe that water after biosorption becomes with a slightly brown or green color. Previous studies on *Sargassum* biomass revealed a Total Organic Carbon (TOC) around 24 mg L^{-1} in a fixed-bed column. Other values are as high as 55 mg mL^{-1}. The organic leaching could lead to secondary pollution that would retard the application of biosorption composites [119]. On the other hand, poor mechanical properties, especially for powder samples, require the necessity to modify the raw biomass for an extensive application in biosorption process. To face this problem, there are two main options: encapsulation (active or inactive entrapment) and surface modification [120]. Regarding the encapsulation, various supporting materials of organic and inorganic nature have been evaluated. Through this strategy, the leaching is reduced but, at the same time, the mass transfer would be reduced. The chemical modification approach could be less expensive than entrapment materials with no affections in the mass transfer [78].

1.2.1.4 Biosorption capacity of hydrocarbons

The biosorption capacity in this work is defined as the plot of the equilibrium concentration in aqueous media versus the hydrocarbon adsorbed in the biomass, biosorption data is obtained in batch runs with a fixed value of temperature, electrolytes, and pH [121]. The plot receives the name of biosorption isotherm. Data from biosorption isotherm constitute a valuable tool for predicting and comparing the biosorption efficiency of various biomass sorbents. A few reports regarding the

removal of hydrocarbons could be found in the literature. The primary results are presented in Table 1.7.

Table 1.7 Comparative summary of adsorption capacities achieved by a diverse of algae biomass and biosorbents in other studies.

Specimen	Pollutant	Biosorption Capacity $\mu g \cdot g^{-1}$	Initial Concentration mg/L	Reference
Sargassum sp.	Phenanthrene	430-460	1.00	[119]
Spirulina	Phenanthrene	4800	1.29	[119]
Brown algae	Phenanthrene	2300	1.29	[122]
Porphyra	Phenanthrene	9178	1.29	[122]
Rice bran	Benzene Toluene	520 690	ND	[9]
Horseradish pods	Benzene Toluene	620 830	ND	[9]
Activated carbon fiber cloth	Benzene	300-375	ND	[9]
Gran. active carbon bed	Toluene	163-267	ND	[9]
Activated carbon bed	Benzene	650	ND	[9]
Activated carbon	Toluene	260	ND	[9]

1.2.1.4.1 Main biosorption models

There are two-, three- and even four- parameter of empirical equations to correlate the biosorption isotherm data. The simpler two parameters models (Langmuir and Freundlich) are usually preferred. There is no strong reason to employ complex adsorption isotherm models because both equations well-fit most of the biosorption data. However, recent works have used three-parameter models such as the Redlich-Peterson and Sips models to describe the biosorption isotherm [79]. Sips adsorption isotherm equation could commonly offer a good fit because it was optimized for heterogeneous systems like most of the biosorbent constituents.

An extended description of biosorption models will be presented in the following chapters.

1.2.1.5 Factors affecting hydrocarbon biosorption

1.2.1.5.1 Ionic strength

The ionic content in the aqueous solution produced a significant effect in the sorption performance in aquatic media. In most of the cases, a lower biosorption capacity was registered at moderate to high ionic strength values (I > 0.6 M). This phenomenon is because the biosorption interaction included, but is not limited to sorbent – solvent, sorbent – container surface; salt – solvent, salt – solvent and salt – sorbate. The elevated concentration of ions in the solution is expected to interact more strongly with water molecules that the HC – water interaction, therefore, reducing the solubility of the aqueous solubility of HC and forcing the adsorbates to interact with other surfaces such as the biosorbent [119].

1.2.1.5.2 pH

Some of the robust evidence supporting a significant role of ionic interactions and repulsions come from studies of the pH effect. Previous reports on the biosorption of phenols and other weakly acidic compounds found that difference on the removal capacity was strictly related to the difference between the pH values and the pK_a value of the organic compounds. In the case of non-polar hydrocarbons like BTEX and naphthalene, the molecular form does not suffer changes in the whole range of pH, because dispersive and hydrophobic interactions are dominant [123].

1.2.1.5.3 Temperature

Temperature is also an important parameter influencing the biosorption process. Change in temperature alters thermodynamic parameters, resulting in a variation of the sorption capacity. The thermodynamic nature of adsorption could be exothermic or endothermic. In endothermic biosorption, an increase in the temperature produces

an increase in the uptake. Contrary, an increase in temperature hinders biosorption capacity in the case of exothermic sorption processes [124]. A previous study on the removal of phenanthrene onto *Sargassum* biomass an endothermic process was elucidated [119].

1.2.1.5.4 Agitation

A few studies incorporate the effect of speed of agitation in biosorption of HC. The relevant study of Chung [119] verified the increase of the kinetic constant (*k*) in concordance with the increase of the agitation rate. Regardless the revolutions per minute (rpm), the adsorption capacity in equilibrium remain almost the same.

1.2.1.5.5 Competition for adsorption sites

In past studies, the adsorption of phenol and pyrene registered competitive behavior in biomass but not in the case of activated carbon [9]. The relevant report of Rodriguez-Hernandez [125] on the equimolar competition of BTEX *in Macrocystis Pyrifera* biomass reported that the affinity followed the next order E > X > T > B in deionized water and dissolved organic matter solutions, showing an affinity for more hydrophobic compounds.

1.2.1.6 Biosorption kinetics

Biosorption kinetics shows the rate of solutes bonding on the surface of particular biomass. The description of the kinetic phenomenon is complicated due to many stages of happening the process. Kinetic studies provide relevant information about the possible mechanisms of biosorption that consists in (a) diffusion (bulk, external al intraparticle), and (b) the actual biosorption process [126]. In general, it is assumed that sorbate transport occurs in the following steps: (a) the first involves external diffusion of the adsorbate to bulk and the internal parts of the biosorbent; (b) the second step involves the transport of the sorbent from the solution to the solid phase. Numerous kinetic models are available to fit the kinetic data, which provides

information regarding the controlling step of the process and the probable binding mechanism [45]. In a vast number of biosorption studies founded in the literature, kinetic data was adjusted to kinetic models based in chemical reactions, especially pseudo-first and pseudo-second-order, (also known as Lagergren and Ho model, respectively). The primary assumption of these models is that the rate of biosorption is proportional to the number of free sites on the surface of the sorbent, depending on the power of the equation [127].

1.2.1.6.1 Empirical and diffusional models

Dynamic of the biosorption processes could also be evaluated by using diffusion models [128]. These models established that the step that limits the rate of biosorption is related to the diffusion of the molecules. [129]. The Weber-Morris intraparticle diffusion model is the most extensively reported correlation. Authors argued that its application is only suitable for the first stage of adsorption. Other models like Chrastil diffusive model allows the calculation of the kinetics in systems limited by diffusion, and the Reichenberg model permits the calculation of the phase that limits diffusion that takes place in the boundary film and the pores of the sorbent [130].

1.2.1.7 Biosorption mechanisms

Biosorption processes of nonpolar hydrocarbons include a combination of several mechanisms including mainly dispersive, hydrophobic, cation-π, and van der Waals attractions [125], which are briefly described in Table 1.8. In the case of dyes, chelating and ionic interchange binding should be considered [40]. Previous studies point out the role of certain salts (sodium, potassium, calcium, and magnesium) along the ion exchange interaction. The probable mechanisms could be hypothesized by the characterization of surface structure and functional groups by different methodologies like FT-IR (Fourier Transform Infra-Red), SEM (Scanning Electron Microscopy), Raman microscopy, XPS, potentiometric titration, among others [131].

Table 1.8 Possible seaweed components capable of interacting with aromatics.

Cellular component	Type of interactions	Observations	Reference
Proteins	NH − π	Primary amine, Van der Walls interactions	[132]
Ashes	Cation−π	Ca, Na and K ions produced by cellular lysis and dissolved organic matter	[133]
Lipids	Hydrophobic	Lipid fraction	[122]
Alginates	OH—π	—OH groups point to the aromatic ring.	[132]
Polysaccharides (Carrageennan, ulvans and fucoidans)	OH—π , CH_3−π	Active sites available by cellular lysis	[109]
Cellulose	Van der Walls interactions	CH_3− (metil); CH_3−O−R (metoxhy); (carbonyl) C=O; OH− (hydroxil)	[112]
Nonhydrolysable compounds	Hydrophobic	Long chain alkyls, waxes, lignin	[111]

1.2.1.8 Flow-through adsorption experiments

The most critical aspect of the scale-up of adsorption processes involves the determination of the effluent concentration profile as a function of throughput effluent (volume or time) [124]. This profile, commonly known as the breakthrough curve, represents the specific combination of equilibrium and rate factors than control process performance for a specific objective. The breakthrough curve can be obtained by passing through an adsorption column an inlet with the solute and registering the concentration of the outlet as a function of either volume of effluent or time [23]. The modeling of the shape of the breakthrough curve is very complex and include several models as Thomas, Bed Depth Service Time (BDST), among others, with the porpoise to obtain the necessary parameters for scale-up of adsorption systems [135]. A few studies have reported the use of different biosorbents for continuous adsorption of organic dyes. For that reason, more efforts

are necessary to assess the performance of biosorbents for extended HC applications.

1.2.2 Adsorption of hydrocarbons by composites of chitosan/graphene oxide composites

Graphene oxide (GO) has a sum of features to become a potential adsorbent such as remarkable mechanical properties, impermeability, electrical conductivity and a broad theoretical surface area [64]. However, one of the main limiting factors is the irreversibility of the graphene sheets aggregation due to the strong intermolecular van der Waals interactions, which can even reduce the surface to non-detectable values.

Chitosan (CS) is a natural polymer derivate from the deacetylation of chitin, and for that reason possess a large quantity of hydrophilic functional groups (amino and carboxylic groups). For the previous reason, this molecule is readily protonated. CS molecules have been extensively used as a binding agent for the synthesis of composites and immobilization of microorganisms. The recent available literature related synthesis of graphene oxide and chitosan composites has registered a relevant increment along the time. The primary fields interested in these materials are chemistry and medical development. The active sites of GO can interact with the CS polymer by hydrogen bonding and electrostatic interactions.

1.2.2.1 Methodologies for composite synthesis

Preparation of composites by chitosan is driven by amino features, which are obtained by the dissolution of CS in acidic media. GO-CS composites have demonstrated peculiar properties, which would be useful for practical application in many research fields [136]. The primary synthesis procedures contempt: (a) wet spinning and electrospinning for the production of fibers, (a) manufacture of hydrogels and aerogels and (c) formation of composites by in-situ polymerization and solution mixing. In the specific case of adsorption applications, the strategies above (in-situ polymerization and solution mixing) are the main reported synthesis procedures, and are described as follows [137]:

- Solution mixing: Is a process in which graphene and second component are mixed in a form that the second component is inserted in the graphene via a solvent. In a later stage, the composite is formed with a reducing agent. Li et al. [58], prepared a magnetic chitosan graphene oxide (MCGO) and employed ionic liquids to complete the synthesis procedures for the removal of Cr^{3-}.
- In-situ polymerization: In this methodology, graphene and monomers are mixed, and monomers aggregate between the layers of graphene by an initiator.

A summarized previous synthetized GO-CS composites for the removal of organic pollutants is presented in Table 1.9.

1.2.2.1.1 Optimization procedures

One of the primary goals of the adsorption studies is to find a suitable material with a high affinity for the adsorbate(s) of interest. In the case of CS-GO composites, many combinations could be added from the precursors for the synthesis of the final material. When a study involves a large number of variables, it is useful to identify the optimal combination of factors and interactions among factors that would bring close to the goal [138]. The defined goal is achievable by using statistical-based multivariate design methods such as factorial design and response surface methodology (RSM), which reduces the number of experiments, cost, and the time consumption, needed for the research and provides an appropriate model for process optimization [139]. The first step is to identify the primary variables (factors) involved and their impact on the result (response). This step could be defined by a factorial design procedure which would define the variables and interactions with higher significance in the process. In the following step, a maximum or minimum in the response could be founded by RSM methodologies [140]. A valuable activity before any procedure is to perform previous tests to verify the interval of interest of the variables that would generate the desired response. The development of optimization procedures is well described in the literature [138,141]. Previous reports performed these methodologies for the synthesis of composites and evaluation of removal capacities [139,142].

Table 1.9 Selected reports for the synthesis of GO-CS composites.

Target pollutant	Graphene synthesis	Crosslinking agent	Composite shape	Particular analysis	Chitosan properties	Reference
Only characterization	Hummers	Tetraethylorthosilicate (TEOS)	Film	FT-IR, XRD, EDS, TGA, SEM, mechanical strength	DD: 75 – 85 MW: low	[92]
Methyl violet Alizarin yellow	Hummers	glutaraldehyde	Film / magnetite	FT-IR, XRD, EDS, TGA, SEM, temperature	DD: 78	[143]
Methylene blue Methyl orange Cr (VI)	Hummers	dimethylformamide	Film	FTIR, XPS. SEM, titration, pH effect, recycle	DD:96 MW: 6.36 X 10^5	[144]
Acid red GR redX-5GN	Hummers	glutaraldehyde	Film / Drop	FTIR, XRD. SEM, titration, pH effect, kinetics	ND	[66]
Methylene blue	Hummers	None	Drop / Magnetite	BET, FT-IR, XRD	DD:96 MW: 6.36 X 10^5	[145]

DD: Deacetylation dergree (%);
MW: Molecular weight (Da);
ND: No data presented

1.2.2.2 Determination of physicochemical properties

Chitosan biopolymer has been combined with GO sheets with a significant difference on methodological procedures and intrinsic properties (e.g., molecular weight, concentration and GO/CS synthesis ratio). Examples are detailed in Table 1.9. The viscosity of CS solutions is a function of the molecular weight and determine the binding performance with GO sheets. On the other hand, the increase of the deacetylation degree is correlated with its biodegradability. In the case of electrospinning procedure, structural conditions are limited regarding the factors above (e.g., concentration, molecular weight and degree of acetylation), behind an absolute limit, a crosslinker is necessary to maintain structural integrity [93]. As would be shown in chapter 5, the molecular weight of chitosan determines its diffusivity into the GO sheets registering a hindering effect as the molecular weight increases.

On the other hand, different chemical modifications could be realized on GO sheets such as oxidations, reductions, use of polymers, cationic surfactants, alkylamines or silylating reagents. More research efforts would be needed to assess the effect of physicochemical modifications in the structural properties of the final composites.

1.2.2.3 Binding mechanisms

Studies related to the adsorption of organic pollutants by graphene oxide establish the existence of defects, edges and groove areas with high energetic sites. Aromatic molecules would tend to interact with these high energetic sites in conjunction with flat surfaces [146]. Additionally, the hydrophobic effect in the case of HC should be considered. The textural properties of graphene may be modified with the introduction of chitosan molecules, which probably create a higher presence of surface crumples and grooves with a high adsorption energy sites. In the case of chitosan, hydroxyl groups could generate van der Waals interactions, particularly in the C–3 position, between chitosan chains and aromatic molecules. Remaining carboxylic groups could also be involved. In the case of anionic and cationic colorants, electrostatic interactions and hydrogen bonding should also be considered between the oxygenated groups of graphene oxide and chitosan, and the substituents groups within dyes structure.

a)

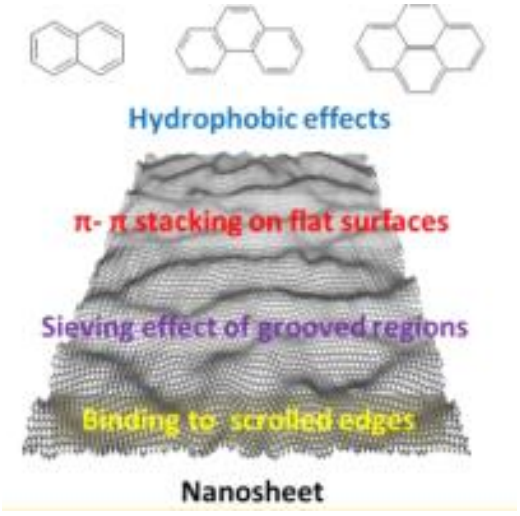

b)

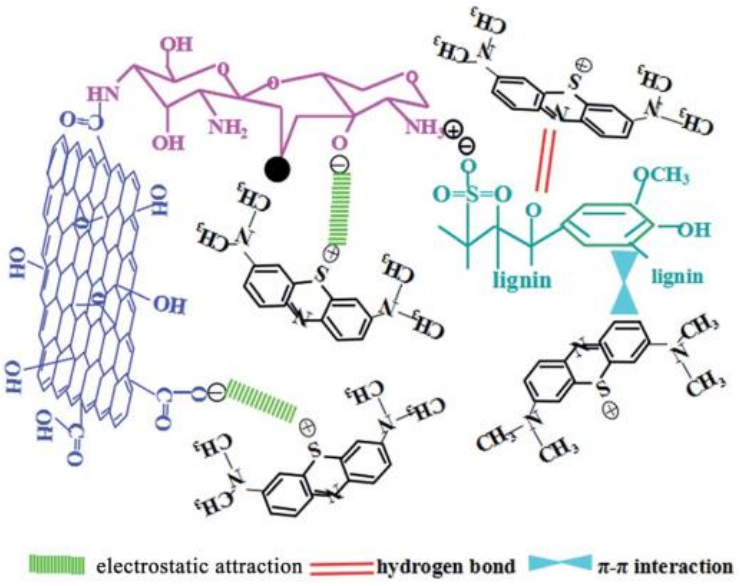

Fig. 1.6 a) Adsorption mechanisms between nonpolar hydrocarbons and GO sheets, b) Adsorption interactions between GO-CS composite and an azo-dye. Adapted from[146,147].

1.2.2.4 Main characterization procedures

The physicochemical characterization of GO-based composites share the same conventional carbon and oxygen spectroscopic analyses The most regular procedures to identify GO-CS matrix involves [148–150] :

- FT-IR. It is common to evaluate signals related to hydroxyl (OH), epoxy (C-O-C) and ketone (C=O) groups. The vibrational frequencies for the stretching 3400 cm^{-1}, 1090 cm^{-1} and a doublet at 1700 cm^{-1}, respectively. The spectrum of CS show two characteristics at 1651 and 1596 cm^{-1}, corresponding to the C=O stretching of –NHCO-, and the –NH- bending of -NH_2, respectively.
- Raman. The spectra of GO consists of two broaden peaks which correspond to the G and D band. The first band around 1580 cm^{-1} is attributed to the ordered crystal structure while D band (approx. 1350 cm^{-1}) is assigned to the disordered structure. The DD band is characteristic of chitosan corresponds

to 2θ = 10.7 ° and 20.3°, usually attributed to the anhydrous crystals (Forms I and II), respectively

- UV-Vis. The characteristic spectra for GO shown an adsorption signal of 190-900 nm. The maximum absorbance is found around λ = 230 nm attributed to $\pi \rightarrow \pi^*$ vibrations.
- XRD. X-ray diffraction shows an only peak around 11°. The peak corresponds to the interlayer distance depending on the GO solvent type. Chitosan reports crystalline reflections in the 2θ from 10 to 80°.
- SEM/TEM. The morphology of GO appears like packed layers with a corrugated surface. TEM is often employed to visualize the number of layers.
- AFM. This technique can visualize the thickness and lateral size of a sample.
- Thermogravimetric Analysis (TGA). GO mass loss starts at a temperature of around 60 °C. A loss of around 60 % of the total weight is usually registered at values up to 300 °C.
- Differential Scanning Calorimetric (DSC). The primary signal of GO appears over 200 °C corresponding to an enthalpy value of 1600 J g^{-1}.

1.2.2.5 Comparison of utilized isotherms

Isotherms can describe how the adsorbate interact with a particular adsorbent. Linear isotherms are not conventional in adsorption of hydrocarbons on GO-CS composites but are the initial section of isotherms for homogeneous surfaces [60]. Langmuir and Freundlich represented the most selected adsorption isotherm equation for adsorption data. As a general characteristic for GO-CS composites, a very sharp initial rise is followed by a plateau [92,96,144,145,147]. For that reason, three-parameter models like Sips would represent a good model to fit the adsorption data of GO-Cs sheets, because it combines both Langmuir and Freundlich characteristics [151].

1.2.2.6 Adsorption kinetics

For almost all the studies, three conventional kinetics models were only considered pseudo-first-order, pseudo-second-order, and intraparticle diffusion models. A particular high adsorption rate of adsorption is registered in the initial adsorption time for the majority of systems [152]. As a summary, most of the systems registered the presence of three stages of adsorption: (a) external surface adsorption, (b) intraparticle diffusion as the rate-limiting stage, and (c) adsorption phenomenon. Furthermore, a more significant part of reports showed that the chemical adsorption was the rate-limiting step as a result of a better adjust of the kinetic data to the pseudo-second-order kinetic model [153,154].

1.2.2.7 Adsorption thermodynamics

Based on the literature review, thermodynamic parameter included Gibbs free energy change ($\Delta G°$), enthalpy change ($\Delta H°$), and entropy ($\Delta S°$) as follows:

$$K_c = \frac{q_e}{C_e} \qquad \text{(Eq. 1)}$$

$$\Delta G° = -RT ln K_c \qquad \text{(Eq. 2)}$$

$$ln K_c = \frac{\Delta S°}{R} - \frac{\Delta H°}{RT} \qquad \text{(Eq.3)}$$

Where R (8.3145 J mol^{-1} K^{-1}) is the ideal gas constant, T (K) is the absolute temperature, and K_c is the thermodynamic equilibrium constant. The values are calculated from the slope and the intercept of the Van´t Hoff linear plots of *log* K_c vs. *1/T*.

As a summary, negative values of $\Delta G°$ confirmed the natural character of adsorption. With an increase in temperature, an increase of $\Delta G°$ is registered, thereby the adsorption capacity with temperature rises. The positive values of $\Delta H°$ defined an endothermic process. Finally, positive values of $\Delta S°$ refers to an increment in the randomness of the system [153,155].

1.2.2.8 Adsorption mechanisms

1.2.2.8.1 Van der Waals and hydrophobic interactions

The London dispersion component of Van der Waals does not consist in the polarity of the molecules rather than the polarizability of the outer electrons of the adsorbate molecule. In this sense, higher forces of attraction are expected from molecules or surfaces with a less capability to share electrons, like those from iodine or bromide ion, or molecules with aromatic rings. –OH and $–NH_2$. Since GO and hydrocarbon present an hydrophobic character, and nonpolar adsorbates are in the same molecular state along experimental conditions, is convenient to suggest van der Waals forces an essential mechanism of interaction [9].

Hydrophobic forces consider the self-association of molecules with an in intrinsic hydrophobic nature (like carbon base materials). The energy of interaction is higher than hydrogen bonds [52].

1.2.2.8.2 π-π interactions

This type of interactions is commonly referred to in the adsorption of organic molecules by carbon-based materials. Consist in the overlapping of the electron density of the aromaticity of GO sheets, and the aromatic rings of adsorbate molecules. An increase of the strength of π-π interactions by the presence of primary sites is well-documented. The interaction could have a “Y” or “T” shape, depending on the orientation of the electron density and the surface or the counterpart.

1.2.2.9 Recyclability of the biomaterials

The use of graphene nanomaterials has shown promising results for the adsorption of hydrocarbon molecules. Limited information is available for the reusability cycles and desorption mechanisms. Previous studies confirmed a reuse rate of 5 times without losses in the removal capacity for dyes and BTEX [156–158]. Moreover, in the case of GO-CS composites, a magnetic β-cyclodextrin-chitosan/graphene oxide material (MCCG) and a magnetic-cellulose graphene oxide composite reported a

lifetime of 5 cycles for the removal of dyes at a concentration of 30 mg L^{-1} with a washing process with ethanol and NaOH [147,159]. A reusability rate of five times was also confirmed for a GO-CS composite for various dyes and heavy metals, with a slight loss of 10% in the affinity for the target pollutants [144].

1.3 GENERAL OBJECTIVE

The purpose of this research is to analyze the biosorption capacity and mechanisms involved in the main soluble-water hydrocarbons (benzene, toluene, and naphthalene) on different types of bio-based adsorbents.
Also, this research focuses on developing and easy method for the synthesis of pillared graphene oxide to generate an adsorbent with high affinity toward the same pollutants.

1.4 SPECIFIC OBJECTIVES

To determine the physicochemical characteristics of three seaweed biosorbents by acid-base titrations, FT-IR analysis, surface area, fiber and proximal content.

To elucidate the biosorption mechanisms involved in the biosorption of water-soluble hydrocarbons at different ionic strength, and pH media.

To determine the production conditions to synthesized a microalgae-based biocomposite for the removal of water-soluble hydrocarbons.

To perform batch biosorption experiments evaluating the effect of pH, ionic strength and dissolves organic matter to analyze the adsorption mechanisms.

To determine the pillared effect of chitosan into graphene oxide to increase the surface area of GO sheets.

To evaluate the batch affinity of a GO-CS composite toward benzene, toluene, and naphthalene y in different adsorption systems.

To study the dynamic adsorption behavior of BTEX and naphthalene by a microalgae-based biocomposite at equimolar conditions and different inlet flows.

1.5 HYPOTHESIS

The biosorption mechanism of benzene, toluene, and naphthalene on macroalgae-based materials will be based on hydrophobic interactions with lignocellulosic fractions and in less degree by London/ van der Waals bonding with oxygen-containing sites of the biosorbents constituents.

The pillared effect of chitosan onto graphene oxide would increase the available surface area, and at the same time, the affinity for the pollutants above.

CHAPTER 2

Biosorption removal of benzene and toluene by three dried macroalgae at different ionic strength and temperatures.

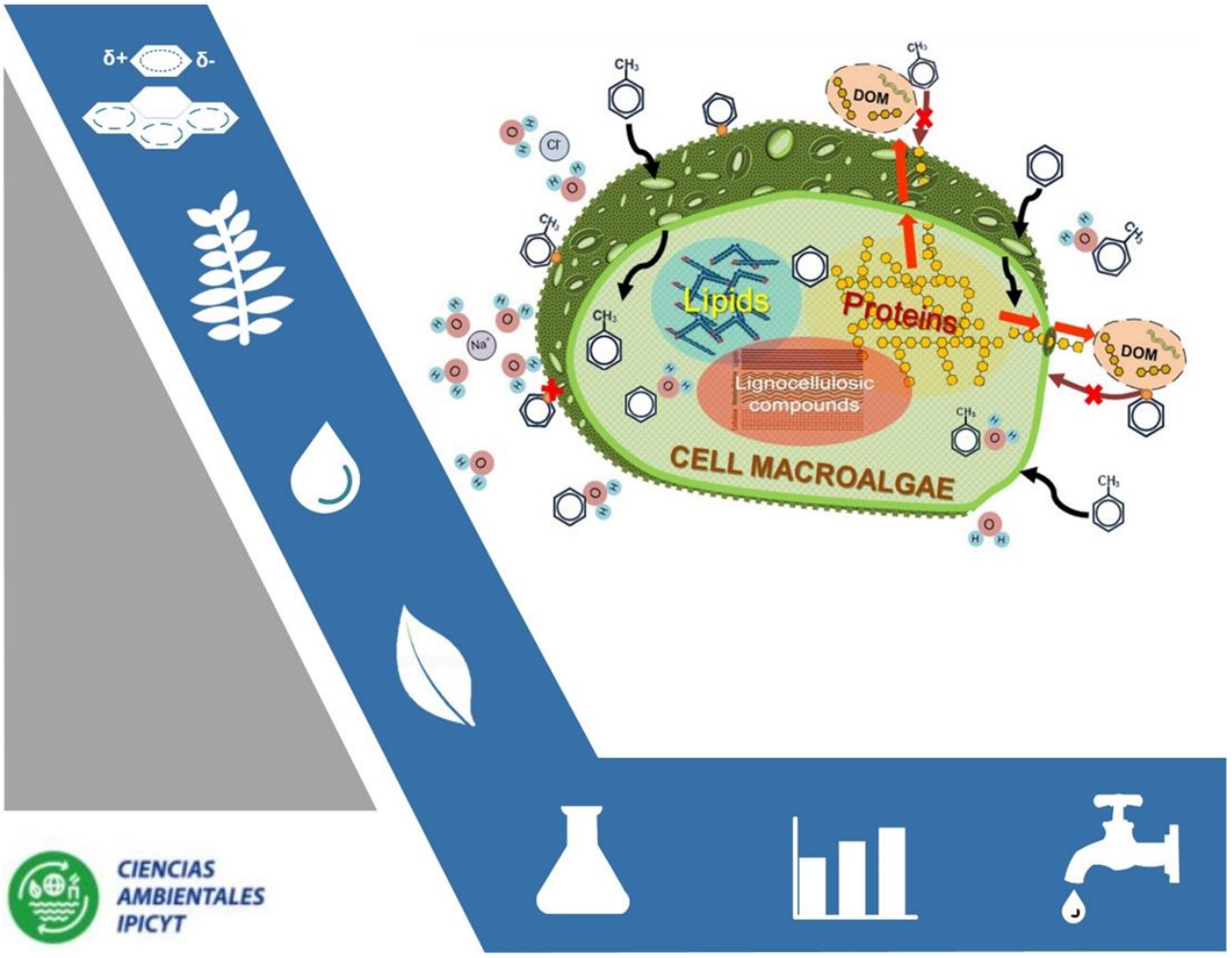

This chapter is adapted from: *Biosorption removal of benzene and toluene by three-dried macroalgae at different ionic strength and temperatures: Algae biochemical composition and kinetics*, 2016, 193, 126-135

2.1 Abstract

The release of low−molecular aromatic hydrocarbons (HC) into natural waters brings severe consequences to our environment. Unfortunately, insufficient information is available regarding the treatment of these pollutants. This work evaluated the use of brown, green and red macroalgae biomass as biosorbents of benzene and toluene, two of the most soluble HC. Raw seaweed biomasses were wholly characterized, then evaluated under different temperatures and ionic strengths to assess their potential as biosorbents and to elucidate the biosorption mechanisms involved. Brown macroalgae registered the highest removal capacities for benzene and toluene (112 and 28 $mg \cdot g^{-1}$, respectively), and these were not affected at ionic strength < 0.6 M. Langmuir and Sips isotherm equations well-described biosorption data, and the pseudo-second-order model provided the best fit to the kinetics rate. Hydrocarbons are adsorbed onto the diverse chemical components of the cell wall by London forces and hydrophobic interactions.

2.2 Introduction

Water pollution by oil spills is a severe problem in petrochemical activities, with a total volume of oil lost to the environment in 2015 of approximately 7,000 tonnes [19]. It has been calculated that around 1 to 3% (sometimes up to 15%) of crude oil can pass into the dissolved state [160], although low molecular aromatic compounds like benzene and toluene, present higher water solubilities and bioavailabilities than other petroleum hydrocarbon components and, as a consequence, have been classified as a risk to the environment [161]. In−situ removal of these pollutants by adsorption onto activated carbon has been considered a more suitable technology than aeration or photocatalysis, mainly due to the hydrophobic nature of the adsorbent, its high surface area and high affinity to a broad type of pollutants [124]. However, the advantages of activated carbon could be restricted for remediation purposes because it has been associated with secondary ecotoxicological effects in sediments [162]. Another viable option is the usage of macroalgae utilized as biosorption matrix, a process that constitutes a low cost and environmentally friendly

alternative for the removal of the dissolved fractions of petroleum [9]. Biosorption involves the passive binding to metabolic inactive materials derived from, i.e., industrial or agricultural by-products, forestry, marine or terrestrial biological materials and microbe biomass [76,163,164]. For the particular case of macroalgae biomass, it is widely available (15.8 million tons harvested in 2010), occurs in a wide variety of habitats (ranging from marine to freshwater), and contains different active sites in its cell structures that are accessible for organic biosorption, i.e. hydroxyl, carboxyl and amine [83,165].

There are three types of macroalgae: red, green and brown [108], but all have cell walls that are complex networks of biopolymers consisting in a skeleton of crystalline and fibrous parts (cellulose, hemicellulose, etc.) and an embedding matrix of specific polysaccharides, proteoglycans and others molecular components that depend on the type of seaweed. Red algae possess sulfated galactans (i.e., carrageenan), and xylan or mannan fibrils (also presented in green algae), which also include mixed glucan or ulvan linkages. Brown algae are comprised mainly of sulfated fucans and alginates [109].

Seaweeds, especially brown algae, have been effectively used as biosorbents for heavy metals [108], dyes [9] and polyaromatic hydrocarbons [119]. Preliminary studies have shown that seaweed biomass can be successfully used to remove many organic pollutants like phenanthrene, phenol, and nonylphenol [119,166]. Unfortunately, the number of studies on water−soluble hydrocarbon fraction is low, with a knowledge gap relative to the ionic strength and temperature effects on benzene and toluene removal. The potential of this technology can be further improved by evaluating the biomass removal capacity for the most water−soluble hydrocarbons (benzene and toluene) under controlled laboratory conditions to increase our knowledge of its use for remediation purposes.

The primary objective of this work was to investigate the influence of ionic strength on the benzene and toluene biosorption capacity of three different types (brown, green and red) of macroalgae biomass. The studies were also conducted at 4 and 25 °C to simulate temperature variations that could be registered along the water column in oil-contaminated waters [167]. Additionally, the chemical and physical

characterization of algae was conducted to provide insights into the hydrocarbons biosorption mechanisms. All samples were thoroughly dehydrated, milled and mixed to avoid any metabolic bioactivity and to assure homogeneous determinations.

2.3 Biosorbents and reagents

Samples of the macroalgae *Macrocystis pyrifera*, *Ulva expansa*, and *Acanthrophura spicifera* (brown, green and red seaweed, respectively) were collected in La Paz, Baja California Sur, Mexico and Ensenada, Baja California, Mexico. The seaweed samples were rinsed with plenty of deionized water (< 11 µS/cm) and dried in an oven at 50 °C during 72 h. Algae biomass was sieved to a particle size of 0.8 – 1 mm with a Mini-Cutting Mill (Thomas Wiley) before used in characterization and sorption experiments. The model soluble HC were represented by benzene and toluene (Sigma−Aldrich, 99% purity).

The adsorption capacities of the inert biomass were determined in different ionic strength solutions: (1) deionized water as control; (2) NaCl solutions with concentrations from 0.3 – 0.75 M; and (3) artificial seawater solution Instant Ocean® (33 g L^{-1}) ≃0.76 M.

2.4 Physical characterization

Surface area ($m^2 \cdot g^{-1}$) and pore size distribution of the macroalgae were calculated by BET isotherms and DFT (Density Functional Theory), respectively, using a Micromeritics ASAP 2020 instrument at 77 K [168].

Proton binding curves and the point of zero charges (pH_{PZC}) were determined by potentiometric titrations (Mettler Toledo model T50) following the established protocol by [62]. A series of 0.1 g biomass samples were placed in 50 mL NaCl solutions with different ionic strengths (I = 0.01, 0.15, 0.3 and 0.45 M). The system

was allowed to equilibrate for 16 h, and then the experiment initiated. The pH solution was adjusted to pH three by adding 0.1 N HCl.

During the titration, the solution was continuously stirred in the N_2 atmosphere to avoid the interference of CO_2. NaOH standard (0.1 N) was used as titrant. The titration curves consisted of about 50–70 experimental points between pH values of 3 to 11 because of the buffering effect of water at pH < 2 and > 12 [169]. The resulting titration curves were transformed into proton binding curves Q (pH) using the numerical procedure SAIEUS (Solution of the Adsorption Integral Equation Using Splines) which indicates the total amount of protonated sites [170]. Raw biomass was ground with KBr pellets and studied by a Thermo Nicolet 6700 in transmittance mode in the range of 600 − 4000 cm^{-1}, with a four cm^{-1} resolution and 64 scans. The ash content of samples was determined by a TGA−Thermo Cahn thermo−gravimetric analyzer under an air flow rate of 2 mL· min^{-1}, at a heating rate of 5 °C· min^{-1}, up to a final temperature of 900 °C. The degree of swelling (S_w) was determined in triplicate runs by weighing a precise mass of 0.5 g of dry biocomposites which was placed in a beaker at 25 °C with 20 mL of distilled water. The swollen materials were removed from the water and weighted (W_t) after 24 h. The S_w value was computed by the following equation: $S_w = ((W_t – W_o) / W_o)*100$, where, W_o is the mass weight of the dry biomass (t = 0), and W_t is the weight of the swollen material at time t.

2.5 Chemical characterization

An extensive chemical analysis of algae was made to characterize the main molecular structures associated with the HC biosorption. The total nitrogen content in crude protein was determined by the Kjeldahl method [171], using a conversion factor of 6.25 to calculate protein content [172]; crude fat and total sugars were estimated through the fatty acid hydrolysis and by the Fehling – Soxhlet extraction procedure [172,173]. Cellulose, hemicellulose, and lignin were determined by a semiautomatic fiber analyzer (ANKOM Technology, Macedon, NY, USA), which is

based on the use of a neutral and acid detergent methodology reported by Van Soest et al. (1991) [174]. Alginate extraction was carried out using the sequence of ion−exchange reactions proposed by [175]. Sulfated polysaccharides constitute an essential fraction of algal biomass. It was for this reason that the main sulfated polysaccharide (fucans) present in brown algae were characterized according to [138]. The biomass soluble fraction was estimated using a TOC−meter (Shimadzu Co. Model TOC−VCSN), conducted by placing 0.1 g of dry macroalgae in contact with deionized water during 48 h and then filtering it through a 0.22 µm pore size filter. The concentration of inorganic elements in the biomass structure was determined through acid digestion of the ashes (previously obtained by 5 g of biomass in a muffle at 550 °C) during three h using ten mL of a 1:1 (v v^{-1}) mixture HNO_3 and HSO_4 solution. The concentrations of Zn, Ca, Fe, K, Cu, Cr, Ni, Mn, Mg, and Na were determined by inductively coupled plasma−optical emission spectroscopy (ICP−OES) by a Varian 730−ES spectrophotometer.

2.6 Uptake experiments

The benzene and toluene capacity of the raw biomass was determined in deionized water and saline solutions of different concentrations [176,177], including the maximum solubility of each compound (Table 2.1). The salting coefficients κ_s of the hydrocarbons were calculated according to the Setchenov equation $log(S_o/S) = \kappa_s C$, where S_0 is related to the solubility of benzene and toluene in water, and is equal to 1800 and 515 mg L^{-1}, respectively [178].

An amount of 0.1 g of each biosorbent was added to 35 mL of an aqueous solution that contained different concentrations (non-competitive) of the organic compound. All experiments were performed at least in duplicate. Amber glass flasks with Teflon taps were used leaving no headspace to avoid volatilization. Once sealed, the flasks were placed in a shaker set at 120−130 rev min^{-1} for 48 h at 25 °C. The initial and equilibrium concentrations of the adsorbates were determined by an UV−Vis (Thermo Aquamate) spectrometer set at a wavelength of 254.5 and 261 nm for benzene and toluene, respectively. At least five blanks with the same amount of

biomass (no HC added) were run simultaneously as controls to correct the final HC concentration for the desorbed organic matter in solution. Hence, the final HC concentration was calculated by subtracting the average value of the blank samples to the value of the equilibrium hydrocarbon concentration in batch systems. The amount of HC uptake q_e (mg g^{-1}), was calculated by the following mass balance equation:

$$q_e = \frac{V}{m}(C_0 - C_e) \qquad \text{(Eq. 2.1)}$$

Where C_0 and C_e are the initial and equilibrium concentrations (mg L^{-1}), V is the volume of the solution (L), and m is the mass of the adsorbent (g). Experimental values were fitted to Freundlich, Langmuir, and Sips adsorption isotherm equations to determine the extent of uptake in the adsorption process. The Langmuir model [179] has the following form:

$$q_e = \frac{q_{max} b C_e}{1 + b C_e} \qquad \text{(Eq. 2.2)}$$

where C_e (mg·L^{-1}) is the residual (equilibrium) concentration in the liquid, q_e (mg·g^{-1}) is the amount of hydrocarbon adsorbed in the solid phase, q_{max} is the maximum monolayer cover capacity (mg·g^{-1}), and b is the Langmuir isotherm constant (L·mg^{-1}).

The Freundlich model is represented by the following equation [180]:

$$q_e = K_F {C_e}^{1/n} \qquad \text{(Eq. 2.3)}$$

where K_F is the Freundlich isotherm constant ($mg^{1-(1/n)}$ $L^{1/n}$ g^{-1}), which is related to adsorption capacity of HC and n is an equilibrium constant related to the adsorption affinity of the binding sites for the pollutants.

The Sips model can fit data by both Langmuir and Freundlich type sorption effects and has three parameters: b, q_{max} and $1/n$ [151] and is included next:

$$q = \frac{b q_{max} C_e^{1/n}}{1 + b C_e^{1/n}} \qquad \text{(Eq. 2.4)}$$

Computations were made by using the STATISTICA software, and the parameters estimation was achieved using a nonlinear estimation method (Rosenbrook and quasi−Newton). The best−fit correlation model was selected verifying the best

regression correlation coefficient (R^2) and the least sum square error (SSE) based on the following equation:

$$\sum_{i=1}^{n}\left(q_{e,calc} - q_{e,meas}\right)_i^2 \qquad \text{(Eq. 2.5)}$$

Where $q_{e,calc,}$ and $q_{e,means}$ are the calculated and measured sorption capacities at equilibrium (mg g^{-1}), respectively.

Temperature effect on sorption and desorption experiments

The effect of temperature on the benzene and toluene biosorption capacity was studied at 4 and 25 °C in under different ionic strength solutions (*I*= 0.3, 0.45, 0.6, 0.75), as well as with a synthetic seawater solution (≃ 0.76 M). The hydrocarbon biosorption capacities of these experiments were calculated using equation (1). Desorption experiments were also conducted using hydrocarbon−loaded adsorbents which were filtered, rinsed with three mL deionized water to remove contaminant excess and subsequently immersed into 35 mL of a solution with the same ionic strength and temperatures at which the biosorption experiments were conducted. Next, the system was stirred at 120 rpm for 48 h and the benzene and toluene leached were determined by UV−Vis spectrophotometry, as already explained in section 2.6.

Table 2.1 Maximum concentration of hydrocarbons used in the biosorption experiments.

	Maximum solubility [mg/L]					
Solvent	D.I. H_2O[1]	NaCl 0.3 M	NaCl 0.45 M	NaCl 0.6 M	NaCl 0.75 M	Instant Ocean[2]
Benzene	1800	1573	1470	1375	1285	1391
Toluene	515	445	414	385	358	379

[1] Deionized water
[2] Instant Ocean solution (33 g·L^{-1}) ≃ 0.76 M

Biosorption kinetic experiments

To elucidate the potential rate-limiting steps of biosorption, kinetics studies were carried out using 0.1 g of the biosorbent which was placed in contact with the initial benzene and toluene concentrations in deionized water solutions as indicated in Table 2.1. A total of 15 bottles were prepared for benzene and toluene solutions respectively, which were kept at a constant temperature of 25 ºC and stirred at 120−130 rev/min. At pre-set time intervals, a sample was collected to determine the concentrations of benzene and toluene. The constant rates of adsorption were determined by the pseudo−first, pseudo−second, and intra−particle diffusion equations. The *pseudo−first−order kinetic equation* is given by:

$$ln(q_e - q_t) = ln(q_e - k_1)t \qquad \text{(Eq. 2.6)}$$

Where q_t and q_e are the adsorption capacities at time t (h) and equilibrium, respectively, and k_1 (h^{-1}) is the pseudo-first order rate constant calculated from the slope obtained by plotting $ln\ (q_e - q_t)$ vs $.t$.

The pseudo−second−order−kinetic equation can be represented by:

$$\frac{t}{q_t} = \frac{1}{k_2 q_e^2} + \frac{1}{q_e}t \qquad \text{(Eq. 2.7)}$$

Where k_2 is the pseudo−second order rate constant of sorption ($mg \cdot g^{-1}\ h^{-1}$), q_e is the amount of pollutant adsorbed at equilibrium ($mg^{-1}\ g^{-1}$), and q_t is the amount of pollutant adsorbed at any time t ($mg^{-1} \cdot g^{-1}$). The *intraparticle diffusion equation* describes the influence of diffusion on the solute uptake mechanism by a linear plot of the form:

$$q_e = k_3 t^{1/2} + C \qquad \text{(Eq. 2.8)}$$

Where k_3 ($mg \cdot g^{-1} \cdot h^{1/2}$) is the intraparticle diffusion rate constant, and C is the intercept of equation (8).

2.7 Characterization analysis

The chemical composition of the biomaterials is affected by seasonal, temporal and spatial variations of environmental factors like water temperature, salinity, light, and nutrients availability [173]. This study reveals that carbohydrates represent the main structural component of the macroalgae biomass reported herein (15.9, 16.02 and 11.8% for the brown, green and red macroalgae, respectively, Table 2.2), followed by hemicellulose (13.57, 9.30 % in the green and red macroalgae samples). The protein content in brown seaweeds was the second highest component with 13.4 %, whereas a lower content was measured in green and red seaweeds (2.8−7.1 % dry weight). These results are comparable with those reported in the literature and compiled in Table 2.3.

Table 2.2 Chemical composition of the seaweeds used in the experiments (% dry weight).

	Macrocystis pyrifera (brown)	*Ulva expansa* (green)	*Acanthophora spicifera* (red)
Total carbohydrates	15.9	16.02	11.8
Proteins	13.4	7.1	2.8
Lipids	0.5	0.44	0.40
Hemicellulose	5.56	13.57	9.30
Cellulose	1.44	1.85	1.30
Lignin	9.67	8.53	7.99
Alginates	9.1	2.4	1.8
Fucans	2.66	ND	ND

ND= Not determined.

Table 2.3 Proximate comparative results from the biosorbents of study.

Sample	Carbohydrates	Lipids	Proteins	Reference
Macrocystis pyrifera	22.3	ND	0.21	[76]
	ND	3.02	7.17	[113]
	15.9	0.5	13.4	This study
Ulva expansa	ND	0.5	14.7	[113]
	16.02	0.44	7.1	This study
Acanthophora spicifera	30	2.7	7.49	[115]
	11.8	0.4	2.8	This study

ND Not determined

The total carbohydrate sources differ according to the species. The typical constituents of the brown algae are integrated by cellulose fibrils and two main types of matrix polysaccharides: alginates and fucans. In the case of *Ulva expansa* (green algae), there are three main polysaccharide constituents: amorphous cellulose, polysaccharides containing sulfated groups (mainly ulvans) and starch. Finally, red macroalgae possess cellulose, mannan or xylan fibrils and sulfated galactans (agars and carrageenans) as their principal constituents [109]. Data on cellulose, hemicellulose, and lignin show considerable variation in content in the three seaweeds, which are probably related to environmental conditions affecting macroalgae growth [173]. No comparative data were available in the literature for *A. spicifera*; however, the absence of lignin for some species of brown algae was previously reported [181]. Lignin, one of the most relevant fractions, is an amorphous heteropolymer composed mainly by phenolic propylbenzene skeletal units that exhibit an aromatic nature especially suitable for the removal of aromatic hydrocarbons. This hydrophobic character is shared with hardly hydrolyzable polymers like cellulose and hemicellulose [182]. Because of the complexity of most macroalgae biopolymers, it is very probable that several interactions can passively take place in the system between HC and active sites at the same time.

Textural properties of the biosorbents

The BET surface area of all the biosorbentes was less than 0.3 $m^2 \cdot g^{-1}$ with a considerable percentage (> 85 %) associated with micropores and mesopores. Similar values of 0.2 and 0.3 $m^2\ g^{-1}$ were obtained earlier [76] for *M. pyrifera* and *U. pinnatifida*. The extent of the biosorption capacity of our biosorbents could be limited by the narrow micropores volumes (Table 2.4), which may produce diffusional restrictions due to the small cross-section area of the adsorbates (25.3 and 28.5 $Å^2$ for benzene and toluene, respectively) plus the solvation shell hydration complex [183].

Table 2.4 Textural properties of the biosorbents.

	A_{BET} ($m^2 \cdot g^{-1}$)	$A^{\dagger}_{micro}{}^{1}$ ($m^2 \cdot g^{-1}$)	$A_{meso}{}^{2}$ ($m^2 \cdot g^{-1}$)	$A_{macro}{}^{3}$ ($m^2 \cdot g^{-1}$)	$V^{\ddagger}_{micro}$ ($cm^3 \cdot g^{-1}$)	V_{meso} ($cm^3 \cdot g^{-1}$)	V_{macro} ($cm^3 \cdot g^{-1}$)
Macrocystis pyrifera	0.126	0.030	0.020	4.7×10^{-3}	2.1×10^{-5}	1.7×10^{-4}	2.7×10^{-4}
Ulva expansa	0.169	0.049	0.033	0.020	1.1×10^{-5}	3.1×10^{-4}	6.4×10^{-4}
Acanthrophora spicifera	0.212	0.055	0.042	0.019	2.3×10^{-5}	4.9×10^{-4}	9.3×10^{-4}

$A^{\dagger}$ = Surface area.
$V^{\ddagger}$ = Pore volume.
[1,2,3] micro−, meso−, and macropores, respectively.

FT-IR analysis

An indirect chemical determination of the different biopolymers constituting the cell wall of macroalgae was conducted with FT−IR spectroscopy, and potentiometric titrations techniques (Table 2.5) showed that the significant bands identified by FT−IR were between 4000 cm^{-1} and 500 cm^{-1}. The FT−IR analysis also showed, in all the spectra, broad bands at 3800−3000 cm^{-1} that correspond to hydroxyl (−OH) and amine (−NH) groups which can be associated to different polysaccharides and amino acids, respectively. The bands found in the interval 2848 – 2855 cm^{-1} could be attributed to aliphatic chains of lipids [122], whereas the band 2908 − 2915 cm^{-1} can be assigned to hydrocarbon (−CH) stretches. The bands at 1638, 1645 and 1648

cm^{-1} could correspond to antisymmetric carboxylate groups ($-RCOO^-$) associated with alginate carboxylate but are also related to the presence of primary amides in amino acids. Polysaccharides of the biomass were identified by the C−O−C group found between 1145 and 1160 cm^{-1}. Finally, sulfated polysaccharides and amino acids were also observed at the broadband located between 1155 and 980 cm^{-1} [184].

Table 2.5 FTIR characteristic bands of the macroalgae Macrocystis pyrifera (brown), Ulva expansa (green) and *Acanthophura spicifera* (red). Symbols: α, stretching; β, bending.

Brown	Green	Red	Vibration assignment	Possible source
3800 – 3000			(α) H−O; (α) N−H	Sugars and amino acids
2915	2908	2913	(α) C−H (sp^3)	Mainly sugars
2848	2855	2849	(β) C−H	Aliphatic chains; Lipids
1638	1645	1648	(β) N−H; (α) CO_2 antisymmetric	amino acid side chains; alginate and proteins
1407	1417	1410	(α) CO_2 symmetric; (β) O–H	Alginate and aminoacids; cellulose
		1367	(α) O=S=O antisymmetric in sulfonate	Fucans
1338	1340		(α) COH	Mainly sugars
1244		1248	(α) C−H	Mainly sugars; Hemicellulose
1155	1145	1148	(α) C−O−C	Polysaccharides
1074	1066	1068	(α) C−O−C symmetric; (α)S−O; (α) C−N	Mainly sugars; fucans, amino acids
1020		1022	(α) C−O stretching ring	Cellulose and hemicellulose
822	830	813	(α) C−O−C; (β) N−H	Mainly sugars; proteins
592	595	597	(α) C−O−C; (β) O=S=O	Mainly sugars; fucans

Potentiometric titrations

A wide interval of point of zero charges (pH_{PZC}) values (3−8) have been reported (Table 2.6) for different species of brown, green and red seaweed [185,186]. The high pH_{PZC} of 9.7 observed in *A. spicifera* may be a consequence of the presence of amines (i.e., lysine and methionine amino acids), and secondary by phenolic groups present in the galactans and carrageenans which are active during alkali conditions associated to the NaOH titration [187,188]. Potentiometric titrations were conducted in I < 0.5 M because of deviations in the reproducibility of the Davies equation at

higher *I* [170]. It is no possible to elucidate the location of the acid functional groups in dehydrated biomass because plasmalemma permeability allows the titration of inner and outer groups [189]. However, all detected pK_a values could be associated with the composition of the cell wall (Table 2.6) based on previous reports [189,190]. In all three samples, pK_a titrations above eight could be associated to amines (pK_a 8.0−11.0), sulfhydryl (thiol) (pK_a 8.0–10.0) and hydroxyl groups (pK_a 9.5–13) [191].

Table 2.6 Acid dissociation constants (pK_a) and point of zero charge (pH_{PZC}) determined by potentiometric titration with 0.1 M NaOH. The probable structures associated with the pK_a constants are also included.

Sample	pH_{PZC}	pK_a	Acid Group	Possible associated compounds
Macrocystis pyrifera (brown algae)	8.2	4.1, 5.6	Carboxylic	Alginates, proteins, and glycoproteins
		6.9	Fosfonate	Phospholipids
		8.3	Amine	Amino acids
		10.3	phenolic, sulfhydryl (thiol)	Polysaccharides, proteins, and glycoproteins
Ulva expansa (green algae)	6.6	3.8, 5.5, 7.5	Carboxylic	Uronic acid, Amino acids
		11.0	Amine, hydroxyl or sulfhydryl	Amino acids
Acanthrophora spicifera (red algae)	9.7	4.3	Carboxylic	Uronic acid, Amino acids
		6.1	Imidazole	Amino acids
		9.4	Amino	Amino acids
		11.0	Sulfhydryl (thiol)	Amino acids

About brown seaweed, the carboxyl groups of alginate were reported more abundant than any other carboxyl or amine from proteins [113]. For green algae, its different pK_a's values are comparable with those reported for *Spirulina* species, *D. tertiolecta* and *Ulva lactuca* species [189]. The pK_a values between 4 and 6.5, were attributed to either a separate carboxyl or adjacent to hydroxyl in *ortho*−position, and also to a hydroxyl with carbonyl or the second hydroxyl in *ortho*−position [189]. In the particular case of *A. spicifera,* similar pK_a results have been observed in other red

algae species, like *Polysiphonia lanosa* and *Palmaria Palmata* [192]. On the other hand, the proton binding curves (Fig. 2.1a-c) corresponding to the three biosorbents showed that an increase in the ionic strength (from 0.01 to 0.45 M) did not significantly alter their surface charge distribution (Table 2.6). It has been reported that at ionic strengths higher ($I \geq 5$ M) than the ones used in our experiments, the number of protons adsorbed in *U. lactuca* increased [189].

Ash content

The inorganic matter of the biomass provides vital functions such as control of osmotic pressure and the acid-base equilibrium. This mineral content is related with: (1) water soluble salts in the cultivation environment, and (2) minerals and mineral microelements, like calcium and magnesium, associated with proteins and several sulfated and branched polysaccharides [193]. A high ash value (> 30 wt. %) was detected in the samples, where the concentration of minerals followed the next order (Table 2.7): K> Ca> P≥ Na for brown algae and K > Na > Ca for green and red biomass.

The most abundant inorganic elements in the sample under study (mg $g_{macroalgae}^{-1}$) were Sr (0.05 to 0.279), Fe (0.258 to 0.684), Al (0.110 to 0.723) and Mn (0.005 to 0.075). These results are comparable with those reported by Mohammadi M. et al. (2013) [115].

Finally, dissolved organic carbon (DOC) was used as a measure of organic biomass leaching to the liquid phase, representing all covalently bonded carbon in the organic molecules present in the biomass and dissolved in water. DOC value represents 5, 6 and 7 % of the total dry weight for the brown, green and red macroalgae, respectively.

Table 2.7 Ash composition of the biosorbents used in this study.

Elemental content (mg·g macroalgae^{-1})			
Element	*M. pyrifera* (brown)	*U. expansa* (green)	*A. spicifera* (red)
K	36.72	28.86	18.91
Ca	3.86	2.21	2.94
P	3.14	0.96	1.29
Na	2.80	3.36	3.91
.Mg	0.70	0.74	0.72
Si	0.32	0.21	0.06
Sr	0.28	0.03	0.05
Fe	0.26	0.68	0.54
B	0.12	0.07	0.12
Al	0.11	0.48	0.72
Mn	0.01	0.08	0.01
Total Ash (wt%)	43.2	31.7	52.5

2.8 Biosorption isotherms

Adsorption isotherms were carried out without controlling the pH to avoid volatilization of the HC. The maximum concentrations evaluated were those located near the aqueous solvation limit of benzene and toluene. The parameters of the adsorption equations in addition to the R^2 and the error functions are shown in Table 2.9. In all the cases, the Langmuir and Sips equations were ones that best fitted the experimental data with the minimum SSE (Fig. 2.1d). To predict the affinity between the sorbate and the sorbent, a dimensionless constant known as separation factor was computed according to the equation:

$$R_L = \frac{1}{(1+bC_o)} \qquad \text{(Eq. 2.9)}$$

where b (L·mg^{-1}) is the Langmuir or Sips constant. The R_L value indicates if the sorption process is irreversible (R_L = 0), linear (R_L = 1), unfavorable (R_L > 0), or favorable (0 < R_L < 1). Our R_L values (0.02−0.85) indicate that biosorption of hydrocarbons on brown, green and red seaweeds is favorable. All n values from the

Langmuir–Freundlich (LF) equation were found to be in the range of 0.1–10 suggesting physical biosorption that is favorable [194] as it is described below.

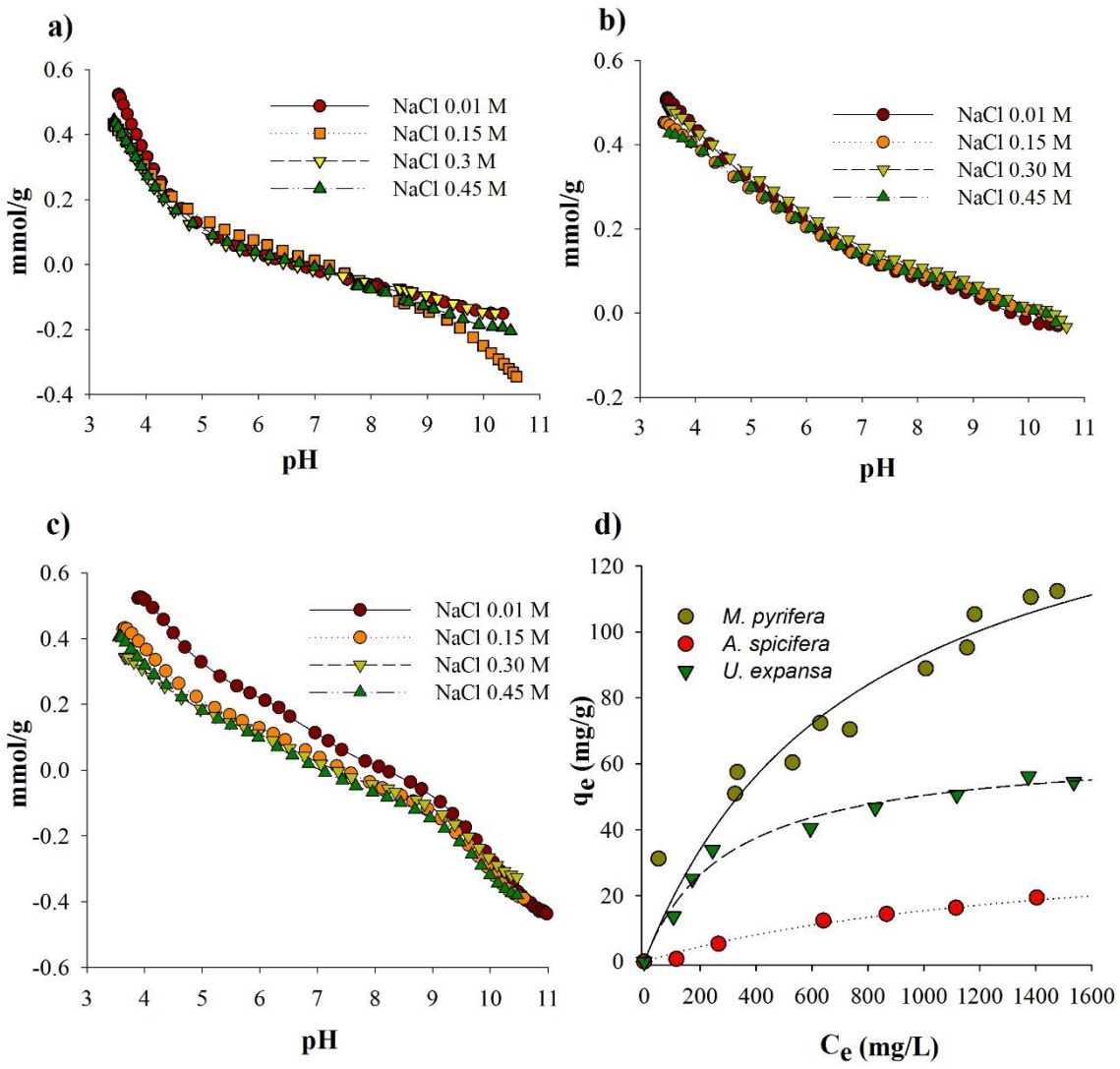

Fig. 2.1 (a) Surface charge curve of *Ulva expansa* at different ionic strengths as a function of pH; (b) Surface charge curve of *A. spicifera* at different ionic strengths; (c) Surface charge curve of *M. pyrifera* at different ionic strengths; (d) Adsorption isotherm of benzene at initial pH 6 − 8.7, and 25 °C. The lines represent the Langmuir isotherm equation.

The observed high fit to the LF isotherm is related to the saturated concentrations of stock solutions: at low concentrations, the LF isotherm is reduced to the Freundlich

equation, but at high sorbate concentrations, the LF isotherm approximates the Langmuir features [120].

Biosorption of aromatic compounds is a complex phenomenon because the orientation of the molecule should be accounted for [60]. Moreover, preliminary assays showed that benzene molecules generate Van der Waals interactions, and, in minor quantity, hydrogen bonding with water [61].

Table 2.8 Parameters of the isotherm equations, correlation coefficients (R^2) and error function values of the models for organic compounds adsorption.

	M. pyrifera		*U. expansa*		*A. spicifera*	
	Benzene	Toluene	Benzene	Toluene	Benzene	Toluene
Langmuir						
Q_{max} (mg·g^{-1})	164.76	47.49	63.39	28.89	38.71	45.99
b (L·mg^{-1})	0.0013	0.002	0.003	0.026	0.0001	0.0011
R_L	0.30	0.22	0.16	0.02	0.85	0.34
SSE$^{\beta}$	756.30	19.88	50.15	12.64	5.97	13.79
R^2	0.94	0.97	0.99	0.98	0.99	0.95
Freundlich						
n	0.485	0.70	0.37	0.28	0.69	0.81
K_F	3.14	0.36	3.64	5.21	0.12	0.11
SSE	516.38	30.20	93.53	53.47	12.48	16.79
R^2	0.96	0.96	0.97	0.94	0.97	0.94
Langmuir - Freundlich						
b	0.001	0.0001	0.004	0.019	0.003	0.002
Q_{max} (mg·g^{-1})	130	28.07	67.24	28.06	18.56	22.84
n (L·mg^{-1})	1.12	1.69	0.95	1.10	0.99	1.49
R_L	0.36	0.85	0.12	0.03	0.16	0.22
SSE	303.16	8.15	50.11	12.11	10.12	9.01
R^2	0.97	0.99	0.98	0.98	0.98	0.97

$^{\beta}$ SSE= Sum of squared error

A good fit of the data to the LF isotherm equation ($r^2 \geq 0.97$), allowed to calculate the maximum removal capacities of adsorbed HC per m^2 of biosorbent (assuming that adsorption occurs on a monolayer). These calculations assumed an equilibrium concentration C_e of 1400 mg L^{-1}, and a cross-sectional area of the adsorbates of 25.3 and 28.5 Å^2 for benzene and toluene molecules, respectively [183]. These maximum removal capacities were compared with the maximum coverage capacity

of the biomass. According to our calculations, the maximum contribution of HC monolayer on the biosorbent does not exceed 1 % in all the cases, suggesting the formation of HC multilayers on the macroalgae. However, this calculation presents limitations that should be taken into consideration because the swelling (S_w) degree of the biomass (557, 270 and 857 for brown, green and red samples, respectively), should produce a noticeable increase in surface area and, therefore, a more active physical and chemical biosorption.

In this work, the biosorption capacity decrease in the order *M. pyrifera* > *U. expansa* > *A. spicifera*, for benzene and toluene, respectively. The differences in HC sorption may be related to different cellular components among the species. Brown algae have proved to contain fucans, cellulose and high quantities of alginate [195] as previously indicated. Active groups of macroalgae compounds, especially lignin and alginate, have been reported to have high affinity to HC and metals [196]. This sum of binding affinities may explain the superior biosorption capability of benzene by brown algae in comparison to other samples. In the case of toluene, the biosorption capacities reached similar values, probably because of diffusional restrictions of toluene present in the pores of the brown macroalgae, which showed a low surface area. It is possible that the higher ash content of *M. pyrifera* promotes cation – π interactions that diminish the diffusion of toluene to the pores of brown seaweed. There are no available reports concerning *A. spicifera,* but probably the biosorption mechanism is mainly related to the presence of hydrophobic structures, as previously reported [109]. Also, the low biosorption capacity of *A. spicifera* would be related to the higher ash content (> 50%) and the lower content of protein, lipid and cellulose fractions compared to brown and green biomass.

In this regard, the constituents of the cell wall provide a diversity of functional groups capable of binding hydrocarbons [132–134] and, as a consequence, many biosorption mechanisms could be involved in the overall process (Table 1.8). Furthermore, due to the complexity of biomass constitution, many of these interactions probably co-occur at multiple degrees [197]. The biosorption mechanism of aromatic hydrocarbons is a current and relevant research topic.

Recent studies [122,166] that evaluated the partition of phenol, nonylphenol and phenanthrene pollutants among different macroalgae fractions found that the initial concentration, lipid fraction, ionic strength, H/O atomic ratios and poly(methylene) carbon were the main factors influencing the sorption capacity of seaweeds.

Effect of ionic strength and temperature on biosorption

The presence of dissolved salts can modify the biosorption capacity of seaweeds. Considering that salinity in natural waters can reach values of up to 0.7 M [167], it is important to evaluate the performance of biosorbents as a function of this variable simulating conditions from fresh to saline waters. The presence of salts modified the biosorption capacity of seaweed (Fig. 2.2a,c,e). In the case of benzene and toluene the biosorption capacity changed little until salinity reached I = 0.45 M. As shown by our potentiometric titrations, the increase in I produced no change on the surface charge of the material, results supported by [189], who reported that acid functional groups were stable under a wide ionic strength interval (I = 0.01 – 5 M). However, when the systems reached a value of I = 0.6 M, an important decrease in biosorption capacity was observed primarily for Instant Ocean solutions, probably because this solution includes different ions ($I \approx$ 0.76 M) and organic matter that may block pores, preventing the diffusion of the adsorbate to the active sites. Also, hydrophilic interactions from inorganic content may be enhanced by the increase of I, generating biosorption competition by water clusters [119]. Also, higher salt content resulted in a lower biosorption capacity of a metal–complex dye by fungi biomass [198]. Furthermore, it was observed that desorption increased with an increase in the ionic strength of the solution (Fig. 2.2b,d,e). We can speculate that high salt concentrations promote more interactions between electrolytes and water, forcing the sorbed pollutants to interact with other surfaces and, hence, overcoming most of the unspecific interactions with the biomass [119]. Finally, a slight decrease of biosorption was observed when the temperature decreased from 25 to 4 ºC, possibly due to the reduced molecular mobility and probability of interaction between the active sites and the pollutants [124]. This phenomenon due to less mobile of

molecules was previously reported from activated carbons from low-cost biomaterials [8]. In the case of toluene, low desorption values were observed, this could be explained by its high reactivity and molecular area, that enhance interactions as reported to activated carbon [199].

2.9 Kinetic experiments

The experimental data of the relative concentration of benzene and toluene as a function of time (Fig. 2.3) were fitted to the pseudo−first, pseudo−second and Weber−Morris kinetic equations (Table 2.10). Generally, green and red biomass showed two different stages of biosorption, with the first stage showing high sorption uptake (50% of the total biosorption capacity), during the first minutes of the experiment, followed by a much lower rate and essentially constant after 60 min. The samples reached steady states within 1 – 6 h. The overall removal rate in the case of brown seaweeds included an additional second phase showing a slow rate of uptake attributed to competition for the surface active sites of the biomaterial. Half of the overall removal was achieved within 4 h.

The calculated correlation coefficients (R^2) indicate that the experimental data can be better fitted to a pseudo−second order reaction (corroborated with minor values of SSE). The rate constants of sorption (k_2) were between 0.003 – 0.25 mg g^{-1} h^{-1}, suggesting that the removal rate of benzene and toluene is a function of the square concentration of the aromatic molecules [186]. Based on the above results, 6 h was selected as the optimal equilibrium contact time for *U. expansa* and *A. spicifera* samples and, 30 h for *M. pyrifera* biomass.

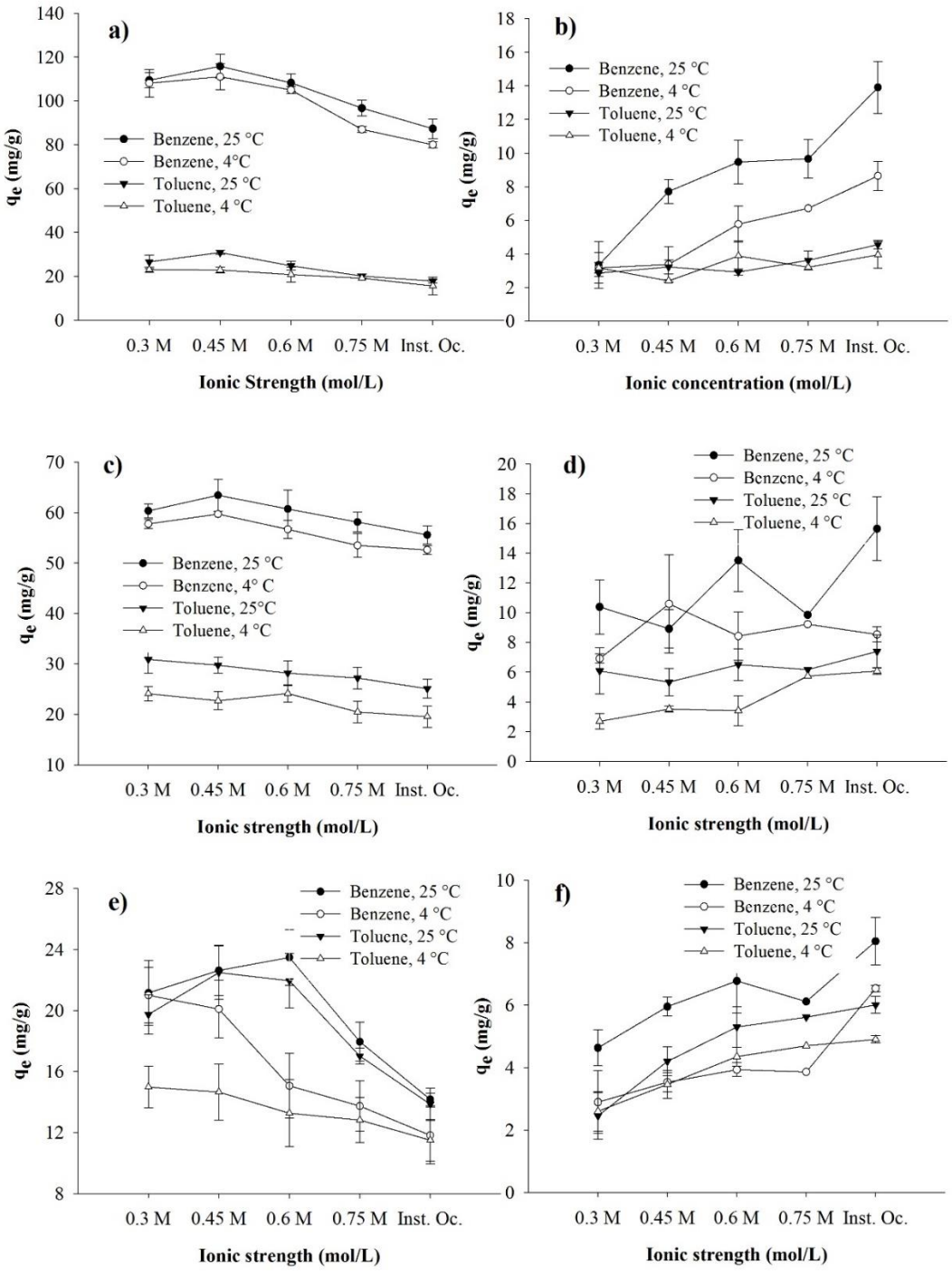

Fig. 2.2 Effect of the temperature and ionic strength on the sorption capacities of benzene by *M. pyrifera*, *Ulva expansa* and *A. spicifera*, respectively (a, c, e); Effect of the temperature and ionic strength on the biodesorption capacities of benzene by *M. pyrifera*, *Ulva expansa and A. spicifera,* respectively (b, d, f).

Our results indicate that the removal capacities of the fresh macroalgae biomaterials are comparable with other studies that employed cellulosic−based materials (Table 2.11). Based on benzene removal results, and making a comparison at an equilibrium concentration of 1400 mg·L^{-1} we can conclude that biosorption capacity represents 20 − 30 % of the maximum adsorption capacity of different carbon-based materials reported in the literature [9]. It is reasonable to conclude that macroalgal biomaterials could offer promising possibilities as biosorbents of soluble HC, not only in fresh water but also in a wide range of saline systems and seawater. Also, these biomaterials have unique features that can make them attractive regarding cost and availability.

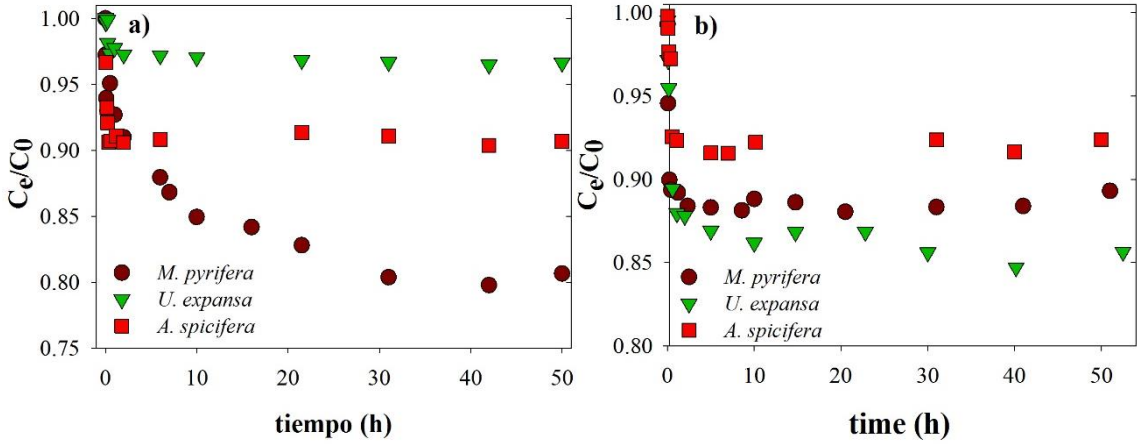

Fig. 2.3 Toluene biosorption rate onto biosorbents under study at an average initial concentration of 530 mg·L^{-1} at 25ºC, 120-130 rev/min.

Table 2.9 Pseudo-first order, pseudo-second order and Weber-Morris rate equation parameters for removal of hydrocarbons by biosorbents in different solutions.

	M. pyrifera		*U. expansa*		*A. spicifera*	
	Benzene	Toluene	Benzene	Toluene	Benzene	Toluene
Pseudo-first order						
k_1 (h^{-1})	0.089	0.06	0.03	0.07	0.09	0.04
q_e ($mg \cdot g^{-1}$)	91.42	5.78	13.13	18.72	10.82	10.99
SSE^{β}	13580	3904	14176	1789	1806	274
R^2	0.89	0.52	0.85	0.85	0.89	0.66
Pseudo-second order						
k_2 ($mg \cdot g^{-1} \cdot h^{-1}$)	0.01	0.11	0.13	0.08	0.04	0.76
q_e ($mg \cdot g^{-1}$)	103.9	27.23	70.51	27.17	20.79	17.73

SSE	543	181	11	59	186	22
R^2	0.98	0.95	0.99	0.98	0.96	0.98
Weber-Morris model						
k_3 ($mg \cdot g^{-1} \cdot h^{1/2}$)	23.16	7.43	73.21	11.83	4.06	8.05
C	16.12	10.03	11.48	4.49	4.88	0.93
SSE	756	184	186	167	163	43
R^2	0.97	0.63	0.82	0.73	0.66	0.81

SSE^{β}=Sum square of errors

Table 2.10 Comparative summaries of adsorption capacities achieved by a diverse of algae biomass and biosorbents in other studies.

Specimen	Pollutant	Biosorption Capacity $\mu g \cdot g^{-1}$	Initial Concentration mg/L	Reference
Sargassum sp.	Phenanthrene	430-460	1	[119]
Spirulina	Phenanthrene	4800	1.29	[122]
Brown algae	Phenanthrene	2300	1.29	[122]
Porphyra	Phenanthrene	9178	1.29	[122]
Biosorbent	**Pollutant**	**Biosorption Capacity $mg \cdot g^{-1}$**	**Initial Concentration $mg \cdot L^{-1}$**	**Reference**
Rice bran	Benzene Toluene	520 690	ND	[9]
Horseradish pods	Benzene Toluene	620 830	ND	[9]
Activated carbon fiber cloth	Benzene	300-375	ND	[9]
Gran. active carbon bed	Toluene	163-267	ND	[9]
Activated carbon bed	Benzene	650	ND	[9]
Activated carbon	Toluene	260	ND	[9]
M. pyrifera	Benzene Toluene	112 28.07	1800 515	This study
U. expansa	Benzene Toluene	55 28.06	1800 515	
A. spicifera	Benzene Toluene	20 16	1800 515	

ND = No data reported

2.10 Conclusions

The ionic strength effect on the benzene and toluene biosorption capacity of three representative species of macroalgae was evaluated. No significant effects on the seaweeds surface charge and their biosorption capacity were observed at least up to an *I* of 0.6 M. The biosorption mechanism involves hydrophobic interactions with lipids and lignocellulose fractions and, to a lesser degree, nonspecific van der Waals interactions with carbohydrates and proteins. The biosorbents under study remove soluble HC in water and could be considered as an alternative to diminish the toxic effect of soluble hydrocarbons in aquatic ecosystems.

CHAPTER 3

Chitosan-based composites as potential water-soluble hydrocarbons biosorbents.

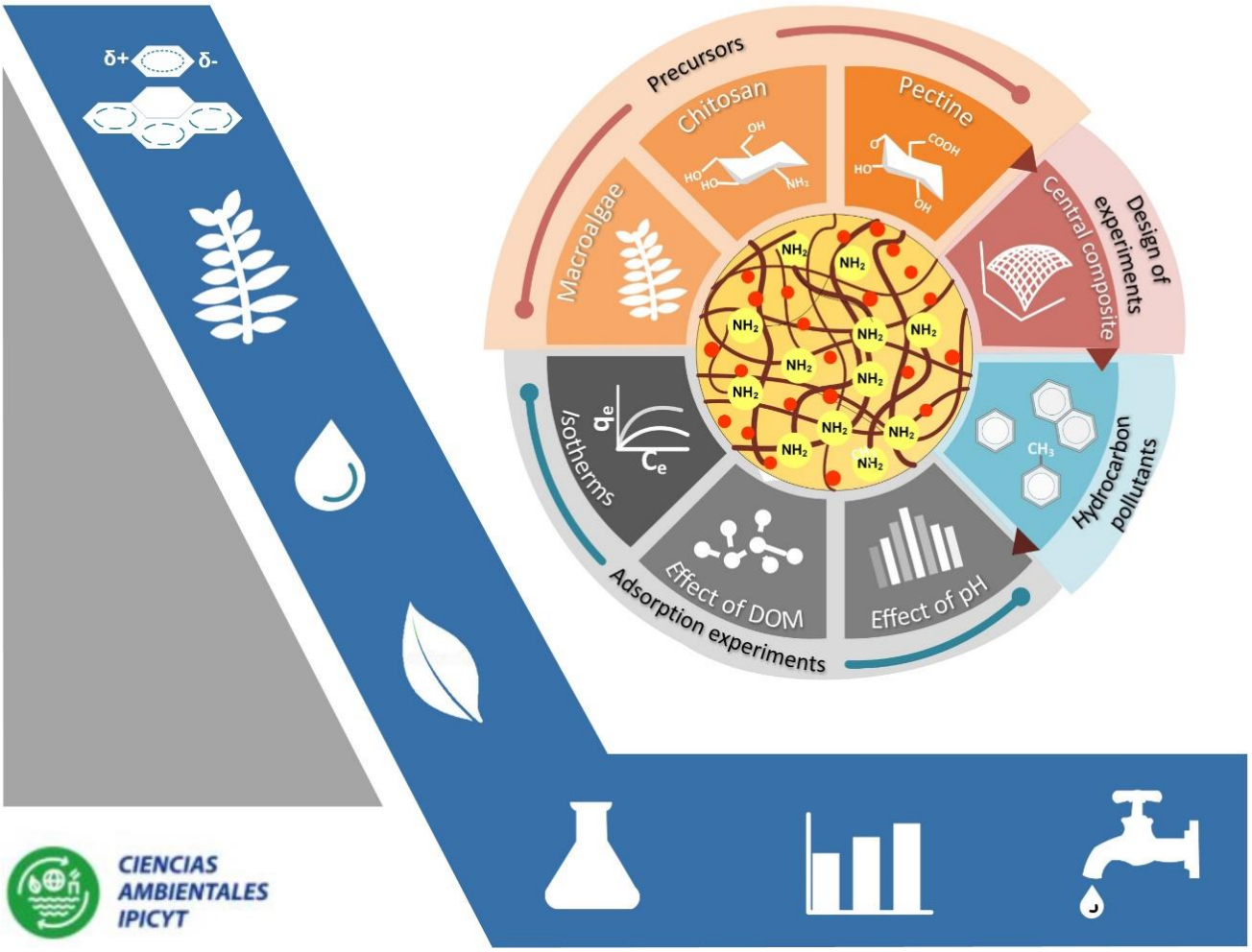

This chapter is adapted from: *Chitosan-macroalgae biocomposites as potential adsorbents of water-soluble hydrocarbons: Organic matter and ionic strength effects*, 2018, 197, 633-642.

CHAPTER 3

3.1 Abstract

Nowadays the recovery of low-molecular soluble aromatic hydrocarbons (HC) released into natural bodies of water continues to be a challenging task. These contaminants bring severe consequences to the environment and the human health. Biosorption on macroalgae (Ma) biomass seem to be a potential alternative to due to low costs and high availability, but the low strength and density are essential drawbacks to handle, start up and operate continuous biosorption units. In this study, chitosan (Ch) and pectin (Pe) were employed as precursors to synthesize a new Ma−Ch−Pe composite enhancing the stability and applicability of macroalgae biomass towards the removal of soluble HC pollutants. The biocomposite synthesis was based on a factorial design and a posterior response surface methodology. The optimized biocomposite (75.4%, 19.8 and 4.8% for macroalgae biomass, chitosan, and pectin, respectively), was characterized and evaluated under different ionic strengths, pH values, and organic load to determine their potential as biosorbents and to elucidate the adsorption mechanisms involved. Removal capacities were 58.68, 16.64 and 6.13 mg g^{-1} for benzene, toluene, and naphthalene, respectively. The adsorption capacity was slightly influenced by the pH (3-9) and diminished with ionic strength values up to I > 0.6 M. The presence of dissolved organic matter (DOM) enhanced the removal of HC by providing hydrophobic sites to the biosorbents. Moreover, the biosorption data was well-described by Sips adsorption isotherm, and the pseudo-second-order equation represented the best fitting model for the biosorption kinetics. The biosorption mechanisms included hydrophobic effect by the algae fraction and London forces between the HC and the diversity of functional groups present offered by the precursors.

3.2 Introduction

Crude oil is one of the three primary fossil fuels, along with coal and natural gas [200]. When operational or accidental oil spills occur on bodies of water, even after applying clean-up technologies, water-soluble aromatic compounds from oil may persist and continue to produce adverse effects on the ecosystem and human health [29]. Around 1 to 3% (sometimes up to 15%) of crude oil can pass into a dissolved state [160]. Data from oil production have shown that the main aromatic compounds (> 96 %) in produced water are BTEX (benzene, toluene, ethylbenzene and xylene), followed by 2- and 3- ring polyaromatic hydrocarbons (PAHs) as naphthalene (3%), and at the end larger PAHs (<0.2 %) [201]. Different methodologies have been suggested for soluble hydrocarbon removal and involve filtration, aeration, biodegradation, and photocatalysis [45,161,202,203]. These techniques have a different degree of success, but sensible disadvantages including high-energy requirements, long periods of treatment, and expensive equipment. Sorption including different adsorbent media such as carbonaceous materials, natural products, and wastes have proven to be an efficient, rapid and feasible alternative for soluble hydrocarbons removal in water [51,204,205]. Remarkable importance is noted for biosorption over the last few years because it was reported that this technology could be from 20 to 36% less expensive in comparison with conventional systems respectively [75,206]. Macroalgae (Ma) biosorption processes constitute a cost-effective and environmentally friendly alternative for the removal of petroleum-based soluble compounds [9,79]. Furthermore, seaweed can be farmed in water by avoiding any competition with food production [207,208]. *M. pyrifera* is a broadly distributed macroalgae (Pacific and Southern oceans) and is the largest algae which size ranges from 70-80 m with an annual growth rate of 50 m in suitable conditions [208]. Regardless of these promising outcomes, the physical characteristics (small particle size, low strength, and density) of such biomaterials are not viable for continuous process operation and make biomass challenging to manage [80]. Therefore, the biomass immobilization techniques are one crucial issue to improve the practical application of macroalgae biomass on biosorption processes. The use

of flocculant agents as an active immobilization technique has received special attention, in particular, polysaccharides as chitin and its derivate chitosan, a highly available food processing by-product [209]. Chitosan is a linear polymer with a predominant amount of positively charged amino groups and a well-known affinity toward pollutants like metal ions and colorants. On the contrary, pectin (Pe) is a polyanionic compound composed predominantly by galacturonic acid units linked through α-(1-4) chain [85,210]. Pectin molecule is extensively used in the food industry for its well-known thickening, stabilization and gelling properties [211], and also known for its decisive health-related role with numerous pharmaceutical uses [212]. The biopolymer-biopolymer interactions between the two oppositely charged polymers (chitosan and pectin) could increase the compatibility and stability of the biosorbents. This mechanism creates new structures that are called polyelectrolyte complexes. Though there are numerous publications on the formation of composites with chitosan for metals and nutrients biosorption purposes [213], it is still of interest to further integrate Ma−Ch−Pe composite via precipitation method to enhance their capabilities for practical applications on water-soluble hydrocarbons removal.

The primary objective of this research was to determine by a factorial design, and by a response surface methodology, the proportion of *M. pyrifera*, chitosan, and pectin that confer to the synthesized composites a greater ability to remove aromatic hydrocarbons. Later, the capacity of these composites to remove benzene, toluene, and naphthalene under different scenarios of ionic strength, pH and dissolved organic matter in natural water was determined. Complete physicochemical characterization of the biosorbent was performed to establish the adsorption mechanisms.

3.3 Materials and Methods

Chitosan (Ch) (with a molecular weight of 50,000 - 190,000 Da and a ≥ 75 % degree of deacetylation) and pectin (Pe) (galacturonic acid ≥ 74 %) were purchased from Sigma−Aldrich Co. Ltd. Other reagents, namely, acetic acid (HAc), NaOH and NaCl were obtained from J.T. Baker Co. Ltd. The macroalgae sample *Macrocystis pyrifera*

(Ma), was collected in La Paz, Baja California Sur, Mexico and Ensenada, Baja California, Mexico. Dried biomass was rinsed with plenty of deionized water (<11 µS cm^{-1}) at 50 °C. Finally, the sample was sieved to a particle size of < 250 µm with a Mini-Cutting Mill (Thomas Wiley) before used in sorption experiments and characterization. The model organic pollutants included in this work were benzene, toluene, and naphthalene (Sigma–Aldrich, 99% purity).

Preparation of Ma-Ch-Pe biocomposite

The Ma−Ch−Pe biocomposites were prepared by dissolving a definite amount of pectin (Pe) powder (up to 2 g) in deionized water. At the same time, 3 − 5 g of chitosan were suspended in the pectin solution. Then, 50 mL of HAc 5% (v/v) were added to the mixture and stirred continuously for 30 min. The synthesis was followed by the addition of a specific amount of the macroalgae biomass (Ma), and the final composite was stirred for another 12 h. The homogeneous (Ma−Ch−Pe) solution was fully poured through a drop system (Fig. 3.1a) into a 25% NaOH solution for hydrogelation, according to a previous methodology [214]. The obtained hydrogels were washed with distilled water to neutral pH and dried at room temperature for 48 h. The average particle size could be controlled from 3 – 6 mm by changing the tip of the syringe.

3.4 Optimization approach

Factorial design

A screening experiment involving a three-factor two-level full factorial design (2^3 runs) was employed. Preliminary experiments were conducted to select the suitable high and low levels (Table 3.1). Moreover, Table 3.2 shows the design matrix for the total ten experiments, and the q_e measured in each run, with the low and high levels as specified in Table 3.2. The design included two center points to have an estimate for the experimental error [139]. Benzene was selected as aromatic hydrocarbon

model, its removal by the composite was the response variable. All determinations were replicated at least twice. The results were examined with Design Expert software v.6.0 to determine the central interactions and effects.

Table 3.1 Experimental intervals and levels used in the factorial design.

Factors	Coded symbol	Low level (-1)	High level (+1)
Chitosan (g)	A	3	5
Pectin (g)	B	0	2
Algae biomass (g)	C	2.7	5.4

Response surface design (RSD)

Response surface methodology (RSM) is a mathematical and statistical approach used for working with specified ranges of the input variables to find the factor settings capable of improving the performance of a process, for example, to maximize the capacity of adsorption of an adsorbent [215]. RSM is often employed after a thorough screening using full or fractional factorial experiments [141]. Therefore, to achieve the highest amount of benzene adsorbed by a Ma−Ch−Pe biocomposite, a non-replicate face-centered cube central composite design was used. Initial amounts of Ch (20 - 40%) and Ma (60 − 80%) were selected as independent input variables. Regardless of the non-significant effect of pectin observed in the factorial design, five wt % of this polymer was added to the Ma/Ch mixture to increase the solution viscosity and mechanical strength [93]. Finally, the hydrogelation procedure was performed as described above.

Five central points were established to provide a reasonably stable variance of the predicted response [216]. The range, levels, and responses of the researched variables are presented in Table 3.1. Treatments were performed randomly, and the results were analyzed using the statistical program Design Expert® v.6.0. The significance of the models was tested by variance analysis (test F), R^2 coefficient and significance of the independent variables were also calculated ($\alpha = 0.05$).

Biosorption properties testing

The selected Ma−Ch−Pe composite was evaluated by several physicochemical analysis as follows: surface area (m^2 g^{-1}) and pore size distribution of the samples were calculated by BET isotherm and DFT (Density Functional Theory), respectively, with a Micromeritics ASAP 2020 apparatus at 77 K [168,217]. Potentiometric titrations were performed in an automatic titration system (Mettler Toledo T70) for proton binding curves and point of zero charges (pH_{PZC}) determinations. A mass of 0.1 g was placed in 50 mL of a 0.1 NaCl solution. The proton binding curves were generated through the transformation of the experimental titration data (50-70 points) by using the SAIEUS program.[169,170]. Interactions between biocomposite precursors were studied by using a Thermo Nicolet 6700 FT-IR in transmittance mode within the range of 600-4000 cm^{-1}, with a 4 cm^{-1} resolution and 128 scans.
The X-ray diffraction (XRD) patterns of the biocomposite were obtained with a step time of 10 s and 2θ of 0.01° with an XRD D8 Advanced-Bruker Axs (Cu Kα radiation λ = 1.546 Å). Powder samples were employed in the analysis.

The degree of swelling (S_w) was determined in triplicate runs by weighing a precise mass of 0.5 g of dry biocomposites and placed in a baker at 25 °C with 25 mL of distilled water. The swollen materials were removed from the water and weighted (W_t) after 24 h. S_w value was computed by the following equation: $S_w = ((W_t - W_o) / W_o)*100)$. Where, W_o is the mass-weighted of the dry biocomposite (t = 0), and W_t is the mass weight of the swollen material at time t.

Chemical stability was determined by contacting the solids in acidic water, which is based on a previous methodology [209]. Briefly, a specific mass of biocomposite was placed in acidified water (pH = 5) at 25 °C. The mixture was shaken at 120 rpm until the pH of the solution has no change. The solids were separated by filtration and dried at 70 °C for 48 h. The chemical stability was the percentage of mass loss at the initial and final stage.

3.5 Equilibrium experiments

For experimental design essays, benzene was selected as the model pollutant, but in the case of the selected biocomposite, toluene and naphthalene were also tested. The removal capacity of the optimized Ma−Ch−Pe biocomposite was determined under deionized water including the maximum solubility of each compound [177]. In all the cases, evaluations were conducted by adding 0.1 g of each sorbent to a series of 35 mL amber glass flasks that contain a specific amount of benzene, toluene or naphthalene, specified in Table 2.1. The experiments were carried out at 90 - 100 rev min^{-1} and 25 °C. The concentrations of benzene, toluene, and naphthalene in solutions were determined using a UV-Vis (Thermo Aquamate) spectrometer at a wavelength of 254.5, 261 and 284 nm, respectively. At least two blanks with the same amount of biocomposite (no HC added) were run simultaneously as controls along the sorption samples to correct the final HC concentration and ultraviolet adsorption for the desorbed organic matter. The adsorption capacity q_e (mg g^{-1}) of the aromatic compounds was computed by the following Eq. (3.1):

$$q_e = \frac{V}{m}(C_0 - C_e) \qquad (3.1)$$

where C_0 and C_e are the initial and equilibrium concentrations (mg L^{-1}), V is the volume of the solution (L), and m the mass of the adsorbent (g). The equilibrium data for adsorption was evaluated with the Langmuir, Freundlich, and Sips isotherm models described elsewhere [62]. Quasi-Newton algorithms were employed to compute equation parameters using the STATISTICA software V.10. Model selection was based on the statistical values of the correlation coefficient (R^2) and the sum of the sum of the squares error (SSE), according to the following:

$$\sum_{i=1}^{n}\left(q_{e,calc} - q_{e,meas}\right)_i^2 \qquad (3.2)$$

Where $q_{e,calc}$ and $q_{e,meas}$ are the estimated and actual sorption capacities values at equilibrium (mg g^{-1}).

Effect of the pH and ionic strength

The effect of ionic strength was studied under different ionic strength solutions (*I* = 0.3, 0.45, 0.6 and 0.75 M), as well as with a synthetic seawater solution Instant Ocean® (*I* ≃ 0.76 M). The salting coefficients κ_s of the hydrocarbons were calculated to determine the organic dissolution rates at different NaCl solutions (Table 1.8). Calculations were performed according to the Setchenow equation $log(S_o/S) = \kappa_s C$, where S_0 is related to the solubility of benzene, toluene and naphthalene in water [178]. Additionally, desorption tests were performed for saline solutions as follows: The 0.1 g pre–adsorbed Ma−Ch−Pe biocomposites were filtered by decantation, rinsed with deionized water to remove contaminant excess and subsequently immersed into 35 mL of water at the same *I* as the previous biosorption runs (100 rev·min^{-1} and 12 h). The organic leached was determined by an UV−Vis spectrophotometer as already mentioned. The amount of desorbed HC was determined by the difference between the HC concentration in the initial solution and that remained in the agitated solution.

The effect of the initial pH in the biosorption of aromatic hydrocarbons was also investigated in deionized water at pH values from 3.0 to 9.0. under the conditions above. The pH of the solutions was adjusted with HCl and NaOH solutions.

Biosorption kinetics

To determine the effect of contact time, a 0.1 g of the selected biocomposite were placed into amber bottles with deionized water at the initial concentration previously specified for benzene, toluene, and naphthalene, respectively. The kinetics were obtained from batch experiments (timescale: 0 to 50 h), containing 35 mL of HC solution stirring at 90 - 100 rev min^{-1} and 25°C. At given time intervals, the sample was collected for analysis, and the HC remaining concentration was determined by UV-Vis spectrophotometer as mentioned above. An approach to describe the biosorption rate was determined by the pseudo-first-order, pseudo-second-order and Weber Morris rate equations as previously reported [218,219].

Effect of dissolved organic matter (DOM)

To evaluate the effects of DOM on the rate of removal of benzene, toluene, and naphthalene, experiments were carried out by using natural water from a reservoir containing 19.3 $mg \cdot L^{-1}$ of DOM. The natural water collected from a reservoir located in San Luis Potosi, Mexico, was filtered through Millipore 0.22 µM nylon filters and was chemically characterized; total organic carbon was measured using a Total Organic Carbon Analyzer (TOC-VCSN Shimadzu), metals concentration was determined by Inductively Coupled Plasma-Optical Emission Spectrometry (ICP-OES, Varian 730-ES).

To verify the aromaticity and humic acids content of the sample, the Chromophoric DOM (CDOM) was measured through UV-Vis spectrophotometric analyses at two specific wavelengths (250 and 350 nm) for the computation of E_2: E_3 ratio and the specific ultra-violet absorbance ($SUVA_{254}$) described elsewhere [220]. Absorption spectra of DOM solution are shown in Fig. 3.1. Finally, anions concentration was analyzed by capillary electrophoresis (Agilent 1600). The summary of the characterization is shown in Table 3.1. Sorption kinetics studies using natural water were carried out, and the data were analyzed under conditions indicated in the following sections.

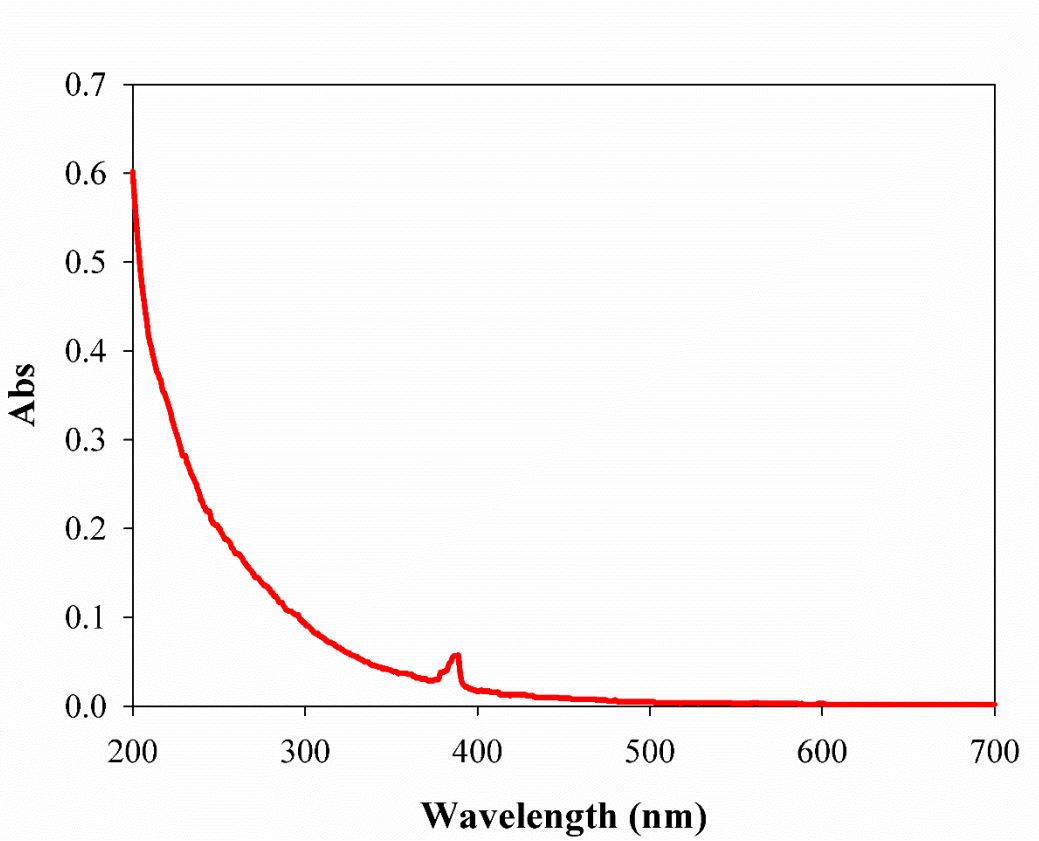

Fig. 3.1 Adsorption spectra of DOM in the sample solution.

Table 3.1 Chemical characterization of natural water used in experimental biosorption procedures.

Parameter	Concentration ($mg \cdot L^{-1}$)	Parameter	Concentration ($mg \cdot L^{-1}$)
DOM	19.26	Ba	0.04
Na	18.95	Co	0.02
Ca	17.34	Mn	0.01
Si	13.42	Cl^{-1}	6.155
K	8.15	SO_4^{2-}	28.5
Mg	3.22	NO_3^-	2.24
Al	1.18	CO_3^{2-}	5.13
Fe	0.55	PO_4^{3-}	3.42
Sr	0.1	pH	7.2

3.6 Optimization results

Design of experiments

A factorial experiment design in conjunction with an analysis of variance was the first approach in optimizing the conditions for benzene removal capacity onto a diverse of Ma−Ch−Pe compositions. The range studied was between 3 and 5 g for chitosan, up to 2 g for pectin, and between 2.7 and 5.4 g for macroalgae biomass. The experimental tests are given in Table 3.2. Based on the previous information, an analysis of variance (ANOVA) and P_{value} significant levels were calculated to check the significance of the effect on benzene biosorption. The statistical parameter P_{value} (more than 0.05) suggests that the model was not significant if we include the overall (Ma−Ch−Pe) interactions. However, in the case of Ma, Ch, and Ma–Ch interaction, significant model terms with more than 95% confidence level were estimated. Based on this, the content of pectin (Pe) was negligible. This finding indicates that the amount of chitosan and macroalgae biomass parameters had the most significant effect in the benzene biosorption capacity. Because of this, the model reduction was suitable leaving only the significant model terms (Ma-Ch interaction).

Table 3.2 Analysis of variance for the factorial model describing the adsorptive capacity (q_e) with the estimate effect and coefficients.

Source	Sum of squares	d.f.[a]	Mean square	F–ratio	*p* [b]
Model	1008.02	3	336.01	31.73	0.0011
A – Ch	501.57	1	501.57	47.37	0.0010
C – Ma	368.08	1	368.08	34.76	0.0020
AC	138.37	1	138.37	13.07	0.0153

[a] d.f.: degree of freedom.
[a] *p*: probability for *F*–ratio test

After the main parameters were identified, subsequent experiments were performed to analyze the nature of interactions among them by a response surface methodology (RSM). The Ma/Ch ratio is critical to the performance of the biocomposite. For an extensive application, it is desirable to use more *Macrocystis pyrifera* in the production of a biosorbent as it plays a crucial role in biosorption and represents the more accessible precursor of the biocomposite [195]. Hence, an upper Ma/Ch ratio was used for the surface response design experiment. Pectin was established to a minimal value (5 % w/w) since this did not have a significant influence on benzene removal but enhanced the mechanical properties of the final material as also reported by Wan Ngah et al. (2011) [210,213].

The design matrix and the corresponding experimental data of the central composite design (CCD) are given in Table 3.3 after tests. The CCD results were fitted to an elliptical second–order polynomial equation: Benzene removal (mg g^{-1}) = 49.05 + 3.31A + 0.54B − 7.55A^2 − 7.35B^2 − 4.79AB. The fit of the model was evaluated by the correlation coefficient, R^2, which was 0.989, indicating that 98.9% of the variability in the response could be explained by the model (Table 3.3). The statistical significance of the second–order model equation was evaluated by an F–test, which reveals that this regression was statistically significant (P < 0.0001) at the 99 % confidence level. The factorial design showed that Chitosan (A), Macroalgae (B) and the Chitosan-Macroalgae (Ch–Ma) interaction, had a highly significant effect (P < 0.0001) on benzene removal.

The contour plot described by the benzene removal is represented in Fig. 3.1b, which shows that the maximum benzene removal capacity was approximately 50 mg·g^{-1}, which corresponds to the central point within the highest contour levels [215]. The optimal concentration for the two precursors obtained from the maximum point of the model was 20.8 % (w/w) for Ch (A) and 79.2 % (w/w) for Ma (B). The model predicts a maximum response of 49.42 mg·g^{-1} at this point. Therefore, the final biocomposite composition was 75.4%, 19.8%, and 4.8% for macroalgae biomass, chitosan, and pectin, respectively.

Table 3.3 Design matrix for the central composite design, levels and responses.

No. Experiment	Factor A Chitosan (g)	Factor B Macroalgae biomass(g)	Response Benzene removal (mg/g)
1	0.3	1.5	25.17
2	0.3	1.7	36.16
3	0.3	1.6	38.55
4	0.4	1.5	40.88
5 CP	0.4	1.6	48.49
6 CP	0.4	1.6	49.93
7 CP	0.4	1.6	49.16
8 CP	0.4	1.6	49.74
9 CP	0.4	1.6	49.19
10	0.4	1.7	41.29
11	0.5	1.5	42.36
12	0.5	1.7	34.18
13	0.5	1.6	43.22

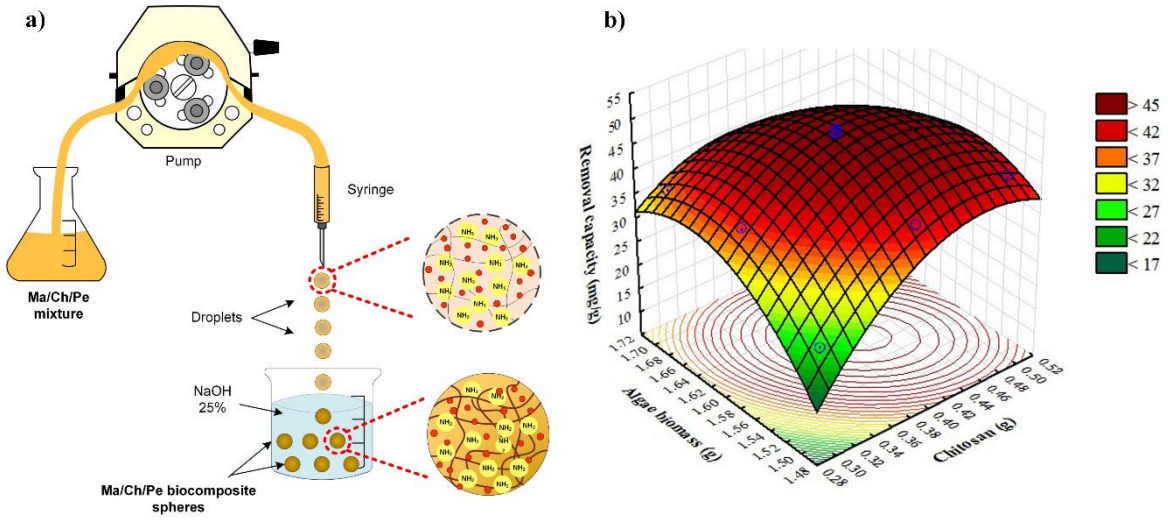

Fig. 3.2 (a) Drop system for biocomposite synthesis; (b) Response surface contour plot of benzene removal (mg g^{-1}) showing the interactive effect of macroalgae biomass (g) and chitosan (g).

3.7 Characterization experiments

FT-IR and XRD analyses

The FT-IR spectrums between 4000 cm^{-1} and 600 cm^{-1} for Ma, Pe, Ch, Ch-Pe and the optimized Ma−Ch−Pe biosorbents (Table 3.4), were compared to elucidate the chemical structure and reaction mechanisms occurring on the biocomposites. The FT-IR spectra of Ch is close to a previous work reported in the literature [99]. The major peaks of Ch were registered at 3352 cm^{-1}, 1654 cm^{-1}, 1590 cm^{-1}, 1424 cm^{-1}, and 1068 cm^{-1}, which corresponds to the N-H stretching vibration, C=O stretching vibration of –NHCO- (acetylated section), N-H deformation of primary amides (formed during deacetylation), -CH bending and C-O stretches, respectively. FT-IR spectra of pectin show bands at 1730 and 1600 cm^{-1} assigned to methyl esterified and vibrations of the O=C-O structure, respectively [221]. The IR spectra of macroalgae biomass indicated a broadband between 3800-3000 cm^{-1} which corresponds to hydroxyl (-OH) and amine ($-NH_2$) groups, which could be associated to polysaccharides and amino acids, respectively [122]. Moreover, the band intensity at 2848 cm^{-1} represents the aliphatic chain of lipids, whereas the peak at 1638 cm^{-1} could be related to the presence of carboxylate groups ($-RCOO^-$) associated to alginate and primary amides of amino acids. Finally, the band at 1155 cm^{-1} was attributed to sulfates polysaccharides and amino acids [79].

In the Ma−Ch−Pe spectrum, the peaks at 2940 cm^{-1} and 1366 cm^{-1} were assigned to C-H from Ma sulfated fucans, and COO^- groups from Ch-Pe. These peaks were downshifted compared to Ch−Pe due to a possible hydrogen bonding between Ma and Ch functional groups. The FT-IR spectrum of Ma−Ch−Pe material indicated that the intensity of the peaks at about 2021 cm^{-1}, 1650 cm^{-1}, 1593 cm^{-1}, 1309 cm^{-1} and 1064 cm^{-1} changed and even some of them disappeared compared to the peaks of Ch-Pe. These results may suggest that in the Ma−Ch−Pe samples, different interactions could occur between functional groups such as N-H, C=C, C-O-C, S-O, and C=N.

The XRD patterns of the Ma-Ch-Pe biocomposite are reported in Fig. 3.2. The XRD profile of Ma-Ch-Pe composite presented two broad peaks at 2θ = 14.69 and 22.8°, which correspond to the presence of amorphous cellulose [222]. However, the reported peaks for chitosan are closer to cellulose values (11.3 and 23°), and both peaks would be overlapped [223].

Table 3.4 FTIR characteristic bands of Ma, Ch, Pe and Ma−Ch−Pe biocomposites.

Ma (cm^{-1})	Ch (cm^{-1})	Pe (cm^{-1})	Ma-Ch-Pe (cm^{-1})	Vibration assignment
3338	3352	3354	3309	H−O; N−H
2915	2916	2918	2940	C−H (sp^3); N-H
2848	2863	-	2863	-CH_2; N-H
-	1748	1730	1764	C=O (-COOH)
1638	1654	-	-	N-H; C=O
-	1590	1600	1597	C=C; C=O
1407	1424	-	1420	-CHO; $CH_3{\cdot}SO_2$
-	1381	-	-	-CH; -SO_2; -CO_2
1338	1313	1222	1316	-CO; SO_2; -CO; -OH
1155	1147	-	-	-CO; C-O-C
1074	1068	1094	-	C-O-C; C-N
1020	1032	1012	1025	C-O
822	892	830	895	C-O-C; S-O; C-N; C-H
592	676	-	680	C−O

Many processes are involved in the biocomposite synthesis reported herein. Chitosan solubilization (pH < 6.5) occurs by protonation of the –NH_2 group (R−NH_2 + H^+ ↔ R−NH_3^+) on the C-2 position of the D-glucosamine repeat unit, transforming the polysaccharide to a polyelectrolyte in acidic media [224]. Chitosan in solution can form electrostatic interactions with the negative unesterified uronic acid residues of pectin (−COO^- $^+NH_3$), allowing the creation of junction zones to form a network [225]. Numerous interactions are involved in the gelation process such as

electrostatic repulsion, “ionic crosslinking,” hydrophobic effects (by − CH_3 group), and hydrogen bonding interactions (groups involved are −OH, −NH, and –C=) [226].

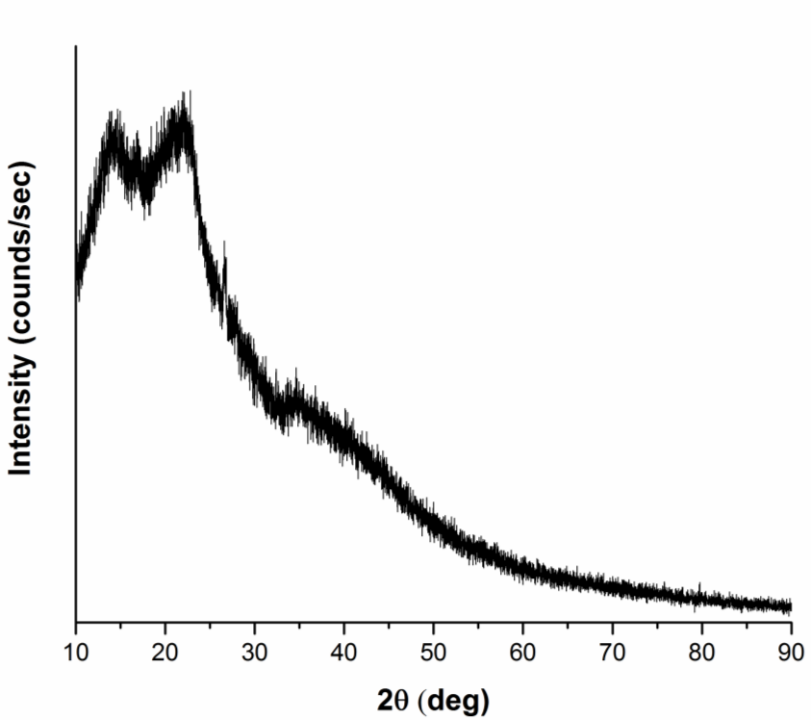

Fig. 3.3 X-ray diffraction pattern of Ma-Ch-Pe biocomposite.

Potentiometric titrations

The surface charge of the biosorbents was determined through potentiometric titrations as a function of pH (Fig. 3.3). Acid dissociation constants were calculated from potentiometric data (Table S8). The titration curve of pristine chitosan shows that under low acidic conditions, the surface registered positive values, but with an increase in pH, the surface charge changed to negative values. The two main basic sites detected from Ch were amine (-NH_2) (pK_a 8-11) and hydroxyl groups, confirmed by previous reports [74]. The point of zero charge was located at pH_{PZC}= 8.2. On the other hand, a marked presence of carboxyl groups (pK_a 3-5) and hydroxyl groups, lowered the surface charge of pectin to negative values, in accordance with previous reports [227].

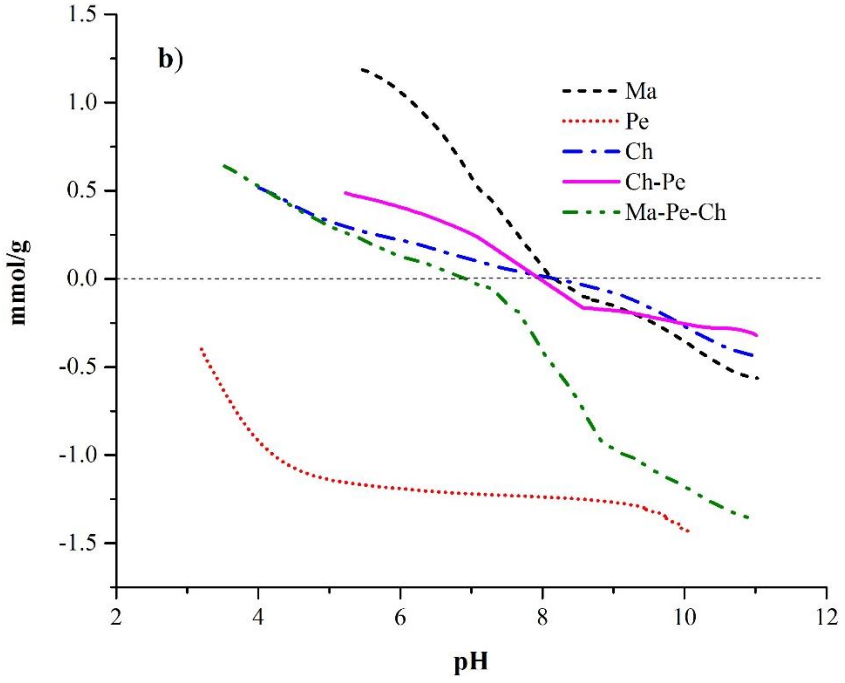

Fig. 3.4 Surface charge Ma−Ch−Pe, Ch-Pe and the precursors Ma, Ch, and Pe as a function of pH.

Table 3.5 Quantity of acidic groups for the sorbents under study determined at an ionic strength of 0.1 M NaCl.

Quantity of acidic groups (mmol·g^{-1})					
Biosorbent	*Strong*	*Weak*		Total	pH $_{PZC}$
	pH < 4	Very weak pH > 7	4 < pH < 7		
Ma[a]	[b]	0.46	0.51	0.97	7.6
Ch	[b]	1.90	[b]	1.90	8.2
Pe	1.36	1.25	0.04	2.65	[c]
Ch-Pe	[b]	0.66	0.17	0.83	8.01
Ma-Ch-Pe	[b]	1.52	0.70	2.22	7.0

[a] Data from a previous report (Flores-Chaparro *et al*, 2017)
[b] Functional group not observed.
[c] No pH_{PZC} observed

The neutralization of the surface charge by Ch-Pe, was probably due to the synthesis of the ion pair ($-COO^- -NH_3^+$) as mentioned above. Moreover, a decrease of the negative surface charge could be associated to the formation of hydrogen bonds between the −OH groups of Ch, and the oxygen atom (-O···HO) from the D-

galacturonic acid unit of pectin [228]. Related to the macroalgae, the carboxyl groups of alginate were the more abundant in the cell wall, and the pH_{PZC} above 8 could be associated with amines (from proteins), sulfhydryl (pK_a 8-10) and hydroxyl groups (pK_a 9.5-13) from alginates, proteins, phospholipids, and polysaccharides, respectively [189]. The dominant presence of weak acidic (i.e., carboxylic and lactonic) functional groups in the Ma−Ch−Pe biocomposites could be related to the presence of lactone and alkaloid groups from Ma polysaccharides, and the dimeric repeating unit of Ch. Moreover, the reported quantity of very weak functional groups (pKa > 7) suggested a structural re-arrangement of hydroxyl and amine groups probably derived from hydrogen bond or London chemical interactions between Ch and Ma during the synthesis process.

3.8 Biosorption studies

The benzene, toluene, and naphthalene adsorption capacity of the selected biocomposite was determined in deionized water at the maximum solubility of each compound (Table S4). Fig. 3.4 shows the nonlinear fitting of the experimental data to Sips adsorption isotherm equation by STATISTICA software v.10. Table 3.6 presents the resulting maximum adsorption capacities (q_{max}) and isothermal parameters. According to the regression coefficient (R^2) and the sums of squares error (SSE), the biosorption process best fits the Sips isotherm. Sips adsorption isotherm equation can describe both Langmuir and Freundlich characteristics for heterogeneous surface systems like in the case of biosorbents. The exponential character of Freundlich equation can only accurately describe the lower concentration ranges by an exponential rise in the amount adsorbed with increasing concentration, while at high sorbate concentrations it shows an asymptotic behavior distinctive of the Langmuir isotherm [229].

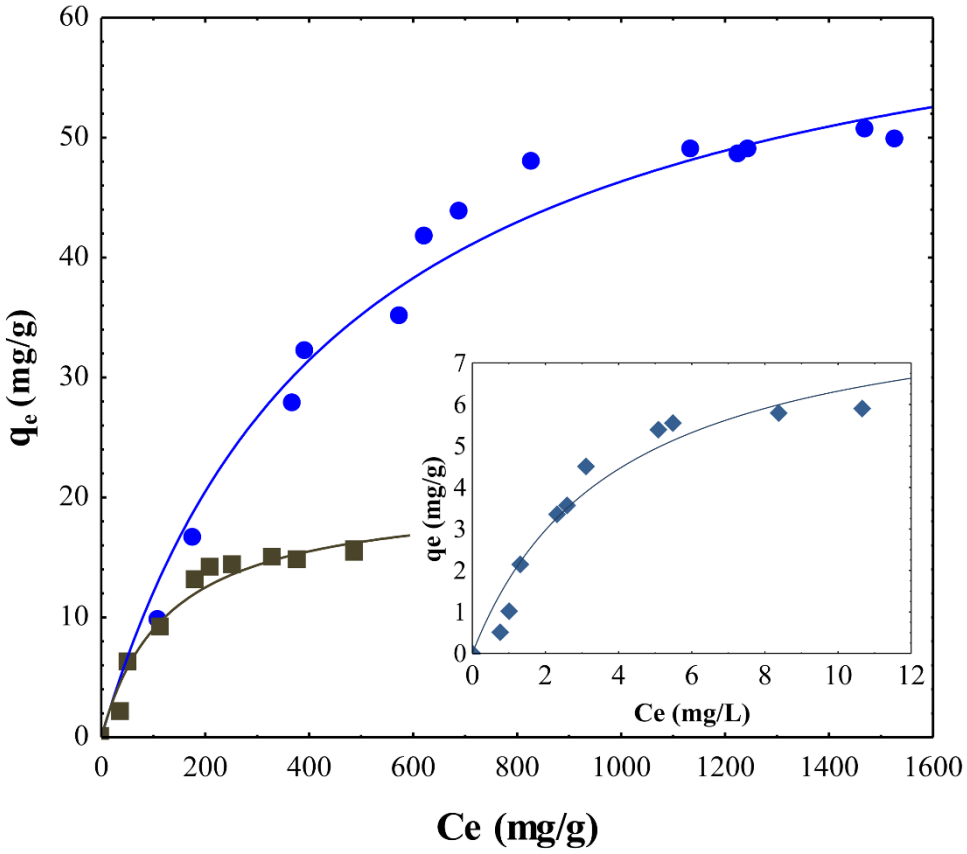

Fig. 3.5 Adsorption isotherm of (●) benzene, (■) toluene and (◆) naphthalene at initial pH 6 − 7, and 25°C. The lines represent the Sips adsorption isotherm equation.

A good fit of the data to the Sips adsorption isotherm ($R^2 > 0.98$) allowed to calculate the maximum removal values (assuming that adsorption occurs on a monolayer) of 58.68, 16.64 and 6.13 mg g^{-1} for benzene, toluene, and naphthalene, respectively (Table 3.6). The exponent *n* value represents the underlying affinity distribution for heterogeneous systems, which can vary from 0 to 1 [129]. The registered ($n > 1$) values for the three molecules under study means that the physical biosorption is more related to Langmuir adsorption behavior in comparison with Freundlich equation, which was also confirmed by the SSE value of Langmuir and Freundlich isotherm equations listed in Table 3.7. A dimensionless constant derived from Sips isotherm known as separation factor (R_L), was computed to predict the affinity between the sorbate and sorbent, indicating a favorable biosorption process. The textural properties of the biosorbent do not present steric limitations for the pollutants

diffusion (Table 3.6). The low surface area of the biosorbents does not entirely explain the affinity of non-polar hydrocarbon, for that reason the adsorption capacity is severely influenced by the biosorbent chemical composition, resulting from the precursors. Former studies established that many acid dyes molecules with one or more benzene aromatic rings are attached in a parallel manner to the amine groups of chitosan, then tend to form subsequent complexes and interactions [85,90]. Otherwise, hydroxyl groups could generate van der Waals interactions and Yoshida hydrogen bonding, particularly in the C–3 position, between chitosan chains and aromatic molecules [230]. Pectin also possesses additional −OH active sites in conjunction with carboxylic groups that contribute to dispersive interactions with the pollutants [211]. The HC biosorption mechanism in the brown macroalgae biomass involves the sum of the interactions occurring with the diversity of chemical components, including hydrophobic effect between lipids and lignocellulosic fractions (cellulose, hemicellulose, and lignin) [127], and to a lesser degree, nonspecific van der Waals interactions with carbohydrates (in particular with alginates) and proteins [132]. The loaded biosorbent with benzene and toluene was lyophilized and characterized by FT-IR in the range of 600 and 4000 cm^{-1}, and the results suggest that all functional groups are involved in the biosorption process, however the –OH and C-O chemical groups registered the main changes, suggesting the primary role of cellulose and hemicellulose in the biosorption process (Fig 3.5).

To elucidate the contribution of the Ch-Pe fraction to the total removal capacity of the Ma−Ch−Pe biocomposite, additional biosorption essays were performed for the three HC under study at the same conditions described in section 2.5. The biosorption was 7.35, 3.83, and 0.94 mg g^{-1}, for benzene, toluene, and naphthalene, respectively, which represents the 15, 24 and 22 % of the total removal capacity of the pollutants above. Therefore, the macroalgae fraction contributes more to the removal of the hydrocarbons, compared to chitosan and pectin immobilizing agents. These results agree with our previous ANOVA analysis where the P-value of pectin

and chitosan factors were higher than 0.05 in the factorial and the response surface methodologies.

Table 3.6 Textural properties of the biosorbents.

	A_{BET} ($m^2\ g^{-1}$)	$A^{\dagger}_{micro}$[1] ($m^2\ g^{-1}$)	A_{meso}[2] ($m^2\ g^{-1}$)	A_{macro}[3] ($m^2\ g^{-1}$)	V_{micro} ($cm^3\ g^{-1}$)	V_{meso} ($cm^3\ g^{-1}$)	V_{macro} ($cm^3\ g^{-1}$)
Ma-Ch-Pe biocomposite	0.119	ND	0.003	1.49×10^{-2}	ND	1.0×10^{-5}	2.0×10^{-5}
Macrocystis pyrifera	0.126	0.030	0.020	4.7×10^{-3}	2.1×10^{-5}	1.7×10^{-4}	2.7×10^{-4}
Chitosan	0.953	0.383	0.201	0.395	ND	1.9×10^{-4}	4.5×10^{-4}

$A^{\dagger}$ = Surface area; $V^{\ddagger}$ = Pore volume;
[1,2,3] micro-, meso- and macropores, respectively.
ND = Not determined

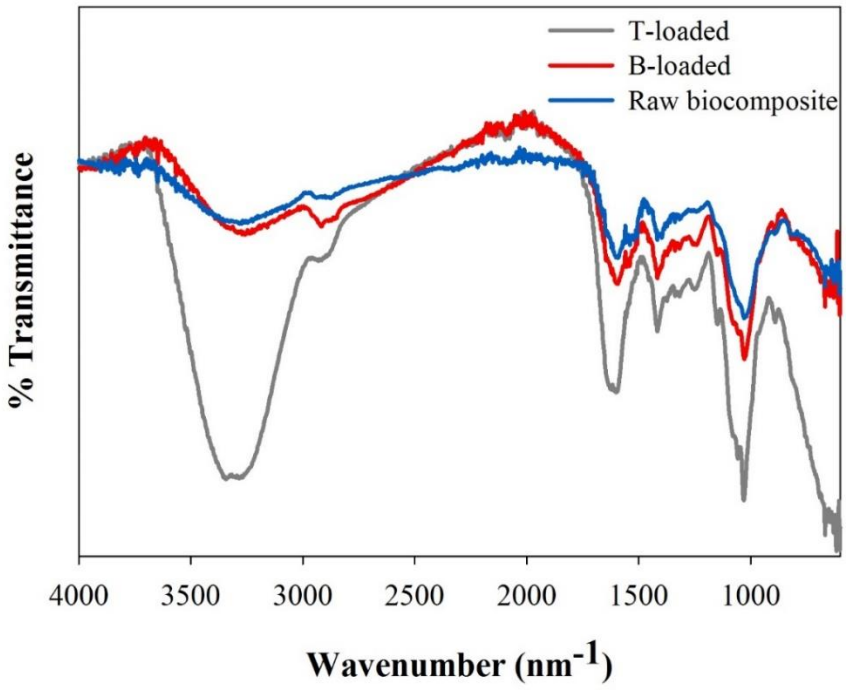

Fig. 3.6 FTIR spectra of the loaded toluene (T) and benzene (B) and the Ma-Ch-Pe biocomposite.

Effect of ionic strength

The effect of competing ions was investigated (Fig. 3.6a). A progressive decrease in the removal capacity was registered from an ionic strength value of 0.6 M. It is

supposed that a high concentration of salts promotes a partial neutralization of the surface charge, followed by the reduction of the electrical double layer by the Na^+ cation. Moreover, the solvated Cl^- anions (radii of 0.202 nm) could improve interactions with the biosorbent surface promoting pore occlusions and avoiding many of the unspecific interactions related to a lower swelling degree (%) about the SW in deionized water. Preliminary studies have shown similar results for different brown macroalgae biomass [231]. Instant Ocean® is a particular case of study because this solution also contains different ions ($I \approx 0.76$ M) and organic matter that may block pores, preventing the diffusion of the adsorbate to the active sites. Also, hydrophilic interactions from the mineral content of the artificial seawater solution may be enhanced by the increase of I, generating biosorption competition by water clusters [121]. It was observed a slight increase in desorption capacity for all the pollutants (Fig. 3.6) because the high ionic concentration of ions also with a low surface area (0.9 and 0.2 $m^2\ g^{-1}$ for chitosan and macroalgae biomass respectively) overcome some of the dispersive adsorbed molecules [119]. However, 88, 76 and 69% of benzene, toluene, and naphthalene, respectively, remained adsorbed to the composites after 12 h exposure to deionized water.

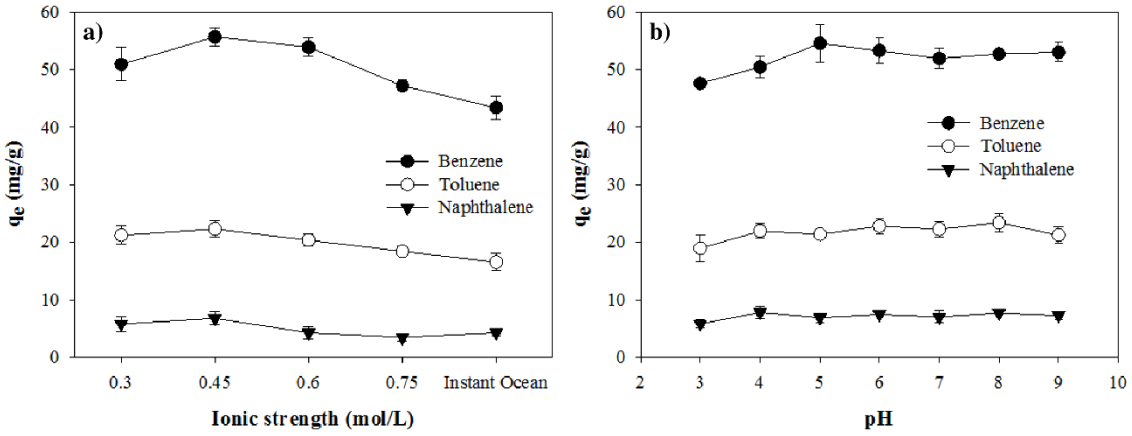

Fig. 3.7 (a) Effect of the ionic strength on the biosorption capacities of benzene, toluene and naphthalene by Ma–Ch–Pe biocomposite; (b) pH effect of benzene, toluene and naphthalene uptake by Ma–Ch–Pe biocomposite.

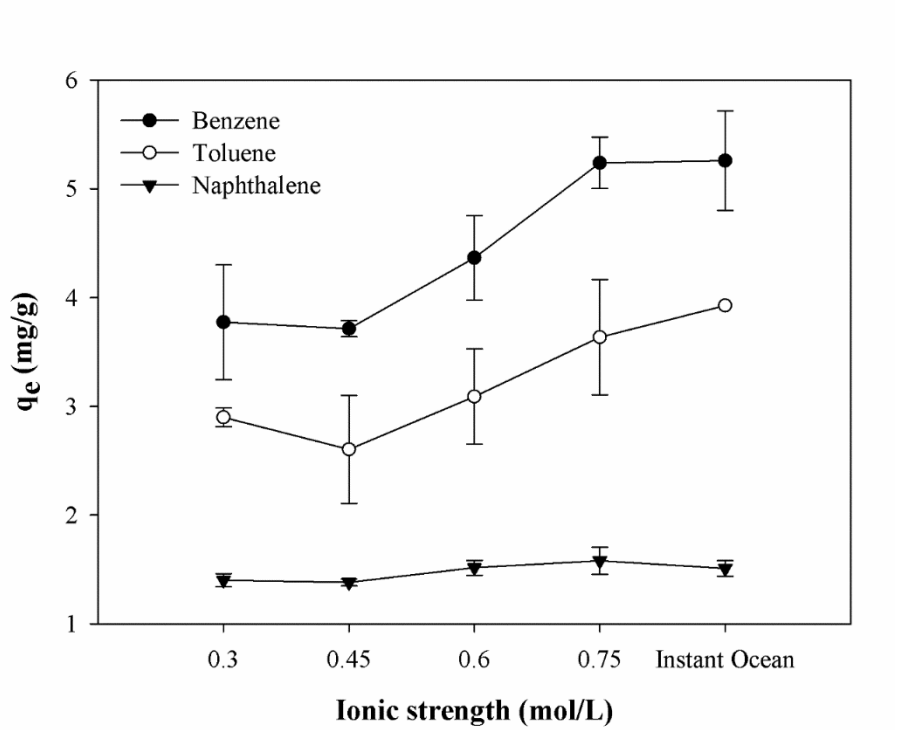

Fig. 3.8 Effect of the ionic strength on the desorption capacities of benzene, toluene, and naphthalene by Ma–Ch–Pe biocomposite.

Table 3.7 Parameters of the isotherm equations, correlation coefficients (R^2) and error function values of the models for organic compounds adsorption.

	Ma–Ch–Pe composite		
	Benzene	Toluene	Naphthalene
Langmuir			
q_{max} (mg·g^{-1})	67.71	20.45	8.80
b (L·mg^{-1})	0.002	0.008	0.255
R_L	0.207	0.186	0.121
SSE	72.10	11.57	2.57
R^2	0.979	0.964	0.973
Freundlich			
n	0.446	0.421	0.516
K_F	2.08	1.25	2.01
SSE	208.11	28.92	5.52
R^2	0.942	0.911	0.887
Sips			
b	0.0004	0.0007	0.227
q_{max} (mg·g^{-1})	58.08	16.64	6.13
n (L·mg^{-1})	1.35	1.61	2.096
R_L	0.587	0.719	0.134
SSE	42.47	4.69	0.35
R^2	0.988	0.985	0.992

3.9 Effect of pH

Fig. 3.6b shows that the pH of the system (5–9) has no significant effect on the removal ratio of the adsorbates. The biosorption capacity minimally changes and is maintained at approximately 50, 20 and 8 mg g^{-1} for benzene, toluene, and naphthalene, respectively. The reinforced Ma-Ch-Pe biocomposite was tested by quantifying its mass loss after being placed in contact with water at a slightly acidic pH (5) during 24 h. Mass loss between 1.2- 2.9 % from the chemical stability essays reflect that the polymeric matrix of Ch covered and strengthened the macroalgae biomass. This data is by the swelling degree (380) of the biocomposite, which is lower than the value of the fresh macroalgae biomass of 570, reported previously [79].

The hydrolytic stability was tested to assess the effect of temperature on the biosorbent constitution (Fig. 3.8). Two samples were stored at 25 and 35 °C for 100 h at neutral pH. Thermal degradation was negligible between the two temperatures, with a mass loss percent of around 15 % in both samples. The water stability of the biocomposites could be associated with hydrophobic polymers like cellulose and chitosan, but higher temperatures may increase inter-chain mobility and the hydrophilic character of the biosorbents.

During the synthesis process, there are remnants of amino groups and carboxylic groups that are not associated by columbic forces in the polyelectrolyte complexes. Free $-NH_2$ and −COOH active sites may form hydrogen bonding with −OH and $-COOCH_3$ from pectin. These interactions are sensible to dissociate in acidic and alkaline mediums, respectively [232]. It was previously reported that in Ch-Pe composites, the swell behavior is limited when 3< pH <8, however, this values significantly increase when pH < 3 and pH> 8 due to the weak intermolecular forces through the dissociation of the hydrogen bonding [93]. These polymers were reported not to precipitate or solubilize until extreme conditions of pH and temperature [233]. However, this phenomenon could explain the lower biosorption values in acidic (3-4) solutions in the present work (Fig. 3.6). Thus, although there was a decrease in the adsorption capacity under the conditions analyzed, compared

to the previously reported capacity for pristine algae [79], Ma–Ch–Pe composites have a significant advantage over previous ones considering the strengthening of their physical properties, which allow them to be applied on a larger scale (e.g. pilot or industrial).

The influence of the surface charge in electrostatic interactions between adsorbate and adsorbent should be observed in organic ionizable compounds (i.e., dyes), but the molecules under study were in the non-ionizable form in the whole ranges of pH [123]. In this case, hydrophobic interactions between the adsorbates and the lignin and lignocellulosic fraction of the macroalgae biomass would remain the main significant fraction for biosorption.

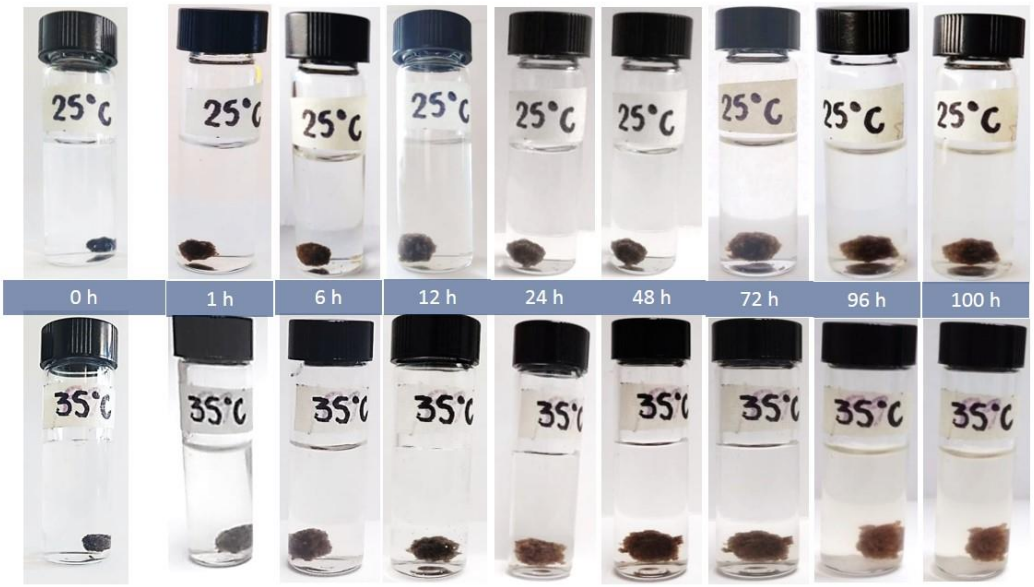

Fig. 3.9 Hydrolytic stability test at 25 and 35°C from 0 to 100 h.

3.10 Biosorption kinetics

To evaluate the effects of DOM on the removal rate of benzene, toluene, and naphthalene, experiments were carried out by using natural water from a reservoir containing 19.3 mg L^{-1} of DOM. The adsorption of HC in the presence of DOM (Fig. 3.9a,b) could be divided into two steps: external diffusion and surface adsorption.

Both were promptly achieved through the former step, and the equilibrium was gradually reached in the second step. These results suggest that except *M. pyrifera* biomass, the biosorption capacity is mainly limited by external diffusion. The kinetic data were found to fit better the pseudo-second-order kinetic equation (Table 3.8), except benzene, which has reported a slightly better approach to the pseudo-first-order equation. HC rate removal increased (Fig. 3.9c) in natural water (NW) compared to deionized water (DW). In this sense, the biosorption capacity increased 33, 61 and 47 % for benzene, toluene, and naphthalene, respectively.

Based on the literature, the natural organic matter may promote a covalent bond with chitosan through carboxylic acid functional groups [234]. The same kind of interaction could be expected from pectin, and the macroalgae biomass, because these fractions share the same surface active sites. Moreover, humic acids, which are present in DOM, have a significant degree of aromatic polymers, chemical compositions, functional groups (aliphatic and alicyclic) and charge density [235]. The light absorbing a fraction of DOM (CDOM) corroborated a high aromaticity degree ($SUVA_{254}$ = 0.976 L mg^{-1} m^{-1}), and the presence of higher molecular weight components like humic acids (E2: E3 ratio = 5.03). Humic acids are hypothesized to have an open network forming aggregates with voids that could join to the Ma-Ch-Pe composites, promoting hydrophobic and π interactions between the biosorbents and the aromatic hydrocarbons, explaining the increase on the removal capacity.

A comparison of the biosorption capacities of the HC understudy on different adsorbent surfaces and cellulosic precursors is presented in Table S11. The Ma−Ch−Pe composite in this study exhibited comparable biosorption capacities and even higher than other natural materials like wood chips or bagasse [9,62,62,236–239]. Additionally, the biosorbent offers all the properties to be used in subsequent flow-through biosorption studies. Additionally, the biosorbent offers all the properties to be used in subsequent flow-through biosorption studies. Further research regarding the effective biosorption of aromatic pollutants by the Ma-Ch-Pe biocomposite and the effect of multi-solute systems will be subject of future publications.

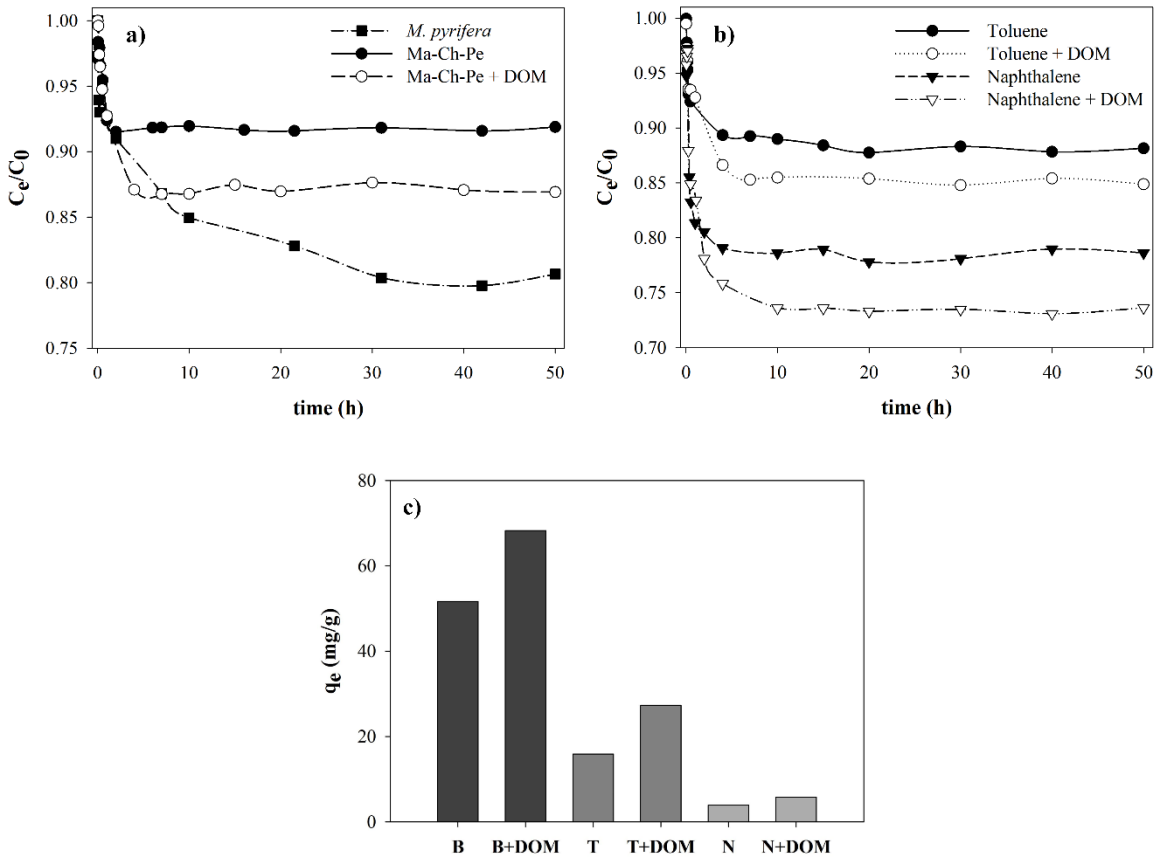

Fig. 3.10 (a) Benzene biosorption rate onto (■) macroalgae biomass, (●) Ma−Ch−Pe, (○) Ma−Ch−Pe and dissolved organic matter (DOM); (b) Effect of DOM in the rate of adsorption of (●) toluene, (○) toluene + DOM, (▼) naphthalene, (▽) naphthalene + DOM; (c) Adsorption capacity of benzene, toluene and naphthalene in the presence of organic matter.

Table 3.8 Pseudo-first order, pseudo-second order and Weber-Morris rate equation parameters for removal of benzene, toluene, and naphthalene.

	MA-CS-Pe Composite.					
	Benzene	B + DOM	Toluene	T + DOM	N	N +DOM
Pseudo-first order						
k_1 (h^{-1})	1.86	0.60	2.69	1.07	0.58	0.33
q_e (mg g^{-1})	51.4	65.4	15.8	25.7	3.95	5.75
SSE^{β}	204.5	666.3	38.4	67.4	2.36	4.32
R^2	0.94	0.91	0.91	0.94	0.92	0.93
Pseudo-second order						
k_2 (mg $g^{-1}{\cdot}h^{-1}$)	0.06	0.014	0.22	0.06	0.22	0.08
q_e (mg g^{-1})	52.9	69.5	16.6	27.0	4.17	6.25
SSE	247.1	423.4	20.2	34.5	1.67	2.70
R^2	0.93	0.94	0.95	0.97	0.94	0.96
Weber-Morris model						
k_3 (mg g^{-1} $h^{1/2}$)	4.85	8.77	1.68	3.38	0.53	0.87
C	26.3	21.72	7.80	8.63	1.17	1.25
SSE	1686	1987	190	312.8	7.71	11.7
R^2	0.53	0.73	0.53	0.73	0.73	0.83

SSE^{β}=Sum square error, calculated by the formula: $\sum_{i=1}^{n}\left(q_{e,cal} - q_{e,meas}\right)_i^2$, where $q_{e,cal}$ and $q_{e,meas}$ are the calculated and measured adsorbate concentrations at any specific time in the case of adsorption kinetics (mg g^{-1}).

3.11 Conclusions

A factorial experiment design in conjunction with a surface response methodology was applied to find the optimal conditions (75.4%, 19.8, and 4.8% for macroalgae biomass, chitosan, and pectin, respectively), to remove the highest benzene concentration from water, as an aromatic hydrocarbon model. The chitosan and algae biomass content were the main factors involved in the process. The biosorption mechanism is a sum of interactions between the diversity of chemical components of the composite precursors and involves mainly hydrophobic effect between lipids and lignocellulosic fractions (cellulose, hemicellulose, and lignin) and non-specific van der Waals interactions with carbohydrates, proteins, chitosan, and pectin contents. The pH of the system (3–9) has no significant effect on the removal capacity because of the non–ionizable character of the HC. The hydrocarbons affinities were not affected at least up to I = 0.6 M, but at higher concentrations, there was a decrease in the adsorption capacity by pore occlusion by water molecules and competition for surface active sites of the biocomposite. The presence of dissolved organic matter enhanced the biosorption capacity by the stimulation of hydrophobic interactions between the biosorbent and the adsorbates. Moreover, the results reported in the present work showed the potential of the synthesized composites to be applied in the removal of benzene, toluene, and naphthalene from polluted natural water in batch processes. Future work to assess the feasibility of the biosorbents will include the setup of a continuous system and incineration technologies of saturated materials. The experiments in the following study will also consider multicomponent systems, the bioavailability, and toxicity to aquatic organisms.

CHAPTER 4

Pillared graphene oxide biocomposite as a potential adsorbent of water-soluble hydrocarbons

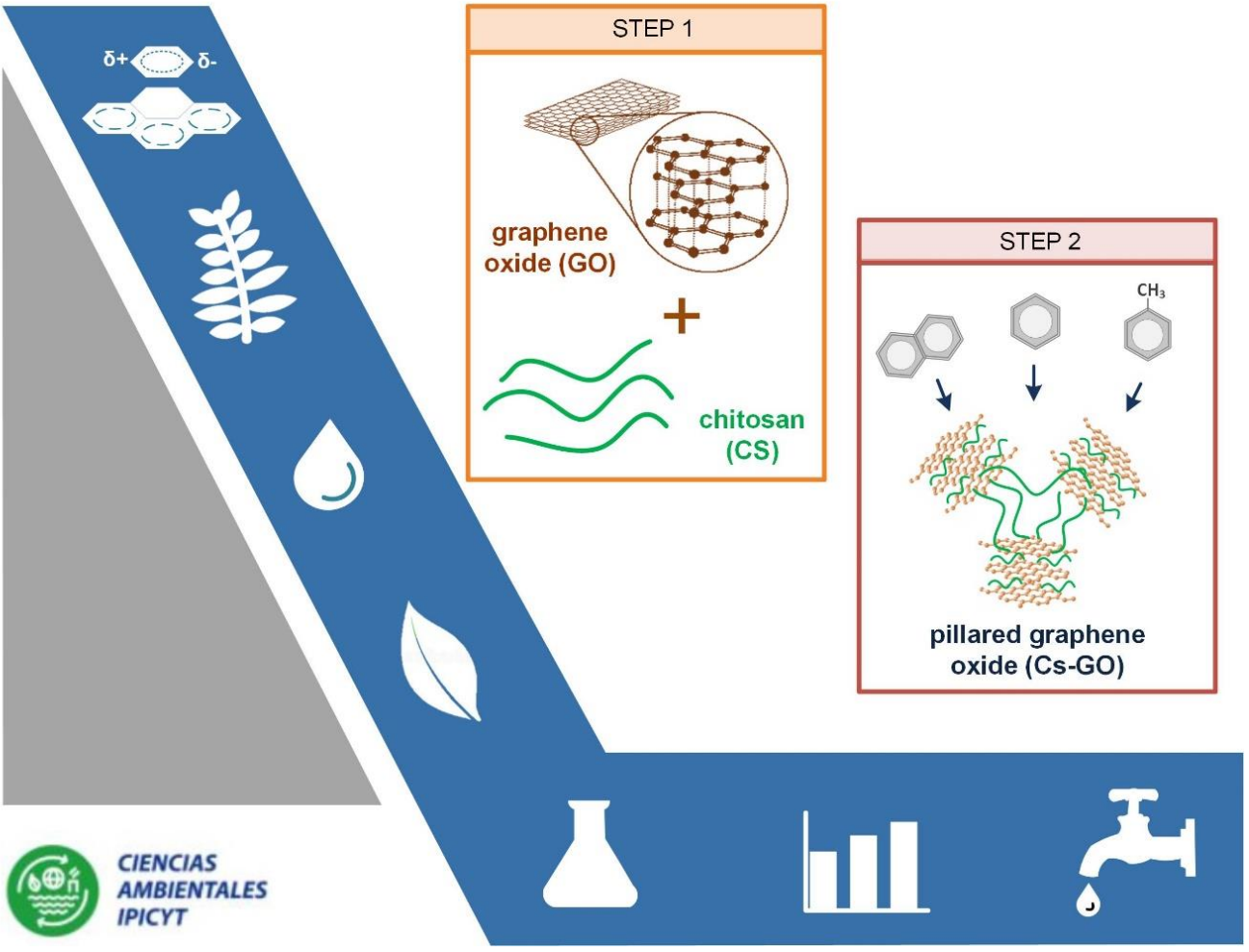

This chapter is adapted from: *Pillared graphene oxide biocomposite as a potential adsorbent of water-soluble hydrocarbons: Effect of pH, organic matter and ionic strength.* In revision.

CHAPTER 4

4.1 Abstract

Graphene oxide (GO) is characterized by containing oxygen groups, and intrinsic properties which make it a potential candidate for many applications through chemical functionalization. However, has a significant disadvantage as low dispersibility in water, causing the surface area to decrease, and therefore, limiting its applications as an adsorbent. Therefore, alternative ways to functionalized graphene oxide with water-dispersable materials are needed to create GO composites for further applications. By introducing molecules or other carbon-based components between GO sheets (pillared agents), an increase in the surface area of the material could be observed. Also, a pillared GO composite may represent an improvement in the removal capacity of the main-soluble hydrocarbons in water (benzene, toluene, and naphthalene). This work is aimed to employ pillared graphene oxide produced by using chitosan at a ratio of CS/GO = 0.1 corresponding to a surface area of 47 m^2/g. The affinity toward benzene, toluene, and naphthalene was evaluated at different systems varying pH, and organic matter content of 19.3 mg L^{-1}. Adsorption data was well-described by Sips and Langmuir adsorption isotherm models. Different pH values in the aqueous media did not influence adsorption performance. Also, in the case of dissolved organic matter, low diffusivity constant values (k_1) were observed. These results show the feasibility of chitosan as a precursor in the development of a surface area of CS-GO composites for the removal of soluble hydrocarbons in water.

4.2 Introduction

The mono-aromatic hydrocarbons benzene, toluene, and the poly-aromatic naphthalene are common pollutants found in gasoline and widely used for numerous industrial applications [239]. These pollutants are a matter of significant concern regarding their high solubility and bioavailability to aquatic organisms [34]. Recent research efforts have been conducted in this field including physicochemical and biological approaches such as advanced oxidation processes, membrane filtration, thermal processes and so on [240–243]. Despite these methods, adsorption

technologies are the most widely applied treatment due to its flexibility, high efficiency, and cost-effective characteristics. Different types of organic [7] and inorganic [73] media were evaluated as adsorbents for water treatment of aromatic compounds. Among all of them, carbon-based materials possess comparatively high surface area, availability of adsorption sites and chemical stability. Moreover, the evaluation of new carbonaceous nanomaterials has grown as potential alternatives to conventional activated carbon (AC) and included carbon nanofibers, carbon nanotubes, fullerene among others [202].

In this sense, graphene, which is a relatively new class of carbon allotrope, and specifically, graphene oxide (GO) has generated numerous scientific reports related to the removal of a wide range of pollutants in water [244]. It is well known that the superior properties of graphene are associated with its single layer. However, GO tends to form irreversible agglomerates or restack to graphite in aqueous solutions through strong π-π stacking and Van der Waals interactions [65]. As with many nanoscale materials, the self-agglomeration of GO particles has restricted its application in large-scale processes [245]. Hence, modification and functionalization of graphene sheets is a critical challenge in the synthesis and control of the aggregation process. This phenomenon can be reduced by the attachment of other small molecules or polymers to the graphene sheets.

The use of flocculant agents as an active immobilization technique could be applied to both problems above, improving the interfacial interaction between adsorbate and the macroalgae biomass or GO sheets. Moreover, the application of polysaccharides as chitin and its derivate chitosan (CS), has received particular attention because possess a remarkable quantity of amine and hydroxyl groups that interact with negatively charged substances and high affinity toward pollutants like metals and dyes [85,210].

In the literature, previous adsorption studies by CS/GO composites employed pre-establish ratios of both precursors for methodology synthesis of the final adsorbent. However, a specific amount of chitosan soluble polymer may promote a pillaring effect in the GO sheets resulting in a noticeable increase in the final CS/GO surface area. Finally, this approach possibly will enhance the affinity toward water-soluble aromatic molecules.

In summary, this investigation will be focused on the synthesis of a pillared GO by chitosan molecules (CS-GO), which will be used for the removal of three of the main soluble hydrocarbons in water (benzene, toluene, and naphthalene). These studies will include the effect of pH and organic matter on adsorption, in conjunction with the physicochemical characterization of the composites to explain the adsorption mechanism(s).

4.3 Material and methods

Chitosan (Ch) (with a molecular weight of 50,000 – 190,000 Da and a ≥ 75 % degree of deacetylation). GO was prepared according to modified Hummers method [246] including the pre-oxidation treatment. A two-step acid-acetone further purified the GO sample–acetone to remove the salt by-products [67]. The GO was further dispersed in water at a final concentration of 2.3 mg/L. The model pollutants will be benzene, toluene, and naphthalene (Sigma–Aldrich, 99% purity).

Synthesis of GO-CS adsorbents

Preparation of chitosan-graphene oxide (CS-GO) composites was made according to previous studies [99]. Briefly, chitosan aqueous was prepared by mixing 0.12 g chitosan powder into 2.5% (v/v) acetic acid solution, then different ratios of GO (25, 50 and 75 % w/w), were dispersed in 10 mL distilled water with sonication to for 10 minutes to form the mixture. Then, the different GO ratios were slowly added to the chitosan solution. The resulted mixture was stirred for at least 12 h and dried in a

vacuum oven for 60 °C. Three types of chitosan were evaluated, a low, medium and high molecular weight samples provided by Sigma-Aldrich.

GO-CS characterization

Quantachrome Autosorb-1 instrument was used to obtain N_2 isotherm at 77 K, from which surface area ($m^2\ g^{-1}$) and were calculated by BET isotherms equation. Surface morphology of graphene oxide, chitosan, and graphene oxide/chitosan composites were characterized using a field emission Scanning Electron Microscope LEO-SEM 1530 VP operating at 5.0 kV for all ranges of resolution. Before imaging, the samples were coated with a layer of AuPd (~2 nm). X-ray diffraction spectrometry was performed with a Bruker AXS D8 with Cu KR radiation, λ = 1.5418 Å. Raman spectroscopy was performed on a Witec Alpha 300 Confocal Raman Microscope. FTIR spectroscopy was performed on a Jasco Instruments FT/IR-4100 with an ATR attenuated total reflectance mode. The zeta potential was evaluated using dynamic light scattering on Malvern Zetasizer Nano – ZS.

Adsorption experiments

The hydrocarbons uptake by pillared CS-GO will be determined in diluted solutions and also in the maximum solubility concentration of each pollutant in water [247]. In brief, 14 mL of a specific hydrocarbon concentration and 5 mg of the GO-CB-CS biocomposite was added into amber glass flasks. Flasks will be sealed and placed in a shaker at 25 °C, at 120-130 rev/min for 4 h. Adsorption kinetics will be studied by adding the mass above of adsorbent to a series of the solution at the same initial concentration of hydrocarbons. The bottles will be incubated, and the samples will be taken at the different time to determine the remaining concentration of HC. The initial and equilibrium concentrations of adsorbates will be determined by a UV-Vis spectrometer at a wavelength of 254.5, 261 and 284 nm for benzene, toluene, and naphthalene, respectively.

4.4 Results and discussion

4.4.1 Physicochemical characterization

Characterization results

Different ratios of chitosan were evaluated to find a pillared effect in the final surface area of the graphene oxide/chitosan composite. After different tests (Fig 4.1a), a CS/GO ratio of 0.1 with unmodified low-molecular-weight chitosan represented the best approach (47 m^2 g^{-1}) in the improvement of the surface area of GO. The pore size distribution was characterized by macro- and mesopores (Fig. 4.1b) In comparison to the surface area value of the precursors (< 2.6 m^2 g^{-1}), this CS/GO ratio represents a significant improvement with adequate adsorbent characteristics. The surface morphology of the GO and CS-GO structures are presented in Fig. 4.2a. GO sheets usually form aggregated structures and typical ripples because of the presence of intermolecular forces (Fig.4.3a) [153]. The introduction of CS molecules certainly enhance the surface area, but a considerable portion of the interlayer surface of GO sheets is still lost (Fig 4.3b,). These results give evidence relevancy of the ratio of a precursor for pillaring porpoises. It was previously reported that a good dispersion of GO sheets enhances the probability of interactions in the suspension [67]. Moreover, the opposite charges within the work solution (pH ~ 4), promote charge stability through the opposite charge of the precursors. Chitosan can be seen inside the graphene oxide layers with an average size of the particles between 3-4 nm.

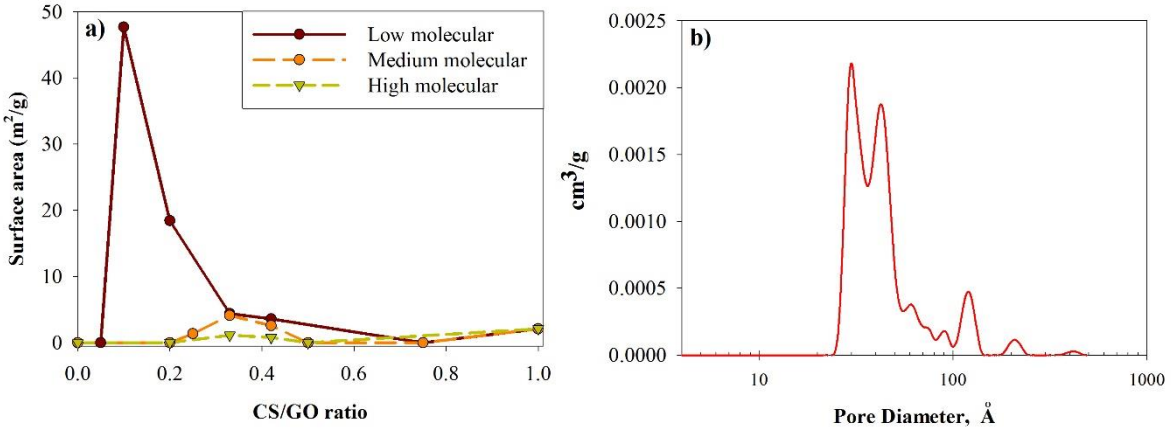

Fig. 4.1 Surface area (m^2/g) of different Cs/GO ratios. The Cs/GO ratio of zero means 100% GO, and a Cs/GO ratio of 1 means 100 % CS.

The zeta potential versus pH profiles of the composites used in this study is shown in figure 4.2b. Zeta potential is a powerful tool for electrical properties and colloidal stability characterization. The zeta potential of the chitosan went from highly positive at pH 3 to slightly negative at pH 10, which can be attributed to the presence of cationic amino groups along the polymer backbone [248]. Graphene oxide presented a negative zeta potential consistent with previous studies [249]. The highly negative value indicates the stability of the suspension [250]. Because of their opposite electrical properties, chitosan can strongly attract negatively charged GO sheets through electrostatic interactions and form multiple hydrogen bonds, increasing the bonding force between GO sheets [136]. Two CS/GO composite profiles are shown in the figure. The zeta potential of the CS/GO 0.25 went from highly positive at pH 3 to highly negative at pH 10. The zeta potential of the CS/GO 0.1 went presented negative values that are consistent with graphene oxide zeta potential [249]. This is an evidence of the well-distributed chitosan inside the graphene oxide layers.

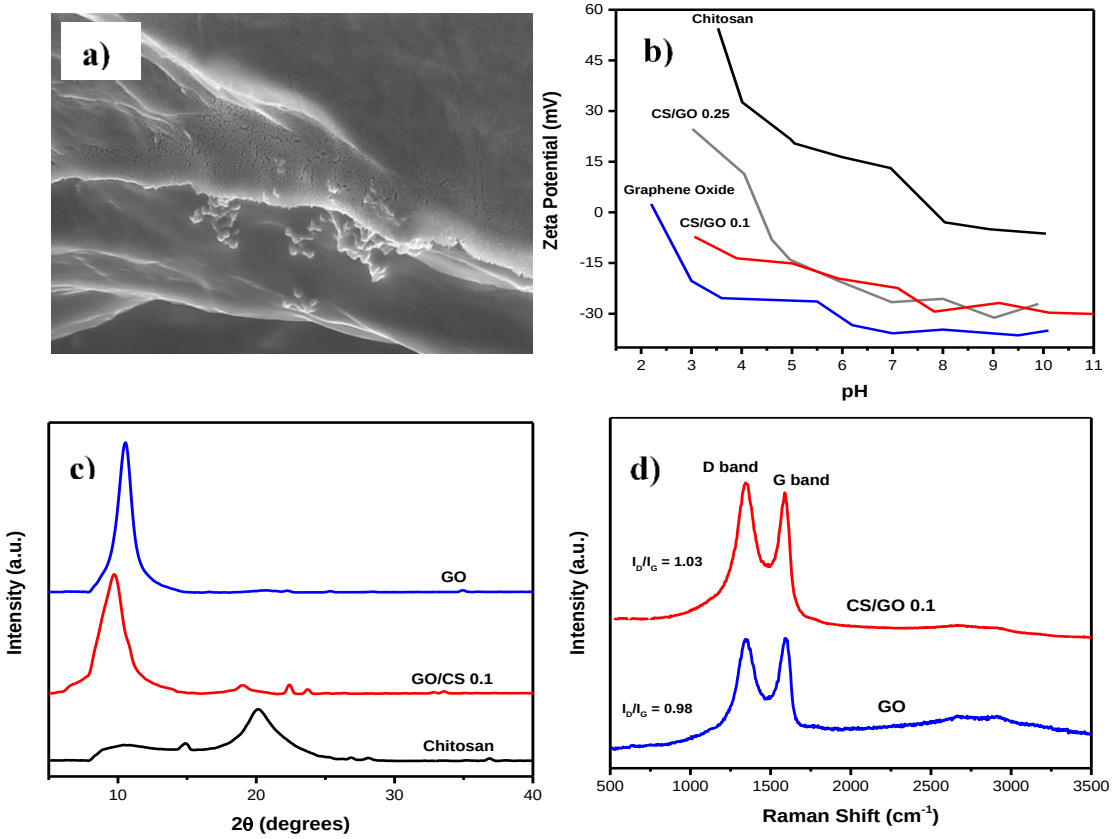

Fig. 4.2 a) SEM image of CS/GO composite; b) zeta potential of GO, CS, and CS/GO composites; c) X-ray diffraction pattern of GO, CS and CS/GO composites, and d) Raman spectra of GO and CS/GO at its optimum ratio

The X-ray diffraction pattern of pure GO has a peak of 2θ = 10.54 (figure 4.2c). The corresponding interlayer spacing is 0.843 nm, which is similar to previously reported for stacked graphene oxide sheets [223]. The interlayer spacing is calculated using Bragg's Law [251]. The chitosan diffraction pattern has two peaks, one at 2θ = 20.5 and a broad peak at 2θ = 10.7. These peaks can be attributed to hydrated and anhydrous crystals, respectively [68]. The CS/GO composite does not present any peaks related to chitosan, which indicates the chitosan is well distributed inside the graphene oxide sheets. The peak at 2θ = 9.7 in the diffraction pattern of the CS/GO corresponds to an increased interlayer spacing of 0.915 nm. The increased interlayer spacing can be associated with the uniform distribution of the chitosan on the graphene oxide layers.

Raman spectroscopy is a useful technique to characterize carbon composite materials. The Raman spectra for the composites in the present study are shown in Figure 2d. The spectrum of GO sheets shows three bands at 1592, 1352, and 2682 cm^{-1}, which can be assigned to the G, D, and 2D bands, respectively. The G band is a result of a C-C bond stretch, being typical for all sp^2 carbon forms [252]. This band is formed from first-order Raman scattering [9]. The D peak is related to vacancies defects and oxidized domains in graphene oxide. Furthermore, it is also well known that the D/G peak intensity ratio can determine the sp^2 area size of graphene sheets containing sp^3 and sp^2 bonds [253]. In the present case, the results indicate that the D/G ratio value changes from 0.98 to 1.03 after the self-assembly of chitosan on graphene oxide layers, as seen in Figure 2d.

The interaction between the amino polysaccharide of chitosan (CS) and GO sheets have been reported through (1) The aforementioned electrostatic interactions of the negative surfaces of GO in solution with the cationic character of CS, and (2) the formation of an amide bond between the amide group of CS and the carboxylic groups of GO [247]. FT-IR spectroscopy and potentiometric titrations confirmed these interactions. Changes in the absorption peaks at 1720 and 1056 cm^{-1} corresponding carboxylic and amide groups, respectively were identified (Fig. 3). Furthermore, a decrease in the peaks of carboxylic and phenolic groups (mention the specific pK_a and concentrations) were detected.

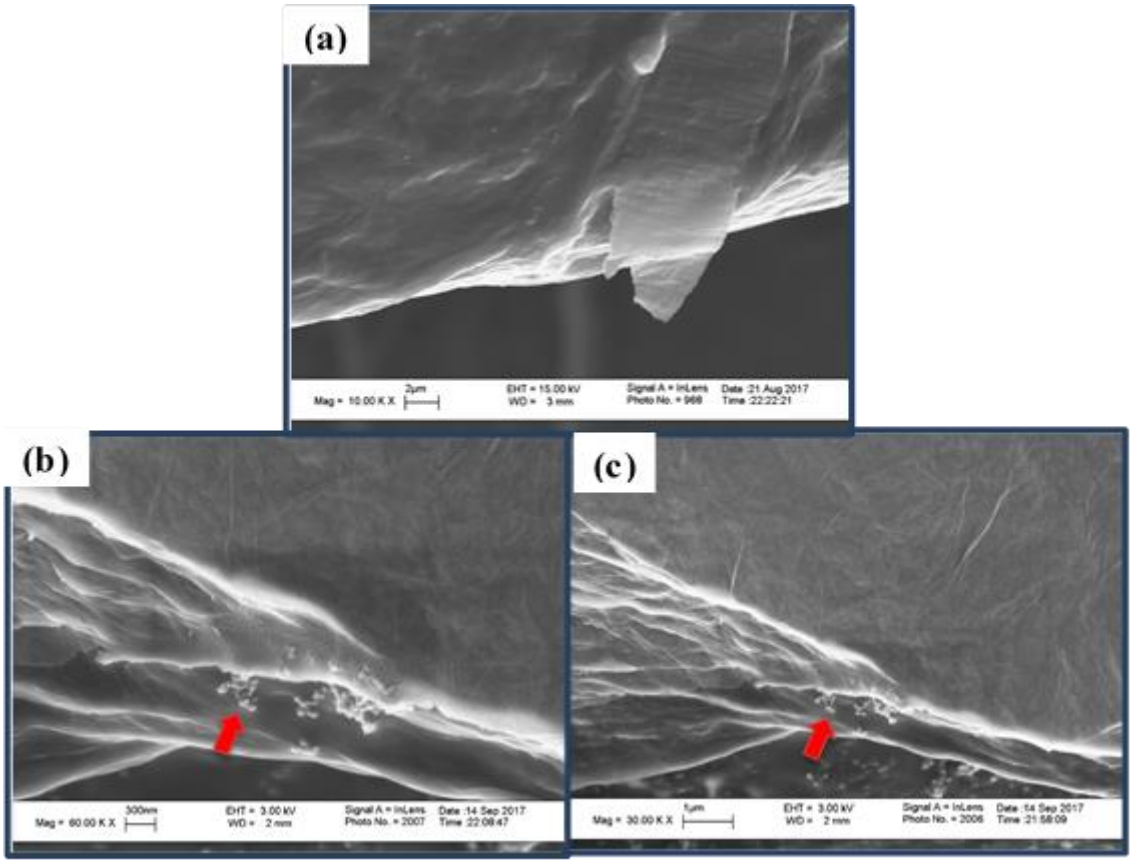

Fig. 4.3 (a) SEM picture of GO (b,c) SEM images of CS-GO composites. The arrows indicate the presence of Cs particle between the GO layers

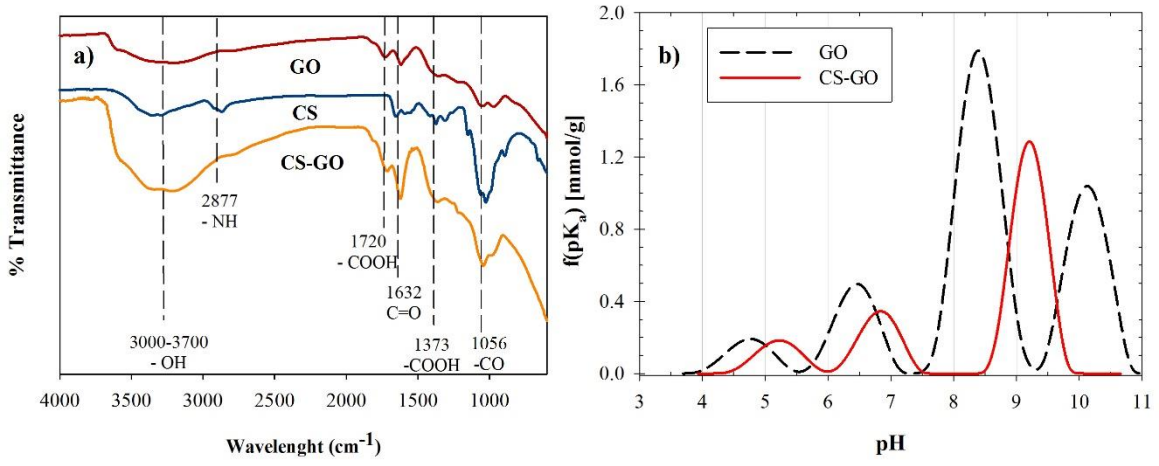

Fig. 4.4 (a) FTIR spectra of the CS/GO composite and the precursors; (b) pK_a distribution for GO and GO-CS composite

4.5 Adsorption experiments

Adsorption points were realized at the maximum solubility value in water (1800, 515 and 31.5 mg/L for benzene, toluene, and naphthalene, respectively) at 25 °C. The CS-GO adsorption data isotherm was described better by Sips isotherm model, however, GO adsorption data registered a best-fit to Langmuir adsorption isotherm equation (Table 5.1). This result is in accordance with previous reports [23].

Table 4.1 Parameters of the isotherm equations, correlation coefficients (R^2) and error function values of the models for organic compounds adsorption.

	CS-GO composite			GO		
	B	T	N	B	T	N
Langmuir						
q_{max} (mg·g^{-1})	278.7	75.77	9.705	34.36	19.02	6.560
b (L·mg^{-1})	7×10^{-4}	0.018	0.149	0.003	0.008	0.026
R_L	0.442	0.097	0.176	0.156	0.195	0.550
SSE	204.6	29.41	0.359	4.320	2.560	0.044
R^2	0.993	0.992	0.994	0.993	0.987	0.994
Freundlich						
n	0.664	0.274	0.432	0.329	0.346	0.719
K_F	1.169	1.169	1.960	2.573	1.808	0.257
SSE	529.7	529.7	1.230	19.50	8.099	0.101
R^2	0.982	0.982	0.981	0.970	0.961	0.988
Sips						
b	3×10^{-4}	0.020	0.149	0.013	0.010	0.041
q_{max} (mg·g^{-1})	260.2	76.83	9.636	41.44	19.23	4.764
n (L·mg^{-1})	1.124	0.961	1.011	0.703	0.957	1.032
R_L	0.649	0.088	0.176	0.041	0.163	0.436
SSE	100.1	29.09	0.360	9.840	2.826	0.097
R^2	0.997	0.993	0.995	0.985	0.986	0.988

The characteristic features of the Langmuir and Freundlich adsorption models describe Sips equilibrium approach of CS-GO isotherm data at saturation and low concentrations. The close difference of heterogeneity constant (n) from unity denotes and homogeneous adsorption on the surface of the adsorbent which was also noted to decrease with the hydrophobicity of the HC. On the other hand,

according to the Langmuir model, the GO isotherm data described homogeneous adsorption with a finite number of identical sites [254].

Comparative adsorption values between the CS-GO composite and GO sheets (Fig.4.5) revealed that the pillared effect of CS between GO sheets resulted in a positive affinity (around 2 to 4-fold increase of the removal capacity) for the pollutants under study. Studies related to the adsorption of organic pollutants by graphene oxide establish the existence of defects, edges and groove areas. Aromatic molecules would tend to interact with these high energetic sites [153]. Additionally, the hydrophobic effect and π-π interactions should be considered. The graphene morphology was modified with the introduction of chitosan molecules, which probably create a higher presence of surface crumples and grooves with high adsorption energy sites. The presence of these new high adsorption sites promote a significant affinity for the hydrocarbons and promoting more typical adsorption mechanisms. In the case of chitosan, recent studies established that benzene aromatic rings are attached in a parallel manner to the amine groups of chitosan, then tend to form subsequent complexes an interactions [85]. Otherwise, hydroxyl groups could generate van der Waals interactions, particularly in the C–3 position, between chitosan chains and aromatic molecules [234].

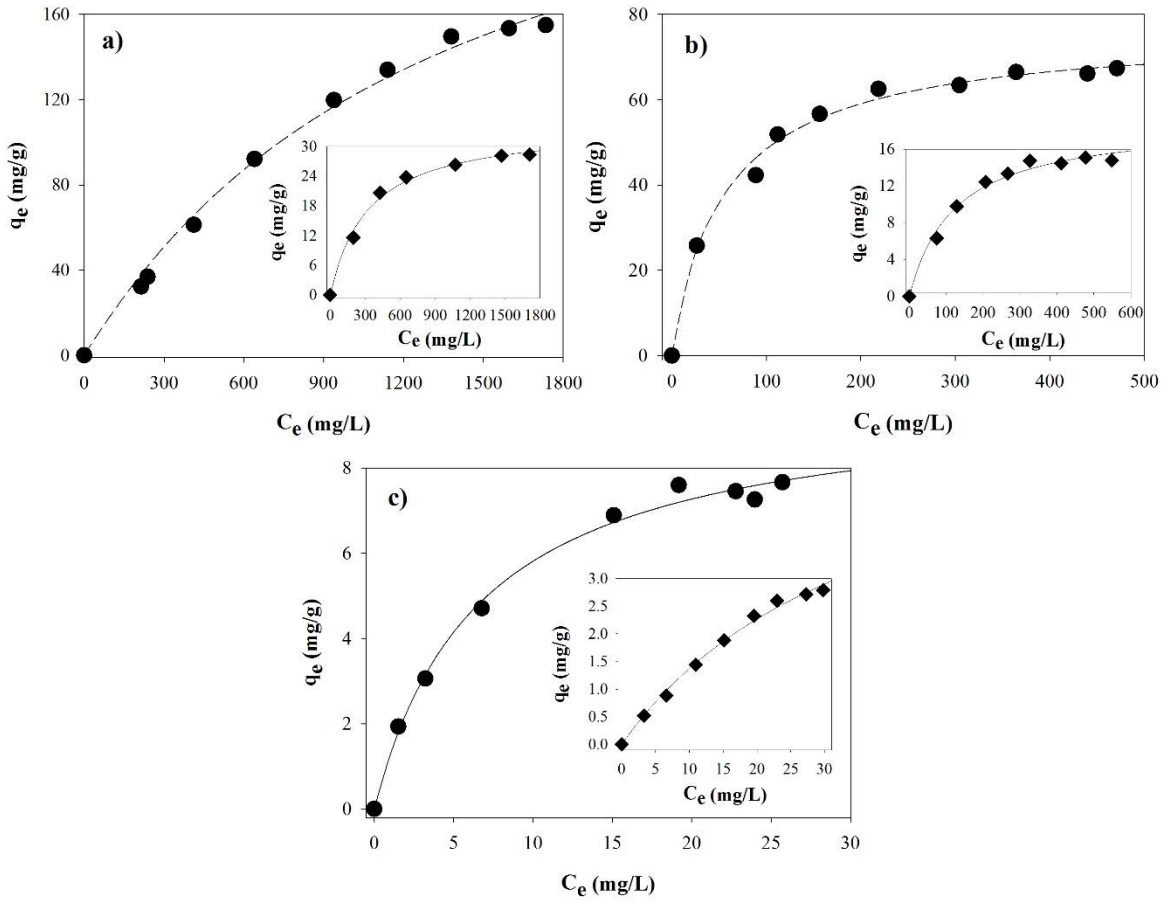

Fig. 4.5 Adsorption isotherm of a) benzene, (b) toluene and (c) naphthalene by (●) CS-GO, (◆) GO at initial pH 6 − 7, and 25°C. The lines represent the Sips adsorption isotherm equation for CS-GO systems and Langmuir for GO systems

4.5.1 Adsorption kinetics

Concerning kinetics tests, a high adsorption rate for the first period of adsorption was revealed in the system (Fig 4.6), reaching the equilibrium in less than 15 min. According to correlation coefficients (R^2 and SSE values), the pseudo-first-order model registered the best fit to the kinetic data in all the systems. This evidence suggests that the kinetics are governed by the rate of surface reactions at the first period, and the system approaches the equilibrium, a change in the mechanisms in registered from surface reaction to intraparticle diffusion. In other words, the quick adsorption at the initial stage revealed a significant number of available sites with a high affinity for the aromatic pollutants.

Dissolved organic matter (DOM) was the fraction of organic substances in a natural water sample that passes a 0.22 μm filter, and is composed of three primary sources: a) terrestrial matter from soils, b) phytoplankton occurring in surface water, and c) synthetic substances of anthropogenic origin. The organic and inorganic fraction was fully characterized and reported elsewhere [125]. The summary of the characterization analysis is presented in Table 4.2. The kinetics results showed a diminish of the adsorption rate of the pollutants with a slight increase in the overall adsorption capacity. This observation was reflected in the comparative lower pseudo-first kinetic constants (k_1).

Table 4.2 Pseudo-first order, pseudo-second order and Weber-Morris rate equation parameters for removal of benzene, toluene, and naphthalene.

	CS-GO Composite.					
	B[α]	B + DOM[β]	T[γ]	T + DOM	N[δ]	N +DOM
Pseudo-first order						
k_1 (h^{-1})	21.77	16.24	15.94	16.36	10.12	4.483
q_e ($mg \cdot g^{-1}$)	148.6	175.4	73.01	98.89	6.577	11.01
SSE[β]	11.80	155.9	187.2	82.06	4.177	8.330
R^2	0.999	0.994	0.966	0.991	0.910	0.936
Pseudo-second order						
k_2 ($mg \cdot g^{-1} \cdot h^{-1}$)	0.236	0.129	0.259	0.229	1.819	0.295
q_e ($mg \cdot g^{-1}$)	157.7	190.8	80.79	108.4	7.390	14.08
SSE	206.1	815.3	374.3	42.78	5.182	12.16
R^2	0.988	0.970	0.931	0.995	0.888	0.905
Weber-Morris model						
k_3 ($mg \cdot g^{-1} \cdot h^{1/2}$)	119.9	150.4	69.18	98.47	6.574	12.41
C	57.01	59.03	21.60	27.20	1.436	0.126
SSE	7217	1088	1920	2614	13.31	25.03
R^2	0.779	0.779	0.648	0.850	0.714	0.807

[α] = Benzene; [β] = Dissolved Organic Matter; [γ] = Toluene; [δ] = Naphthalene

Based on the literature, dissolved organic matter may promote a covalent bond with chitosan through carboxylic acid functional groups [234]. Moreover, humic acids, which are present in DOM, have a different hydrophobic as well as hydrophilic

character, chemical compositions, functional groups and charge density [235]. Through these sites, DOM could join to CS-GO composite adding hydrophobic sites, promoting the hydrophobic and π- π interactions between CS-GO composite and the aromatic hydrocarbons, explaining the increased on the removal capacity.

4.5.2 pH Effect

Fig. 4.7 shows that the pH of the system (3-11) has a significant effect on the removal ratio of benzene at acidic values (pH = 5). On the contrary, pH effect was lower for toluene and naphthalene. One possible explanation is that in acidic media, the CS-GO composite suffered two main changes: (1) a significant quantity of amino groups would be available due to the less amount of epoxy and hydroxyl groups (Fig 3b). The lower capacity could be related to the chitosan dissolution tendency at acidic conditions, or (2) the formation of amido groups after the interaction of the GO carboxyl groups with the chitosan amino groups, which have a highly polar characteristic. However, in the case of toluene and naphthalene, a minor effect was registered possibly by the high energy of adsorption between the CS-GO surface and the molecules under study due to their more hydrophobic character (higher K_{ow} values).

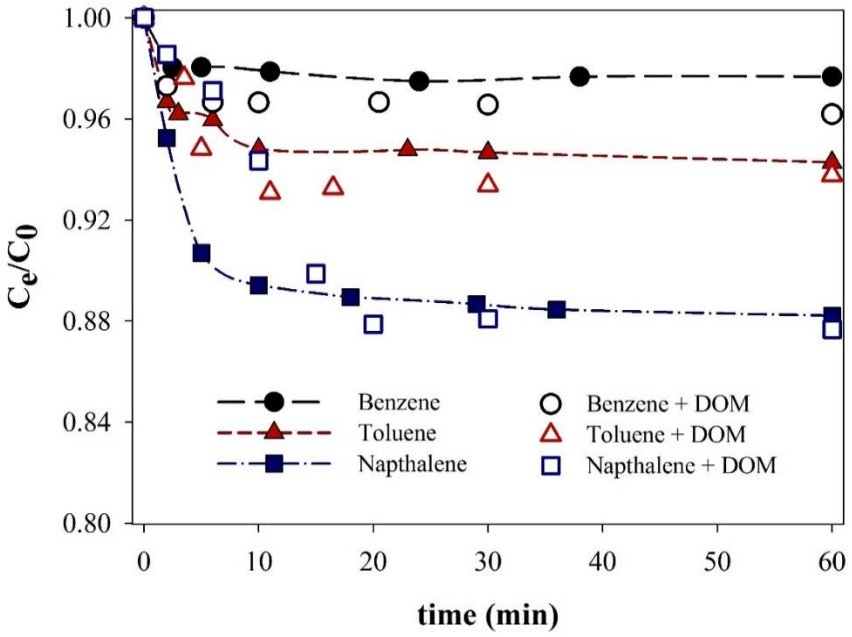

Fig. 4.6 Adsorption capacity of benzene, toluene and naphthalene in deionized water and the presence of organic matter (DOM). Benzene biosorption rate onto (●) benzene, (○) benzene + DOM; (▲) toluene, (△) toluene + DOM; (■) naphthalene, (□) naphthalene + DOM.

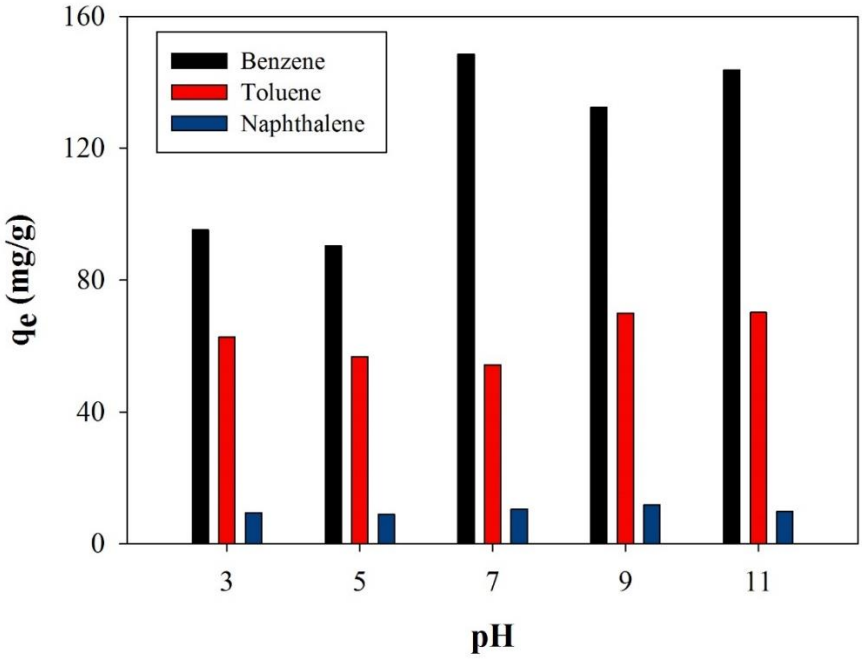

Fig. 4.7 pH effect of benzene, toluene and naphthalene uptake by CS-GO composite.

4.6 CS-GO as an adsorbent of aromatic hydrocarbon

Different pillared agents for graphene and graphene oxide were analyzed in the literature, which mainly included carbon-bases materials like carbon nanotubes, nanocarbon fibers, carbon black and fullerenes [67]. Another type of agents included polymers, metallic cations and in minor proportion organic polymers. For that reason, it is difficult to establish a clear comparison of the pillared capability of chitosan. However, the most similar CS/GO composites reported in the literature, and the target pollutants are presented in Table 4.3.

In the present study, the experimental data confirmed the capability of chitosan, as a soluble polymer to join the interspaces of graphene oxide (0.335 nm). More research in this field would be needed to improve the pillaring methodologies, and to enhance the chemical interaction of the precursors through chemical modifications, and optimum ratios of synthesis.

Table 4.3. Compilation of the main studies regarding the synthesis of CS-GO for the removal of organics in water.

Composite precursors	Target pollutants	Removal capacity (mg/g)	Reference
CS; GO	Methylene blue Eosin Y	320 240	(Chen, 2013)
CS; GO; Fe_3O_4	Methylene blue	180.83	(Fan, 2012)
CS; GO; $FeCl_3 \cdot 6H_2O$; $FeCl_2 \cdot 4H_2O$; gluteraldehyde	Reactive black 5	221	(Travlou, 2013)
CS; GO; $FeCl_3 \cdot 6H_2O$; $FeCl_2 \cdot 4H_2O$; gluteraldehyde; EPC; β-ciclodextrin	Methylene blue	50.12; 84.32	(Fan, 2013)
Cellulose; GO	Methylene blue	70.63	(Shi, 2013)
CS; GO; $FeCl_3 \cdot 6H_2O$	AO7	42.7	(Shesmani, 2014)
CS; GO; $FeCl_3 \cdot 6H_2O$; $FeCl_2 \cdot 4H_2O$;	Fuchsine	75.31	(Leilei, 2014)
CS; GO; Fly ash;	Acid red and cationic red	40 60	(Sheng, 2016)
CS/GO ratio = 0.1	Benzene Toluene Naphthalene	147 60 8	This study

4.7 Conclusions

The synthesis of different CS-GO composites achieved an optimized surface area of 47 m^2/g (ratio CS/GO = 0.1). Different characterization techniques verified the presence of chitosan molecules between the GO sheets, creating grooves and high energetic adsorption sites. The hydrophobic effect and π-π interactions of the GO structures also with chitosan (-OH) functional groups determined the favorable adsorption capacity in comparison with the un-modified GO.

CHAPTER 5

Dynamics biosorption of soluble-hydrocarbon by a macroalgae-based composite

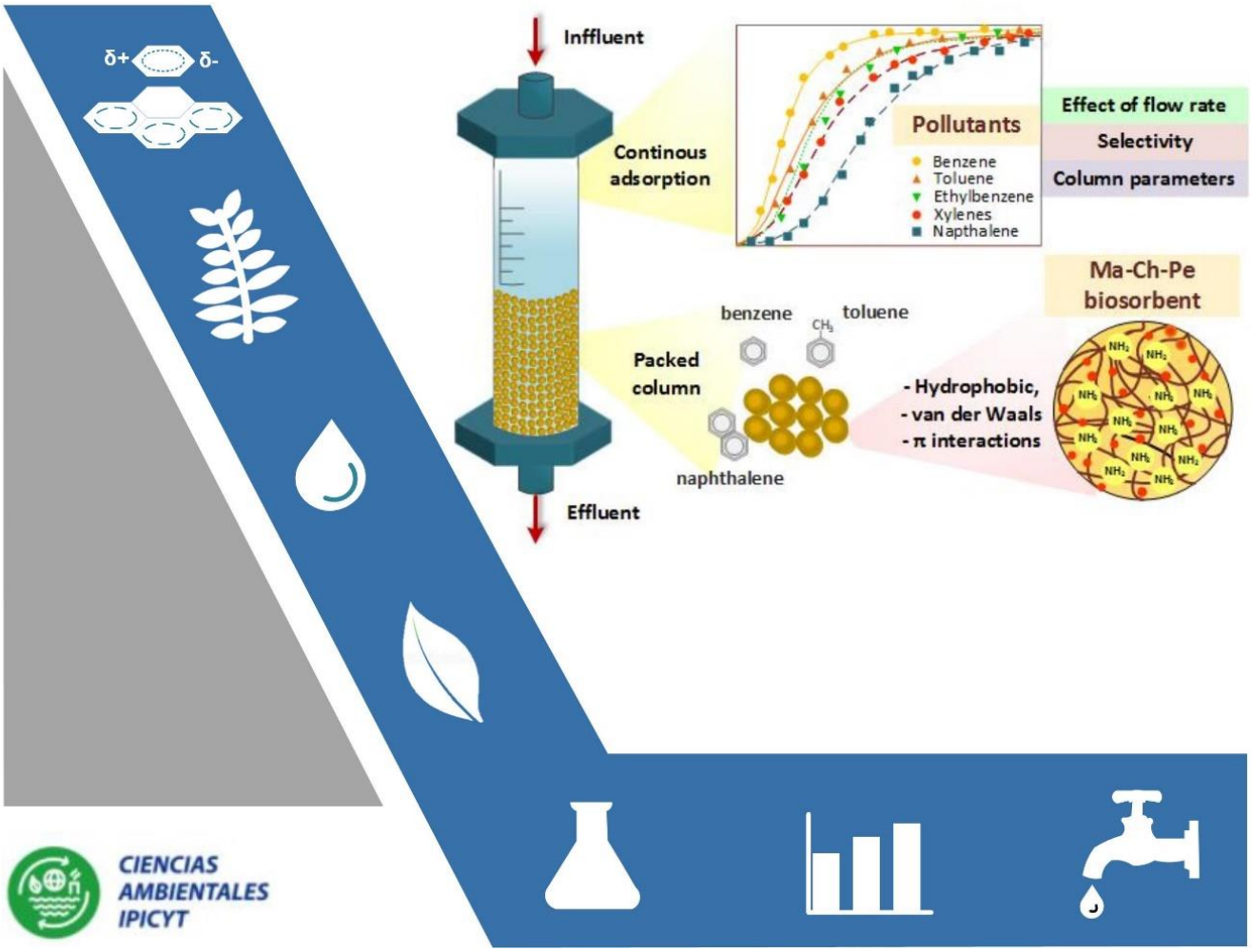

This chapter is adapted from: *Fixed bed biosorption studies for the removal of BTEX and naphthalene onto a macroalgae-based composite. Selectivity and breakthrough modeling.* In revision.

CHAPTER 5

5.1 Abstract

This study aimed to investigate the adsorption capacity of a microalgae-based biocomposite as a biosorbent of water-soluble hydrocarbons like BTEX compounds (benzene, toluene, ethylbenzene, and xylenes), and naphthalene on fixed bed experiments. The effects of the feed flow rate (0.3 - 1.1 mL/min) and equimolar selectivity on the breakthrough characteristics of the biosorption system were determined. The biosorption data was fitted to five well established fixed-bed adsorption models known as Thomas, Clark, Yoon-Nelson, Dose-Response, and BDST. Selectivity on the removal of hydrocarbon was observed based on the molecular weight (hydrophobicity) of the molecules. The biosorption data well-fitted the BDST and Dose-Response models with coefficients of correlation $R^2 > 0.95$ in different conditions. The macroalgae-baed biocomposite shows to be satisfactory for the biosorption water-soluble hydrocarbons.

5.2 Introduction

One of the significant sources of water-soluble hydrocarbons (WSH) is related to petrochemical activities that impact with polluted water and oil spillage [201]. Different approaches have been suggested for WSH such as filtration, aeration, biodegradation and photocatalysis [202,203]. Although these techniques have a different degree of success, they were found to be: (a) energy and chemical-consuming, (b) demands long periods of treatment, and (c) involve expensive costs for equipment and maintenance. Sorption technologies by inactive macroalgae biomass (Ma) have been effectively used for the removal of WSF in previous studies due to its high availability and chemical constitution [10,255,256]. Moreover, during this research, the physical properties of a brown biomass sample were improved through an immobilization technique with chitosan and pectin biopolymers. A design of experiments methodology optimized the final composition of the new biomaterial. Finally, the affinity of the biomaterials for the pollutants under study was evaluated through batch systems at different conditions.

In the literature, many biosorbents were tested in batch systems for different organic molecules. However, the design of an industrial process involves the achievement of additional fixed-column experiments to evaluate the effectiveness of the materials at dynamic conditions [135]. The main objective of this research was to determine the operational parameters of a fixed-bed column packed with our formerly reported macroalgae-based composite. For this purpose, the effect of key design parameters (influent concentration and bed depth) was performed. Moreover, Thomas, Dose-Response, Bed Depth Service Time (BDST), Clark and Yoon-Nelson models were applied to assess the agreement to experimental data.

5.3 Materials and methods

All the reagents used for analysis were of analytical reagent grade supplied by Sigma-Aldrich. The natural water employed in this study was collected from a basin located in San Luis Potosi, Mexico (22° 9′ 00″ N 101° 3′ 15″ W), and filtered through Millipore 0.22 µM nylon filters and was chemically characterized by total organic carbon, metals and anions concentrations as specified in Table 3.1. The inert biomass selected in this study was *M. pyrifera* previously rinsed with abundant deionized water (< 11 µS cm^{-1}), dried at 60 °C for 72 h, milled to powder texture and stored in a free moisture environment.

Synthesis of the biosorbent

The composites were prepared by dissolving a specific amount of pectin (Pe) powder in deionized water. On the other hand, a weighted mass of chitosan (Ch) was suspended in a slightly acidic media (acetic acid 5% v/v). The synthesis was followed by the mixing of both solutions in conjunction with the addition of a precise amount of macroalgae biomass (Ma). A factorial experiment design in conjunction with a surface response methodology was applied to find the optimal doses (75.4%, 19.8, and 4.8% for macroalgae biomass, chitosan, and pectin, respectively), for the biocomposite composition. The homogeneous (Ma-Pe-Ch) solution was entirely

dispensed through a drop system into a 5 % NaOH solution for hydrogelation, according to a previous methodology [226]. The final biomaterials were thoroughly washed with distilled water until neutral pH and then dried at 60 °C for 48 h.

Continuous adsorption experiments

The experimental set-up for a continuous system consisted of a 0.15 m long column with an inner diameter of 25 mm as shown in Fig 5.1. A total mass of 1.4 g of Ma-Pe-Ch biosorbent (600-800 µm of particle size) mixture was uniformly packed into the column with a respective bed height of 5 cm. A disk with 150 µm pore was constructed on the bottom of the glass column to support the biosorbent and also prevent any loss. The continuous experiments were performed under controlled conditions to prevent any hydrocarbon loss. Two primary systems were performed: (1) In the first case, naphthalene was selected and different empty bed contact time (EBCT) were tested. The EBCT refers to the time required for a fluid to pass through the volume equivalent of the media bed and it is expressed by

$$EBCT = V_F/Q \qquad \text{(Eq 5.1)},$$

where V_F is the volume occupied by the biosorbent media (m^3), and Q is the flow rate of the adsorbent, m^3/h. The influent aqueous solution containing a known concentration C_o (2.6 mg/L) was passed in the column bed in a downward manner at a constant flow rate of 1.1, 0.41, and 0.3, and EBCT values of 4, 15 and 20 respectively. (2) In a second system, the equimolar removal rate of BTEX and naphthalene biosorption was performed in the presence of deionized and surface natural water. The effluent solution was collected as a function of the time, and the concentration of each BTEX and naphthalene C_t (mg/L) were determined by HPLC after dilution as previously reported [125]. The breakpoint was considered as the point where effluent concentration reaches 10 % of the influent concentration (C/Ct = 0.1). The time corresponding to this point is the breakthrough time (t_b). When the effluent concentration reaches 95 % of the influent concentration, it is considered the saturation point (referring to saturation time (t_s)).

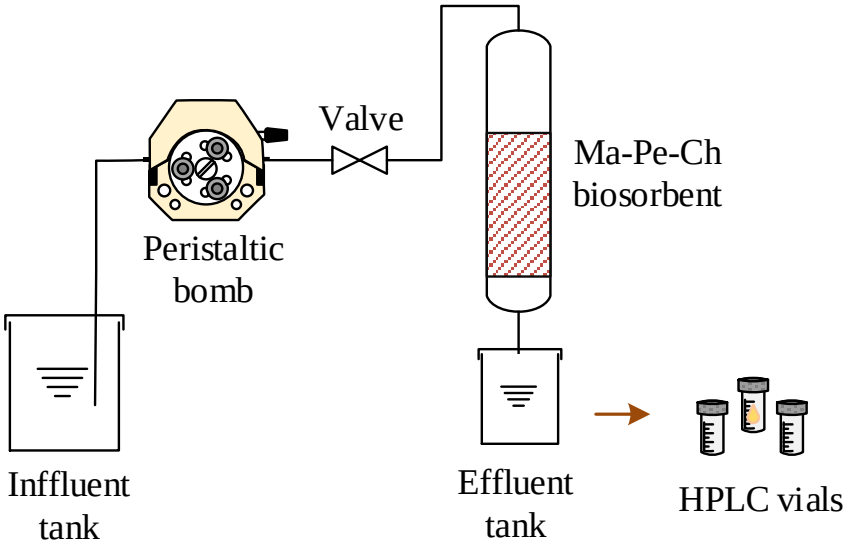

Fig. 5.1 Schematic diagram of the experimental fixed-bed column setup.

5.3.1 Dynamic adsorption models

Thomas model

The theoretical background of the Thomas model [257] implies no mass transfer and axial dispersion. A Langmuir adsorption equilibrium and second-order reversible reaction kinetics determine the adsorption process. This expression is also applied when external and internal diffusion limitations do not limit the sorption phenomenon. The Thomas model is expressed by Eq. 5.2:

$$\frac{C_0}{C_i} = \frac{1}{1+e^{\left[\left(\frac{k_{TH}}{Q}\right)\left(mq_{TH}-C_iV\right)\right]}} = \frac{1}{1+e^{\left(\frac{k_{TH}mq_{TH}}{Q}-k_{TH}C_it\right)}} \qquad (5.2)$$

Where k_{TH} is the Thomas rate constant, and q_{TH} is the maximum adsorption capacity for the hydrocarbons under study (mg/g).

Clark model

This model considers the use of a mass-transfer coefficient in conjunction with the Freundlich adsorption isotherm equation [258], determined by the following expression.

$$\frac{C_0}{C_i} = \left[\frac{1}{\left(1+Ae^{-k_C t}\right)}\right]^{\frac{1}{n_F-1}} \quad \text{with} \quad A = \left(\frac{C_i^{n_F-1}}{C_b^{n_F-1}}\right) e^{k_C t_b} \qquad (5.3)$$

Where n_F is the Freundlich constant (determined for previous equilibrium studies), k_c (min^{-1}) is the adsorption rate constant and C_b (mg/L) the solute concentration at the breakthrough time.

Yoon-Nelson

Yoon-Nelson model [259] identifies that the rate of reduction in the chance of adsorption of adsorbate molecule is proportional to the solute adsorption and the adsorbate breakthrough on the adsorbent. The equation is given as follows (Eq 5.4):

$$\frac{C_0}{C_i} = \frac{e^{\left(k_{YN}t - k_{YN}t_{50\%}\right)}}{1+e^{\left(k_{YN}t - k_{YN}t_{50\%}\right)}} \qquad (5.4)$$

Where k_{YN} is the Yoon-Nelson adsorption rate constant (min^{-1}), and $t_{50\%}$ (min) is the time required for retaining 50% of the initial hydrocarbon concentration (C/C_i =0.5).

Dose-Response model

The Dose-Response model is an empirical equation that diminishes the error resulting from the use of the Thomas models, especially at low and high periods of the breakthrough curve [260], which can be estimated by (Eq 5.5):

$$\frac{C_0}{C_i} = \frac{C_s}{C_i} - \frac{\frac{C_s}{C_i}}{1+\left(\frac{V}{V_{50\%}}\right)} = \frac{C_s}{C_i} - \frac{\frac{C_s}{C_i}}{1+\left(\frac{t}{t_{50\%}}\right)^{\propto}} \qquad (5.5)$$

Where C_s is the solute concentration at t_s and α is the constant of the Dose-Response model.

Bed Depth Service Time (BDST) Model

This model assumes that an external reaction between the solute and the unused fraction of the biosorbent [256] governs the sorption process.

$$\frac{C_0}{C_i} = \frac{1}{1+e\left[k_{BDST}C_i\left(\frac{N_{BDST}}{C_i v}L-t\right)\right]} \quad (5.6)$$

Where N_{BDST} is the biosorption capacity (mg/L), v is the linear-flow velocity of the adsorbates along the bed (cm/h), k_{BDST} is the adsorption rate constant that describes the mass transfer from the liquid to the solid phase (L/mg h), and *L* is the height (cm). The significance of the models was tested by the statistical values of the correlation coefficient (R^2) and the sum of the squares error (*SSE*), according to the following expression (Eq. 5.7):

$$\sum_{i=1}^{n}\left(y_{e,meas} - y_{e,calc}\right)_i^2 \quad (5.7)$$

Where $y_{e,meas}$ and $y_{e,calc}$ are the measured and theoretically calculated dependent variable.

5.4 Results and Discussion

Main biocomposite results

The methodology of synthesis of the biocomposite was previously described. A factorial experiment design in conjunction with a surface response methodology was applied to find the optimal conditions (75.4%, 19.8, and 4.8% for macroalgae biomass, chitosan, and pectin, respectively), for the benzene removal capacity, used as aromatic hydrocarbon model. The chitosan and algae biomass content were the main factors involved in the adsorption process as described below. The biosorption mechanism is a sum of interactions between the diversity of chemical components

of the composite precursors and involves mainly hydrophobic effect between lipids and lignocellulosic fractions (cellulose, hemicellulose, and lignin) and nonspecific Van der Waals interactions with carbohydrates, proteins, chitosan, and pectin contents.

Dynamic adsorption of WSF by macroalgae-based biocomposites

All the breakthrough curves followed the typical S-shape curve ratio of outlet solute concentration to inlet solute concentration (C_t/C_i) in the fluid as a function of time (t in min). At the first stage of adsorption, the HC was rapidly adsorbed on the surface due to the high availability of active sites. When the feed water is introduced through the inlet of the column, the solute is adsorbed most rapidly and effectively by the upper few layers of the fresh biosorbent during the initial stage of the experiment. As the polluted solution continues to flow into the column, the top layers of the sorbent become saturated with the incoming solute and become less useful for further sorption. The process continues until the saturation point reached 95% of the inlet concentration value [261].

Effect of flow rate

The breakthrough curves at three different fluxes 1.1, 0.3 and 0.41 mL/min for EBCT values of 4, 15 and 20 are shown in Fig 5.2. The superficial velocity (v) was 0.99, 0.26 and 0.19 for the aforementioned EBCTs values, respectively. The bed height was constant at 4 cm, and the initial concentration was established at 2.6 mg/L. Breakthrough time reaching saturation was increased with a decrease in the flow rate [255]. At low influent flow, naphthalene had more time to be in contact with the adsorbent, which resulted in a higher removal of adsorbate molecules in the fixed-column. These results are by previous systems for the continuous removal of organic and inorganic pollutants by using biosorbents [255,262].

Dynamic behavior of Ma-Pe-Ch biocomposite beds was calculated using a previously described methodology [263], and the main parameters are compiled in Table 5.1. In this table, V_B is the breakthrough volume at a relative concentration of 0.02 (which was arbitrarily selected). H_{MTZ} is the height of the mass transfer zone, which gives information about the rate of adsorbate removal by the adsorbent. The faster the adsorption rate, the lower is the height of the mass transfer zone. The fractional capacity, φ, is a measure of the efficiency of the biosorbent located within the mass transfer zone. The value S_T express the specific throughput of the adsorbent, which means the mass necessary to treat a specific volume bed beyond an established concentration (0.02). S_{Tobj} has the same principle, but in this case, the reference is given by values suggested by the US-Environmental Protection Agency [24]. In the literature, a quick and sharp breakthrough curve usually show high φ values. On the other hand, gradual, flat breakthrough curves register low φ values. R_{MTZ} is the rate of movement of H_{MTZ}. This parameter is functioned on the affinity of the adsorbate for the biosorbent and is a relevant value for scale-up design because it indicates the rate at which the adsorbent will be exhausted. The results listed in Table 1 shows an increase of V_B and H_{MTZ}, which means that the breakthrough occurs faster at a higher flow rate, by the reduction of the R_{MTZ}. No significant differences were found for φ values, meaning that the removal efficiency is only delimited by the flow-rate.

Figure 5.2 shows a slowing down tendency to reach the saturation value with a decrease in the flow rate. A possible explanation could be related to a decrease of the mass transfer parameter values, which prevent an efficient diffusivity into the internal surface active sites. Low flux values promote an eventual intraparticle diffusion resistance. The linearized Thomas model at different slopes could lead to the computation of different rate constants k_{TH} (mL min^{-1} mg^{-1}) to identify an overall change in the mass transfer rate. In all the cases, two main steps where identified. For example, an EBCT value of 15 registered two different slopes: At the first time period (Fig 5.3), a constant slope is noticeable in the system, especially at intervals below the breakthrough time. At greater times, the slope suddenly change to notable

lower values probably because the internal surface area is completely occupied and the final step of biosorption is only in the external active sites.

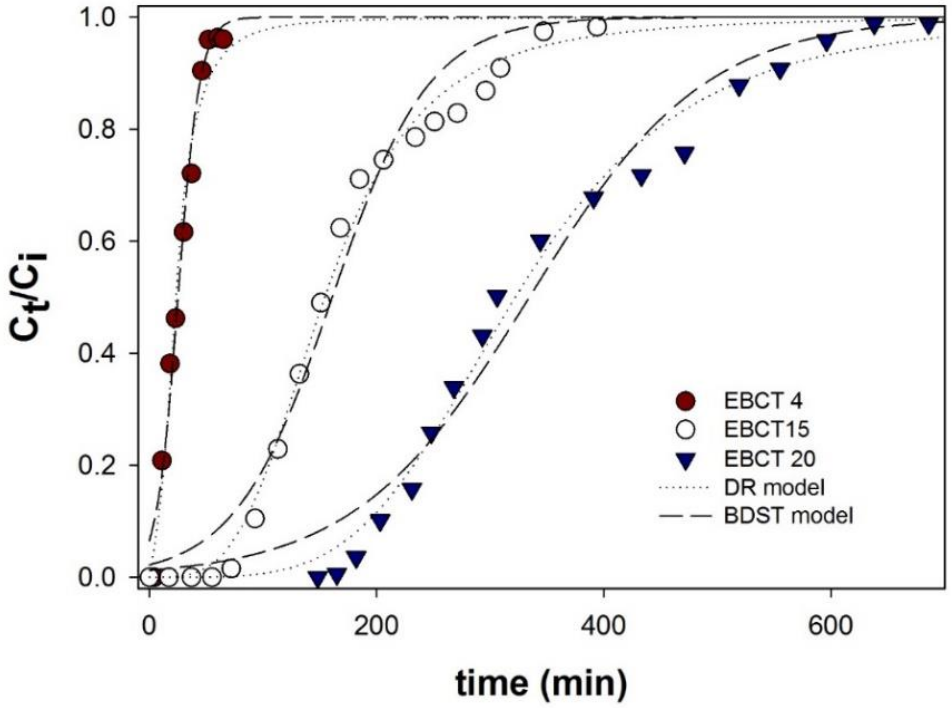

Fig. 5.2 Breakthrough curves for naphthalene at onto Ma-Pe-Ch biocomposite at different flow rates of 1.1, 0.41 and 0.3 mL/min for EBCT values of 4, 15 and 20, respectively.

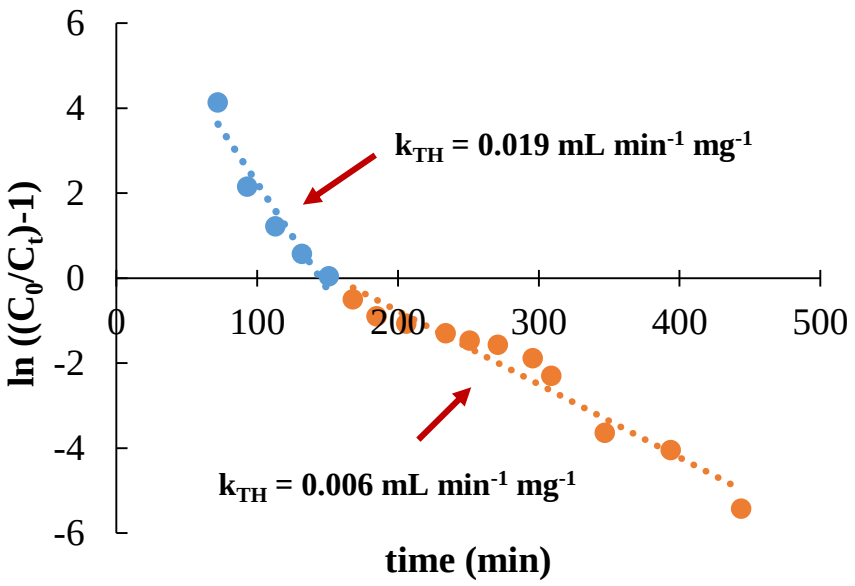

Fig. 5.3 Thomas rate constant for naphthalene removal on Ma-Pe-Ch at an EBCT value of 15.

1.3.2.1 Equimolar experiments

Among the evaluated dynamic adsorption models (Table 5.2 – 5.4), the fitting value of R^2 and *SSE* for Dose-Response and BDST models were the highest for the given experimental conditions. Thus, it could be suggested that an external reaction with no mass transfer and axial dispersion, following a Langmuir adsorption equilibrium, and second-order reversible reaction kinetics [135]. These assumptions are in agreement with our previous batch studies.

Table 5.1 Breakthrough curve parameters of naphthalene removal by Thomas, Dose Response, BDST, Yoo-Nelson and Clark models onto Ma-Ch-Pe biocomposite column (pH = 8 , particle size = 800 µm, room temperature).

	EBCT		
	4	15	20
Thomas model			
K_{TH} [mL(mg/min)]	0.04	0.01	0.008
q_{th} [mg/g]	60.60	125.43	176.09
R^2	0.98	0.97	0.95
SSE	0.02	0.07	0.14
Dose-Response model			
q_D [mg/g]	54.61	120	179.32
a	2.52	3.60	4.25
R^2	0.98	0.99	0.99
SSE	0.02	0.02	0.03
Bed Depth Service Time			
K_{BDST} [L/(mg h)]	0.04	0.009	0.005
N_B [mg/L]	17.09	26.62	42.35
R^2	0.98	0.97	0.97
SSE	0.02	0.07	0.06
Yoon Nelson Model			
K_Y [min^{-1}]	0.107	0.025	0.015
R^2	0.97	0.97	0.95
SSE	0.04	0.09	0.12
Clark model			
K_C [min^{-1}]	0.061	0.014	0.01
R^2	0.98	0.99	0.92
SSE	0.03	0.02	0.17

Table 5.2 Characteristics of biosorbents for the removal of naphthalene of hydrocarbons at 25 °C.

	V_B (mL)	V_C (mL)	H_{MTZ} (cm)	ϕ	R_{MTZ} (cm/min)	$S_{T\ 0.02}$ (mL/g)	$S_{T\ obj}$ (mL/g)
EBCT 4	5.17	6.47	3.53	0.79	0.09	4.23	5.29
EBCT 15	31.00	34.10	3.08	0.79	0.01	23.15	25.46
EBCT 20	52.83	56.43	2.72	0.80	0.01	37.72	40.29

The results of the equimolar experiments of BTEX and naphthalene through deionized and natural water are presented in Fig. 5.4. In general, the experimental data registered a better fitting to D-R, and BDST mentioned earlier. Additionally, the velocity constants of the BDST model (K_B) were higher in the presence of organic

matter because of the competition for adsorption sites (Fig 5.3a). For the same reason, a lower removal capacity was registered as well as the breakthrough time compared with the system in deionized water. This result was corroborated by the removal capacity value of the D-R model. A linear relation was founded between the removal rate (q_e), and the hydrophobicity of the molecules, which has a direct relationship with the partition coefficient of the aromatic hydrocarbons.

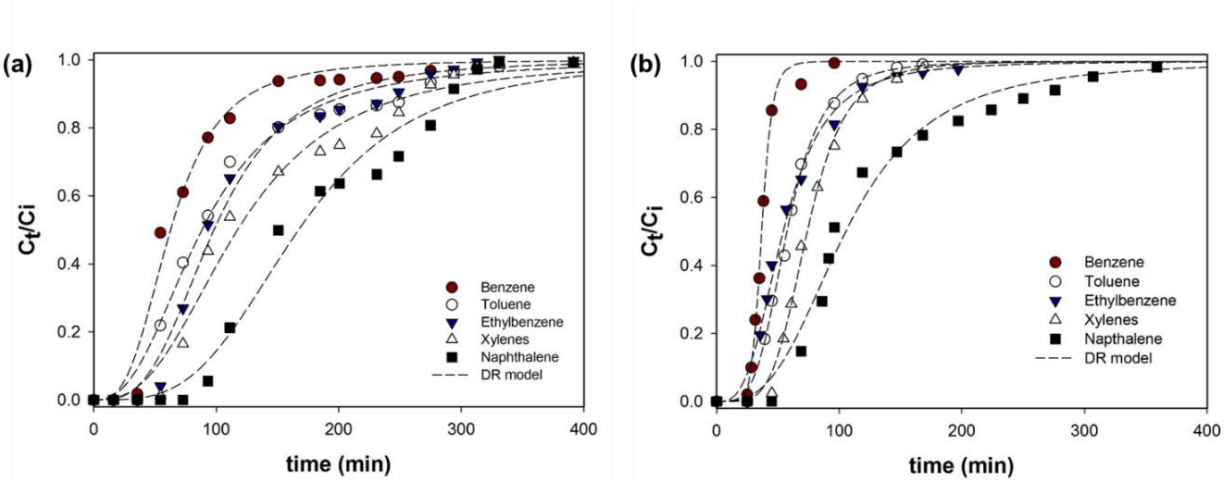

Fig. 5.4 (a) Breakthrough experiments of an equimolar 0.064 mM hydrocarbon mixture of BTEX and naphthalene compounds in deionized water and, (b) natural water on a 15 cm column filled with Ma-Pe-Ch biocomposite. Flow of 0.34 mL/min and empty bed contact time of 17.9 min

Table 5.3 Breakthrough curve parameters of benzene, toluene, naphthalene, ethylbenzene and xylene removal by Thomas, Dose Response, BDST, Yoo-Nelson and Clark models onto Ma-Ch-Pe biocomposite column (pH =8 , particle size = 800 µm, room temperature) in deionized water.

	Pollutant				
	Benzene	Toluene	Ethylbenzene	Xylene	Naphthalene
Thomas model					
K_{TH} [mL(mg/min)]	0.005	0.004	0.004	0.003	0.002
q_{th} [mg/g]	165.90	166.31	209.18	222.05	408.35
R^2	0.95	0.94	0.96	0.94	0.95
SSE	0.07	0.10	0.09	0.11	0.07
Dose-Response model					
q_D [mg/g]	157.41	154.60	200.13	198.03	384.18
a	3.09	2.51	3.15	2.70	3.47
R^2	0.98	0.99	0.98	0.97	0.96
SSE	0.03	0.02	0.03	0.05	0.05
Bed Depth Service Time					
K_B [L/(mg h)]	0.005	0.004	0.004	0.002	0.002
N_B [mg/L]	39.93	39.85	50.34	79.36	98.28
R^2	0.95	0.94	0.95	0.94	0.95
SSE	0.07	0.10	0.09	0.11	0.07
Yoon Nelson Model					
K_Y [min^{-1}]	0.057	0.03	0.042	0.02	0.0184
R^2	0.91	0.94	0.94	0.91	0.88
SSE	0.14	0.01	0.10	0.16	0.15
Clark model					
K_C [min^{-1}]	0.013	0.014	0.018	0.017	0.022
R^2	0.89	0.98	0.98	0.95	0.75
SSE	0.17	0.03	0.03	0.08	0.32

The shape of the equimolar breakthrough curves (Fig. 5.4) shows that benzene is preferentially adsorbed in comparison to the rest of the evaluated molecules. This could be explained by the diffusion coefficients values in free solution [264], which follows a linear trend in base of their molecular weight. For that reason, it is possible that simple aromatic molecules (benzene or toluene) reach quicker the available active sites, avoiding at the same time, the adsorption of larger molecules (e.g., naphthalene). This phenomenon is enhanced by the presence of dissolved organic matter due to the competence of active sites at the bottom of the fixed bed column.

The DOM constituents may attach to the first layers of the fixed column, probably producing diffusional restrictions for larger molecules which registered a slowing down tendency reaching the saturation value of the breakthrough curve (Fig 5.5). According to the literature, the dissolved organic matter contain a significant degree of aromatic polymers, chemical compositions, and functional groups promoting hydrophobic interactions with large molecular aromatic compounds.

Table 5.4 Breakthrough curve parameters of benzene, toluene, naphthalene, ethylbenzene and xylene removal by Thomas, Dose Response, BDST, Yoo-Nelson and Clark models onto Ma-Ch-Pe biocomposite column (pH = 8, particle size = 800 µm, room temperature) in dissolved organic matter (DOM = 19.4 mg L^{-1}) media.

	Pollutant				
	Benzene	Toluene	Ethylbenzene	Xylene	Naphthalene
Thomas model					
K_{TH} [mL(mg/min)]	0.022	0.01	0.006	0.007	0.003
q_{th} [mg/g]	85.57	108.19	117.17	144.27	221.92
R^2	0.99	0.99	0.96	0.98	0.91
SSE	0.007	0.013	0.04	0.02	0.10
Dose-Response model					
q_D [mg/g]	85.10	106.02	111.70	141.15	212.13
a	8.50	4.03	3.10	4.75	3.02
R^2	0.99	0.99	0.99	0.99	0.98
SSE	0.006	0.003	0.012	0.006	0.035
Bed Depth Service Time					
K_B [L/(mg h)]	0.022	0.08	0.006	0.007	0.003
N_B [mg/L]	22.15	27.80	30.32	37.33	57.43
R^2	0.99	0.99	0.96	0.98	0.94
SSE	0.01	0.01	0.04	0.02	0.10
Yoon Nelson Model					
K_Y [min^{-1}]	0.220	0.068	0.057	0.07	0.036
R^2	0.94	0.98	0.96	0.95	0.91
SSE	0.16	0.02	0.04	0.06	0.15
Clark model					
K_C [min^{-1}]	0.08	0.04	0.014	0.024	0.04
R^2	0.97	0.99	0.97	0.96	0.98
SSE	0.03	0.01	0.05	0.05	0.03

5.5 Conclusions

In this study, an optimized Ma-Pe-Ch biocomposite was used for BTEX and naphthalene removal in a fixed-bed column under different experimental conditions. Results showed that the naphthalene adsorption increases by increasing the contact time between the effluent and the adsorbent. The most extensive removal capacity was for naphthalene by the hydrophobicity of the molecules and the partition coefficient to active sites. It has been found that Thomas and Dose-Response models successfully predicted hydrocarbons breakthrough curves obtained under various experimental conditions. Adsorption mechanism revealed by the D-R models suggest a Langmuir and a second order-rate kinetic equation as verified in batch experiments. The presence of dissolved organic matter decreases the removal capacity and increase the kinetics phenomenon due to competition for active sites.

CHAPTER 6

GENERAL DISCUSSION

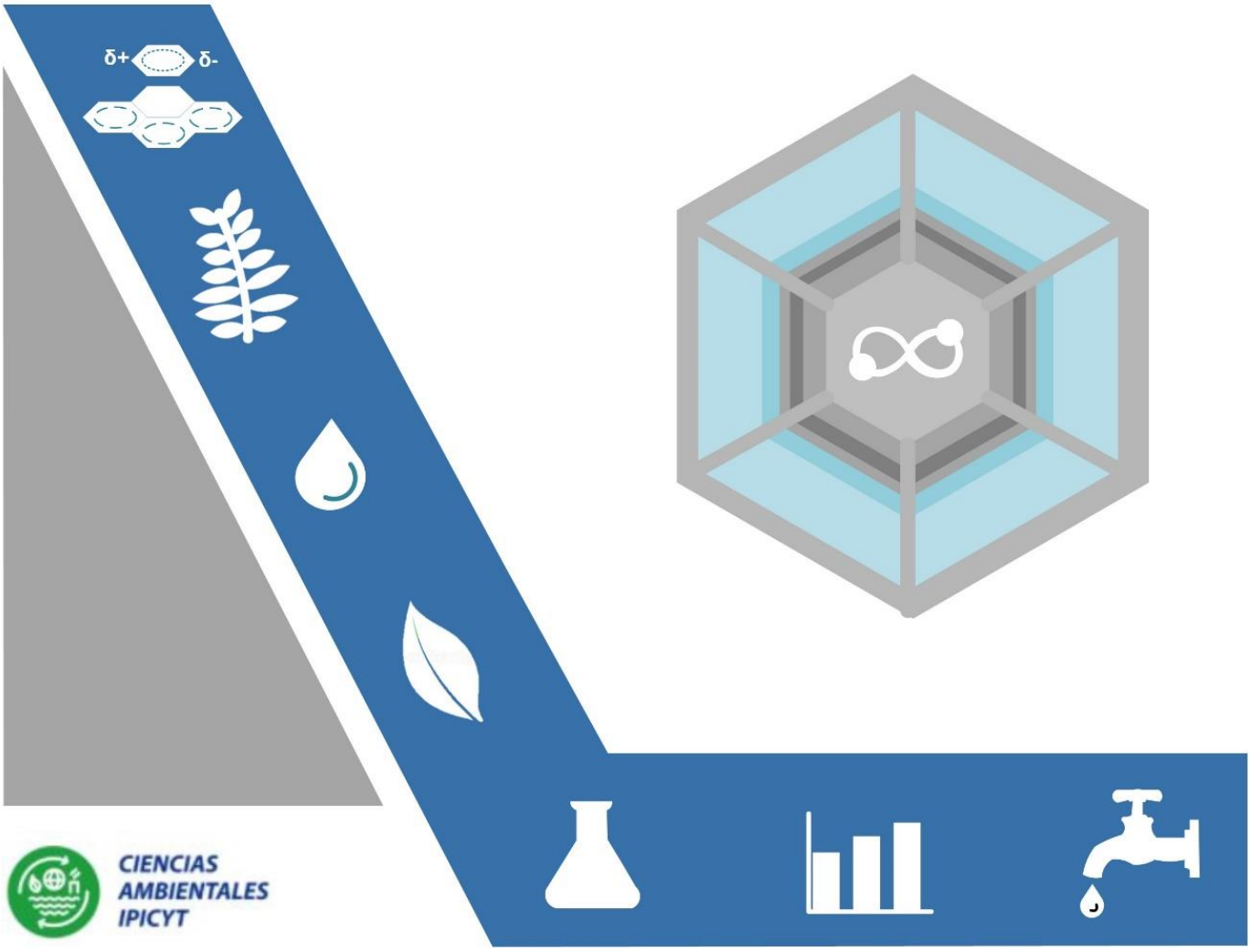

CHAPTER 6

6.1 GENERAL DISCUSSION

The presence of water-soluble hydrocarbons (like BTEX and naphthalene) in water is related with detrimental effects to the environment. Just a minor fraction of their solubility capacity could produce toxic effects in aquatic organisms and human health. The necessity to treat these pollutants is because of its capability to overcome primary and secondary treatments in a wastewater plant. Beyond the extensive list of available technologies to remove these pollutants, the physicochemical strategies of sorption and adsorption are the most selected because of its short periods of treatment with high efficiency. Activated carbon is the most selected adsorbent, but the drive for improved precursors created the field to look for new adsorbents. The use of unemployed resources such as seaweeds represents a potential precursor because there is no competition with food resources. Cultivation and harvesting of seaweed biomass at large scale is a well-establish technology. In this dissertation, one of the main contributions was to found that macroalgae biomass is a competitive biosorbent for the removal of the main soluble hydrocarbons. According to the results, hydrophobic and dispersive interactions govern the biosorption mechanisms, for this reason, proximal and lignocellulosic determinations should be considered as the first step to consider a particular biomass. Brown biomass registered the higher removal capacities.

A crucial analytical aspect is the presence of a dissolved fraction of biomass inevitable release to the aqueous system. A robust technique like high-performance liquid chromatography (HPLC) or gas chromatography (GC) would easily overcome this limitation, but in the case of UV-Vis spectroscopy, the presence of multiple blanks is mandatory. An interesting observation of this fraction is that increases with ionic strength and with temperatures, which is related to the lower stability of the functional compounds within the biomass at extreme conditions.

The appreciable disadvantage of the dissolved fraction in conjunction with low mechanical properties represent the main drawbacks of this technology. For that

reason, in this work, a granulation approach by biomass entrapment was conducted with chitosan and pectin. The biopolymer-biopolymer interactions between two opposite-charge macromolecules enhanced the compatibility and stability of brown biomass. Despite the low surface area, the final material (0.12 m^2 g^{-1}) had a biosorption capacity of 58.68, 16.64 and 6.13 mg g^{-1} for benzene, toluene, and naphthalene, respectively employed. A removal capacity of around 50 % less than the previously tested brown seaweed was registered. This could be related to the immobilization methodology. Improvements in the entrapment techniques would be necessary to increase the availability of surface active sites in the raw biomass.

Finally, the use of natural polymers such as chitosan for the removal of soluble hydrocarbons was applied to attend a well-known agglomeration inconvenient of a carbon-based nanomaterial. The pillared effect of chitosan between graphene oxide sheets was evidenced by an optimal CS/GO ratio. The main advantage of chitosan is its solubility in an acidic media where it can diffuse between some of the GO sheets as could be noted in Fig. 6.1. A clear result was the detrimental effect on the surface area by employing a medium or high molecular weight of CS polymer. The analytical determination of textural properties in CS-GO composites is a challenging task because low masses and volumes may hinder an appropriate pressure difference during the performance of N_2 isotherms. Related to the adsorption tests, the hydrophilicity reduction by the GS-GO composite was traduced in a significant increase of the affinity towards the pollutants under study. A very high uptake rate (less than 10 min) describe a kinetic phenomenon of two main stages: (a) diffusion from the bulk solution to the pores and (b) adsorption process. This means that the separation of the GO was only produced in the edges of GO as shown in Fig. 6.1. Finally, the presence of dissolved organic matter improves the uptake of the pollutants by the attachment of the aromatic fraction of DOM with the basal planes of GO. The presence of humic acids in a 3D forms could increase the number of active sites in the CS-GO composite.

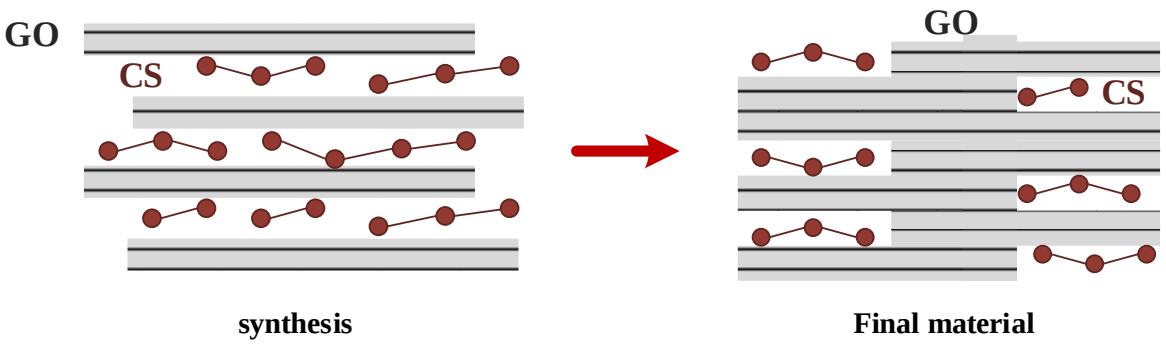

Fig. 6.1 Hypothetical distribution of chitosan between GO sheets during synthesis and final process.

The final section of this thesis dissertation presents the dynamic adsorption evaluation of the previously synthesized biocomposite. The results showed an evident selectivity for the aromatic molecules based on their hydrophobicity degree. A preferential biosorption was observed for light aromatic molecules, which is probably associated with their higher diffusion coefficient values in solution. This phenomenon was more evident in the presence of dissolved organic matter. In this case, DOM components may occlude the transport of large aromatic molecules by the accumulate presence of humic acids in the first layers of biosorbent.

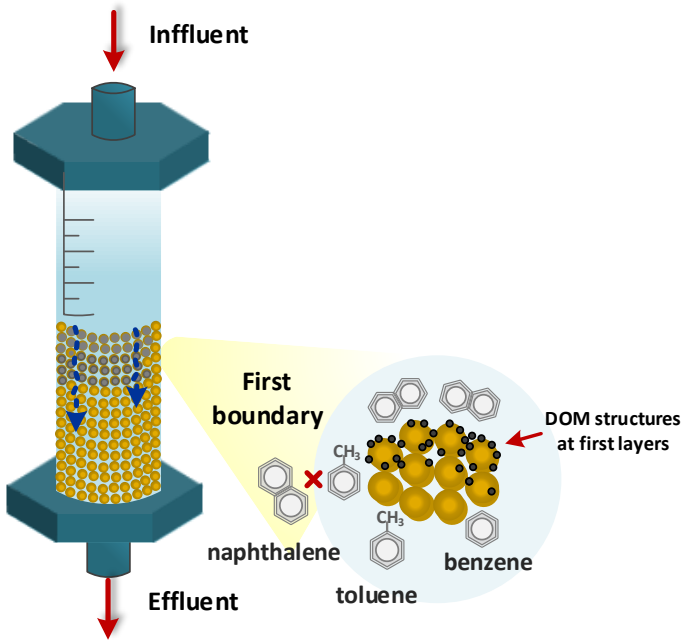

Fig. 6.2 Preferential adoption mechanism of lighter molecules in packed columns with DOM.

On the other hand, the removal efficiency of naphthalene increased with a lower influent flux. The experimental results stated the feasibility of macro-algae based composites for continuous processes, but further test is necessary to analyses the desorption capacity and the effect of increasing DOM along the experimental time. The slowing down effect at different flow rated could be related to the diffusion resistivity generated by an increase in the external mass transfer coefficient. Related to equimolar concentrations,

Comparative results

The data shown in Table 6.1 compiles the information related to the previously described adsorbents. It is noted that significant removal capacity was achieved by the CS/GO composite. These values confirm the higher affinity of the graphitic layers for the pollutants under study. However, the closer biosorption capacity of *M. pyrifera* (a reduction around 20%) highlights the potential use of brown biomass for future applications, even with a significant diminution of the surface area in comparison with the CS/GO composite.

Table 6.1 Comparative results regarding the removal capacity of soluble aromatic hydrocarbons in batch studies. Initial concentration values were 1800, 515.5 and 31.5 mg L for benzene, toluene, and naphthalene, respectively.

Biosorbent	Pollutant	Biosorption Capacity $mg \cdot g^{-1}$	Swelling degree	Surface area (m^2 $g^{-1)}$
M. pyrifera	Benzene Toluene	112 28.07	557	0.13
U. expansa	Benzene Toluene	55 28.06	270	0.17
A. spicifera	Benzene Toluene	20 16	857	0.21
MA-Ch-Pe biocomposite	Benzene Toluene Naphthalene	58.68 16.64 6.13	380	0.12
CS/GO ratio = 0.1	Benzene Toluene Naphthalene	147 62 7.8	N/D	47

The macroalgae-based biocomposite shares a similar affinity with *U. expansa* (green seaweed) biomass, and at the end is located the red macroalgae biomass (*A. spicifera*). The red macroalgae biomass registered poor affinity due to its minor lignocellulosic composition and higher mineral content (almost 50%).

Based on these results, one of the main contributions of this research is the highlight capacity of brown biomass *M.pyrifera* for soluble aromatic compounds. Moreover, the biocomposite synthesis with the brown macroalgae biomass leads the possibility of scale-up applications due to its higher stability and mechanical properties. Finally, the synthesis of biocomposites also contributes to a lower desorption capacity of the pollutants under study.

The application of graphene nanomaterials to water treatment has a valuable potential if a methodology to obtain exfoliated graphene with a few layers is developed. The research about natural polymers as pillaring agents is a relevant field to enhance the mechanical and the available surface area of GO without adverse effects to organisms and human health. The development of pillared composites has a widespread interest in catalysis, medicine, and environmental issues.

CHAPTER 7

FINAL REMARKS

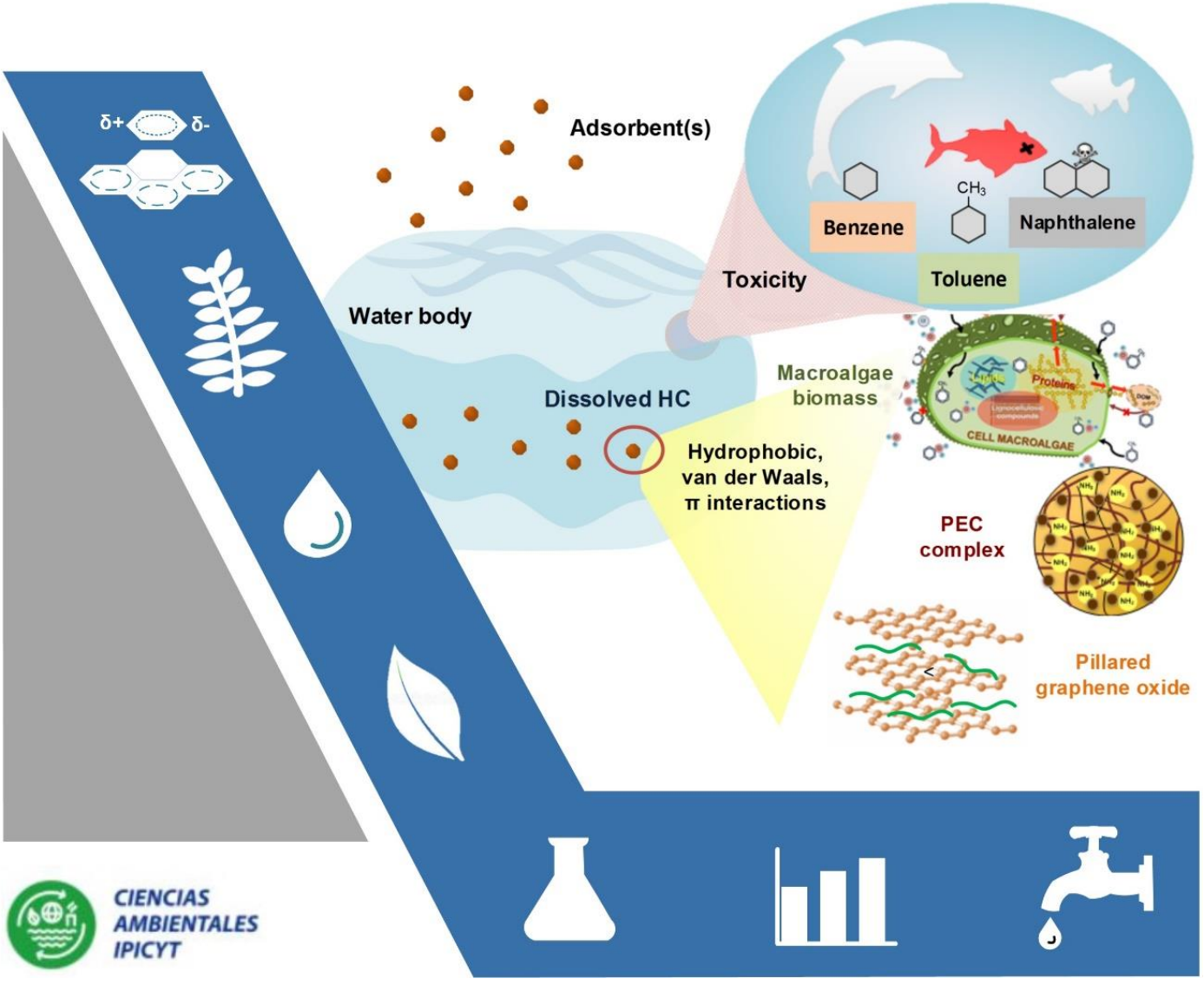

CHAPTER 7

7.1 GENERAL CONCLUSIONS

The present dissertation deal with the use of alternative adsorbents for the removal of the main water-soluble hydrocarbons in batch and continuous systems. According to the results, the macroalgae biomass is feasible for the removal of this kind of pollutants and at the same time promote the consumption of a worldwide available resource. Related to the characterization analyses, it was determined that the main constituents of the macroalgae biomass are carbohydrates, lignin, and proteins. The biosorbents surface charge does not change with ionic strength. In relation with the biosorption tests, removal experiments using different macroalgae biomass followed the next order: *M. pyrifera* $\geq$ *U. expansa* > *A. spicifera*. Additionally, the hydrocarbons affinities were not affected at least up to I = 0.6 M.

For the subsequent synthesis of biocomposites, the optimum content for maximum benzene removal onto Ma−Ch−Pe biocomposites were 20.8% (Chitosan), and 79.2% (Algae biomass), but a 5 % w/w was considered to improve the mechanical properties. The biosorption mechanisms include London and hydrophobic interactions between the sorbents and the diversity of chemical components of the cell wall in addition to chitosan and pectin functional groups. The optimized biocomposites were employed on a fixed-bed column for the computation of column parameters. Finally, the dynamic tests demonstrated the selectivity of the BTEX removal by the hydrophobic character of the molecules.

Finally, the synthesis of pillared GO composite at a CS/GO ratio = 0.1, improved the surface area of GO with a subsequent reduction of its hydrophilic character. Characterization experiments demonstrated the presence of chitosan in the spaced between the GO sheets. Electrostatic interactions and amide bonds are the main mechanisms of synthesis. The presence of dissolved organic matter had a positive effect in the removal of HC, but high acidic conditions hindered the removal capacity attributed to chitosan dissolution.

7.2 FUTURE WORK

Numerous works related to biosorption of pollutants could be found in the literature, but the main drawback in most of the cases is the worldwide unavailability. Seaweed responds in a positive way to this challenge. As shown in the results, brown seaweed possesses remarkable characteristics for biosorption technology. As perspective, it would be useful to search and select a seaweed with a higher lignocellulosic content, and at the same design and effective cultivation and farming for biosorbent production in large scale.

Macroalgae-based composites are the key for scale-up processes, but there is still the necessity to find an optimum immobilization technique that ensures a synergy removal of the organic pollutants. Another important aspect of the synthesis of composites is the research on the mechanical properties, especially in dynamic studies. One remaining test is the to determine the effect of size reduction on sorption capacity and the feasibility of loaded biomass for calorimetric determinations

Related to the pillaring of graphene oxide sheets, following modification may include the chemical modifications of the precursors (chitosan and graphene oxide) to increase the hydrophobic character of the final material and the chemical stability at high acidic conditions. The pillared effectiveness of GO by other natural polymers is an emerging research field.

7.3 LIST OF PUBLICATIONS

- Flores-Chaparro, C. E., M. C. Rodriguez-Hernandez Ruiz, L. F. C., Alfaro-De la Torre, M. C., M. A. Huerta-Diaz & Rangel-Mendez, J. R (2018). Fixed bed biosorption studies for the removal of BTEX and naphthalene onto a microalgae-based composite. Selectivity and breakthrough modeling (*In revision*).

- C. E. Flores-Chaparro, C.J. Barbosa-DeCastilho, I. Külaots, R. H. Hurt, J. R. Rangel-Mendez (2018). Pillared graphene oxide biocomposite as a potential adsorbent of water-soluble hydrocarbons: Effect of pH, organic matter, and ionic strength. (*In revision*).

- April L Rodd, Cintia J Castilho, Carlos EF Chaparro, J Rene Rangel-Mendez, Robert H Hurt, and Agnes B Kane. (2018). Impact of emerging, high volume graphene materials on adverse outcomes in co-exposure with benzo(a)pyrene in brine shrimp and fish liver cells. (*In revision*).

- Carlos E. Flores-Chaparro, Mayra C. Rodriguez-Hernandez, Luis F. Chazaro Ruiz, Ma. C. Alfaro-De la Torre, Miguel A. Huerta-Diaz & Jose R. Rangel-Mendez (2018) Chitosan-macroalgae biocomposites as potential adsorbents of water-soluble hydrocarbons: Organic matter and ionic strength effects (*In revision*).

- Mayra Cecilia Rodriguez-Hernandez, C.E. Flores-Chaparro; Jose Rene Rangel-Mendez (2017). Influence of Dissolved Organic Matter and Oil on the Biosorption of BTEX by Macroalgae in Single and Multi-Solute Systems. *Environmental Science and Pollution Research*.

- Flores-Chaparro, C. E., Ruiz, L. F. C., Alfaro-De la Torre, M. C., M. A.l Huerta-Diaz & Rangel-Mendez, J. R. (2017). Biosorption removal of benzene and toluene by three-dried macroalgae at different ionic strength and temperatures: Algae biochemical composition and kinetics. *Journal of Environmental Management*, 126-135.

- Flores-Chaparro, C. E., Pérez-Martínez, R.M. & Rangel-Mendez, J. R. (2015). Control de derrames de petróleo en cuerpos naturales de agua. *Universitarios Potosinos*, Octubre, 2015, 20-25.

7.4 EXTENDED ABSTRACTS

2016 The American Institute of Chemical Engineers (AIChE)
"Macroalgae and Chitosan-Macroalgae Biocomposite As Potential Adsorbents of Water-Soluble Hydrocarbons: Effect of pH, Organic Matter and Ionic Strength."

7.5 ATTENDANCE TO CONFERENCES

2017 2° AMEXCARB – Asociación Mexicana del Carbono
"Materiales híbridos de óxido de grafeno pilareado con quitosano para la remoción de compuestos aromáticos en agua"
Presentación oral.
IPICYT, San Luis Potosí

2016 The American Institute of Chemical Engineers (AIChE)
"Macroalgae and Chitosan-Macroalgae Biocomposite As Potential Adsorbents of Water-Soluble Hydrocarbons: Effect of pH, Organic Matter and Ionic Strength."
Presentación oral.
San Francisco, CA, EUA

2014 - 2016 5° y 6° Simposio de avances de tesis de Posgrado. Presentaciones orales. Reconocimiento a la mejor presentación oral en 2016
IPICYT, San Luis Potosí

2015 AMEXCARB – Asociación Mexicana del Carbono
"Materiales a Base de Carbono como Adsorbentes de Compuestos Aromáticos en Agua con Diferente Grado de Salinidad"
Presentación oral.
IPICYT, San Luis Potosí

2015 IWA-México 2015- Young Waters Professionals
"Biosorción de compuestos aromáticos por medio de macroalgas en agua con diferente grado de salinidad".
Presentación oral.
IPICYT, San Luis Potosí

REFERENCES

[1] Ucan Marin Francisco, Dupuis Alain, A literature review on the aquatic toxicology of petroleum oil: An overview of oil properties and effects to aquatic biota, Canadian Science Advisory Secretariat (CSAS), 2015. https://www.researchgate.net/publication/273142351_A_literature_review_on_the_aquatic_toxicology_of_petroleum_oil_An_overview_of_oil_properties_and_effects_to_aquatic_biota (accessed June 14, 2018).

[2] S.J. Varjani, R.R. Joshi, P.S. Kumar, V.K. Srivastava, V. Kumar, C. Banerjee, R.P. Kumar, Polycyclic Aromatic Hydrocarbons from Petroleum Oil Industry Activities: Effect on Human Health and Their Biodegradation, in: Waste Bioremediation, Springer, Singapore, 2018: pp. 185–199. doi:10.1007/978-981-10-7413-4_9.

[3] A. Fakhru'l-Razi, A. Pendashteh, L.C. Abdullah, D.R.A. Biak, S.S. Madaeni, Z.Z. Abidin, Review of technologies for oil and gas produced water treatment, J. Hazard. Mater. 170 (2009) 530–551. doi:10.1016/j.jhazmat.2009.05.044.

[4] E.T. Igunnu, G.Z. Chen, Produced water treatment technologies, Int. J. Low-Carbon Technol. 9 (2014) 157–177. doi:10.1093/ijlct/cts049.

[5] R. Crisafully, M.A.L. Milhome, R.M. Cavalcante, E.R. Silveira, D. De Keukeleire, R.F. Nascimento, Removal of some polycyclic aromatic hydrocarbons from petrochemical wastewater using low-cost adsorbents of natural origin, Bioresour. Technol. 99 (2008) 4515–4519. doi:10.1016/j.biortech.2007.08.041.

[6] V.K. Gupta, A. Rastogi, Biosorption of lead from aqueous solutions by green algae Spirogyra species: Kinetics and equilibrium studies, J. Hazard. Mater. 152 (2008) 407–414. doi:10.1016/j.jhazmat.2007.07.028.

[7] V.S. Tran, H.H. Ngo, W. Guo, J. Zhang, S. Liang, C. Ton-That, X. Zhang, Typical low cost biosorbents for adsorptive removal of specific organic pollutants from water, Bioresour. Technol. 182 (2015) 353–363. doi:10.1016/j.biortech.2015.02.003.

[8] I. Ali, M. Asim, T.A. Khan, Low cost adsorbents for the removal of organic pollutants from wastewater, J. Environ. Manage. 113 (2012) 170–183. doi:10.1016/j.jenvman.2012.08.028.

[9] M.A. Hubbe, J. Park, S. Park, Cellulosic Substrates for Removal of Pollutants from Aqueous Systems: A Review. Part 4. Dissolved Petrochemical Compounds, BioResources. 9 (2014) 7782–7925. doi:10.15376/biores.9.4.

[10] A. Abdolali, H.H. Ngo, W. Guo, J.L. Zhou, J. Zhang, S. Liang, S.W. Chang, D.D. Nguyen, Y. Liu, Application of a breakthrough biosorbent for removing heavy metals from synthetic and real wastewaters in a lab-scale continuous fixed-bed column, Bioresour. Technol. 229 (2017) 78–87. doi:10.1016/j.biortech.2017.01.016.

[11] L. Fan, C. Luo, M. Sun, H. Qiu, X. Li, Synthesis of magnetic β-cyclodextrin–chitosan/graphene oxide as nanoadsorbent and its application in dye adsorption and

removal, Colloids Surf. B Biointerfaces. 103 (2013) 601–607. doi:10.1016/j.colsurfb.2012.11.023.

[12] UN-Water, ed., Towards a Worldwide Assessment of Freshwater Quality, (2016). http://www.unwater.org/publications/towards-worldwide-assessment-freshwater-quality/ (accessed September 15, 2017).

[13] UN Environment Programme, A Snapshot of the World's Water Quality: Towards a global assessment, (2016). https://reliefweb.int/report/world/snapshot-world-s-water-quality-towards-global-assessment-enarfrrues (accessed September 15, 2017).

[14] C. Zheng, L. Zhao, X. Zhou, Z. Fu, A. Li, Treatment Technologies for Organic Wastewater, (2013). doi:10.5772/52665.

[15] V. Kumar Gupta, I. Ali, T. A. Saleh, A. Nayak, S. Agarwal, Chemical treatment technologies for waste-water recycling—an overview, RSC Adv. 2 (2012) 6380–6388. doi:10.1039/C2RA20340E.

[16] E. Manoli, C. Samara, Polycyclic aromatic hydrocarbons in natural waters: sources, occurrence and analysis, TrAC Trends Anal. Chem. 18 (1999) 417–428. doi:10.1016/S0165-9936(99)00111-9.

[17] P.F. Kingston, Long-term Environmental Impact of Oil Spills, Spill Sci. Technol. Bull. 7 (2002) 53–61. doi:10.1016/S1353-2561(02)00051-8.

[18] M. Qiao, W. Cao, B. Liu, Y. Bai, W. Qi, X. Zhao, J. Qu, Impact of upgrading wastewater treatment plant on the removal of typical methyl, oxygenated, chlorinated and parent polycyclic aromatic hydrocarbons, Sci. Total Environ. 603 (2017) 140–147. doi:10.1016/j.scitotenv.2017.06.097.

[19] Oil Tanker Spill Statistics 2015 - ITOPF, The International Tanker Owners Pollution Federation Limited, United Kingdom, 2016. http://www.itopf.com/knowledge-resources/documents-guides/document/oil-tanker-spill-statistics-2013/ (accessed April 16, 2016).

[20] I.B. Ivshina, M.S. Kuyukina, A.V. Krivoruchko, A.A. Elkin, S.O. Makarov, C.J. Cunningham, T.A. Peshkur, R.M. Atlas, J.C. Philp, Oil spill problems and sustainable response strategies through new technologies, Environ. Sci.: Processes Impacts. 17 (2015) 1201–1219. doi:10.1039/C5EM00070J.

[21] IOGP, Environmental performance indicators - 2014 data, International Association of Oil and Gas Producers, 2015. http://www.iogp.org/Our-library.

[22] P.W. and G.S.C. Government of Canada, A literature review on the aquatic toxicology of petroleum oil :: Fs70-5/2015-007E-PDF - Government of Canada Publications, (2002). http://publications.gc.ca/site/eng/481102/publication.html (accessed September 15, 2017).

[23] J. Coca-Prados, G. Gutiérrez-Cervelló, eds., Water Purification and Management, Springer Netherlands, 2011. //www.springer.com/la/book/9789048197743 (accessed June 2, 2018).

[24] US EPA, Priority Pollutants, (2013). http://water.epa.gov/scitech/methods/cwa/pollutants.cfm (accessed April 9, 2013).

[25] R.P. Schwarzenbach, P.M. Gschwend, D.M. Imboden, Environmental Organic Chemistry, John Wiley & Sons, 2016.

[26] A.S. Costa, L.P.C. Romão, B.R. Araújo, S.C.O. Lucas, S.T.A. Maciel, A. Wisniewski Jr., M.R. Alexandre, Environmental strategies to remove volatile aromatic fractions (BTEX) from petroleum industry wastewater using biomass, Bioresour. Technol. 105 (2012) 31–39. doi:10.1016/j.biortech.2011.11.096.

[27] C.B. Vidal, A.L. Barros, C.P. Moura, A.C.A. de Lima, F.S. Dias, L.C.G. Vasconcellos, P.B.A. Fechine, R.F. Nascimento, Adsorption of polycyclic aromatic hydrocarbons from aqueous solutions by modified periodic mesoporous organosilica, J. Colloid Interface Sci. 357 (2011) 466–473. doi:10.1016/j.jcis.2011.02.013.

[28] OM Fayemiwo, MO Daramola, K Moothi, BTEX compounds in water - future trends and directions for water treatment, Water SA. 43 (2017) 602–614. doi:10.4314/wsa.v43i4.08.

[29] Y. Liu, E.B. Kujawinski, Chemical Composition and Potential Environmental Impacts of Water-Soluble Polar Crude Oil Components Inferred from ESI FT-ICR MS, Plos One. 10 (2015) e0136376. doi:10.1371/journal.pone.0136376.

[30] O.M. Fayemiwo, M.O. Daramola, K. Moothi, BTEX compounds in water - future trends and directions for water treatment, Water SA. 43 (2017) 602–613. doi:10.4314/wsa.v43i4.08.

[31] K.R. Echols, J.C. Meadows, C.E. Orazio, Pollution of Aquatic Ecosystems II: Hydrocarbons, Synthetic Organics, Radionuclides, Heavy Metals, Acids, and Thermal Pollution, in: G.E. Likens (Ed.), Encycl. Inland Waters, Academic Press, Oxford, 2009: pp. 120–128. http://www.sciencedirect.com/science/article/pii/B9780123706263002234 (accessed December 6, 2013).

[32] E. Rojo-Nieto, D. Sales, J.A. Perales, Sources, transport and fate of PAHs in sediments and superficial water of a chronically polluted semi-enclosed body of seawater: linking of compartments, Environ. Sci. Process. Impacts. 15 (2013) 986–995. doi:10.1039/C3EM00050H.

[33] L. Sørensen, A.G. Melbye, A.M. Booth, Oil droplet interaction with suspended sediment in the seawater column: Influence of physical parameters and chemical dispersants, Mar. Pollut. Bull. 78 (2014) 146–152. doi:10.1016/j.marpolbul.2013.10.049.

[34] J.M. Neff, Chapter 14 - Monocyclic Aromatic Hydrocarbons in the Ocean, in: Bioaccumulation Mar. Org., Elsevier, Oxford, 2002: pp. 225–240. http://www.sciencedirect.com/science/article/pii/B9780080437163500154 (accessed June 21, 2013).

[35] NOM-127-SSA1-1994, (n.d.). http://www.salud.gob.mx/unidades/cdi/nom/127ssa14.html (accessed June 1, 2018).

[36] A short primer on benzene, toluene, ethylbenzene and xylenes (BTEX) in the environment and in hydraulic fracturing fluids - Semantic Scholar, (n.d.). /paper/A-short-primer-on-benzene%2C-toluene%2C-ethylbenzene-in/47088a39aeda3ddd76e67e5e2088faa4a8b86743 (accessed June 1, 2018).

[37] V. Dhananjayan, S. Muralidharan, V.R. Peter, Occurrence and Distribution of Polycyclic Aromatic Hydrocarbons in Water and Sediment Collected along the Harbour Line, Mumbai, India, Int. J. Oceanogr. 2012 (2012). doi:10.1155/2012/403615.

[38] C.M. Reddy, J.S. Arey, J.S. Seewald, S.P. Sylva, K.L. Lemkau, R.K. Nelson, C.A. Carmichael, C.P. McIntyre, J. Fenwick, G.T. Ventura, B.A.S.V. Mooy, R. Camilli, Composition and fate of gas and oil released to the water column during the Deepwater Horizon oil spill, Proc. Natl. Acad. Sci. (2011). doi:10.1073/pnas.1101242108.

[39] H. Agah, A. Mehdinia, K.D. Bastami, S. Rahmanpour, Polycyclic aromatic hydrocarbon pollution in the surface water and sediments of Chabahar Bay, Oman Sea, Mar. Pollut. Bull. 115 (2017) 515–524. doi:10.1016/j.marpolbul.2016.12.032.

[40] M.P. Premkumar, K.V. Thiruvengadaravi, P.S. Kumar, J. Nandagopal, S. Sivanesan, Eco-Friendly Treatment Strategies for Wastewater Containing Dyes and Heavy Metals, in: Environ. Contam., Springer, Singapore, 2018: pp. 317–360. doi:10.1007/978-981-10-7332-8_14.

[41] B.H. Diya'uddeen, W.M.A.W. Daud, A.R. Abdul Aziz, Treatment technologies for petroleum refinery effluents: A review, Process Saf. Environ. Prot. 89 (2011) 95–105. doi:10.1016/j.psep.2010.11.003.

[42] J. Coca, G. Gutiérrez, J. Benito, TREATMENT OF OILY WASTEWATER, in: J. Coca-Prados, G. Gutiérrez-Cervelló (Eds.), Water Purif. Manag., Springer Netherlands, 2011: pp. 1–55. http://link.springer.com/chapter/10.1007/978-90-481-9775-0_1 (accessed April 28, 2013).

[43] F.E.- Fuentes, G.S.- Salas, Evaluación Experimental Del Comportamiento De La Velocidad De Sedimentación De Partículas, Rev. Ing. Univ. Medellín. 11 (2012) 239–250.

[44] O.B. Akpor, U.F. Okolomike, T.D. Olaolu, B.I. Aderive, Remediation of Polluted Wastewater Effluents: Hydrocarbon Removal, Trends Appl. Sci. Res. 9 (2014) 160–173. doi:10.3923/tasr.2014.160.173.

[45] B. Chen, Y. Wang, D. Hu, Biosorption and biodegradation of polycyclic aromatic hydrocarbons in aqueous solutions by a consortium of white-rot fungi, J. Hazard. Mater. 179 (2010) 845–851. doi:10.1016/j.jhazmat.2010.03.082.

[46] K.A. Gallagher, M.G. Healy, S.J. Allen, Biosorption of synthetic dye and metal ions from aqueous effluents using fungal biomass, in: D.L. Wise (Ed.), Stud. Environ. Sci., Elsevier, 1997: pp. 27–50.

http://www.sciencedirect.com/science/article/pii/S0166111697800337 (accessed April 21, 2013).

[47] E. Deniaud-Bouët, N. Kervarec, G. Michel, T. Tonon, B. Kloareg, C. Hervé, Chemical and enzymatic fractionation of cell walls from Fucales: insights into the structure of the extracellular matrix of brown algae, Ann. Bot. 114 (2014) 1203–1216. doi:10.1093/aob/mcu096.

[48] E. Jindrová, M. Chocová, K. Demnerová, V. Brenner, Bacterial aerobic degradation of benzene, toluene, ethylbenzene and xylene, Folia Microbiol. (Praha). 47 (2002) 83–93. doi:10.1007/BF02817664.

[49] T.C. Voice, D. Pak, X. Zhao, J. Shi, R.F. Hickey, Biological activated carbon in fluidized bed reactors for the treatment of groundwater contaminated with volatile aromatic hydrocarbons, Water Res. 26 (1992) 1389–1401. doi:10.1016/0043-1354(92)90132-N.

[50] M. Maretto, F. Bianchi, R. Vignola, S. Canepari, M. Baric, R. Iazzoni, M. Tagliabue, M.P. Papini, Microporous and mesoporous materials for the treatment of wastewater produced by petrochemical activities, J. Clean. Prod. 77 (2014) 22–34. doi:10.1016/j.jclepro.2013.12.070.

[51] S. Lamichhane, K.C. Bal Krishna, R. Sarukkalige, Polycyclic aromatic hydrocarbons (PAHs) removal by sorption: A review, Chemosphere. 148 (2016) 336–353. doi:10.1016/j.chemosphere.2016.01.036.

[52] R.T. Yang, Adsorbents: Fundamentals and Applications, 1st ed., John Wiley & Sons Inc, New Jersey, 2003.

[53] T. Gupta, A.K. Agarwal, R.A. Agarwal, N.K. Labhasetwar, eds., Environmental Contaminants: Measurement, Modelling and Control, Springer Singapore, 2018. //www.springer.com/us/book/9789811073311 (accessed June 3, 2018).

[54] M. Otero, C.A. Grande, A.E. Rodrigues, Adsorption of salicylic acid onto polymeric adsorbents and activated charcoal, React. Funct. Polym. 60 (2004) 203–213. doi:10.1016/j.reactfunctpolym.2004.02.024.

[55] A. Torabian, H. Kazemian, L. Seifi, G.N. Bidhendi, A.A. Azimi, S.K. Ghadiri, Removal of Petroleum Aromatic Hydrocarbons by Surfactant-modified Natural Zeolite: The Effect of Surfactant, CLEAN – Soil Air Water. 38 (n.d.) 77–83. doi:10.1002/clen.200900157.

[56] J.K. Parker, S. Lignou, K. Shankland, P. Kurwie, H.D. Griffiths, D.A. Baines, Development of a Zeolite Filter for Removing Polycyclic Aromatic Hydrocarbons (PAHs) from Smoke and Smoked Ingredients while Retaining the Smoky Flavor, J. Agric. Food Chem. 66 (2018) 2449–2458. doi:10.1021/acs.jafc.6b05399.

[57] R.C. Bansal, Activated carbon adsorption, Taylor & Francis, Boca Raton, 2005.

[58] B. Li, Z. Lei, Z. Huang, Surface-Treated Activated Carbon for Removal of Aromatic Compounds from Water, Chem. Eng. Technol. 32 (2009) 763–770. doi:10.1002/ceat.200800535.

[59] H. Marsh, F.R. Reinoso, Activated Carbon, Elsevier, 2006.

[60] C. Moreno-Castilla, Adsorption of organic molecules from aqueous solutions on carbon materials, Carbon. 42 (2004) 83–94. doi:10.1016/j.carbon.2003.09.022.

[61] G. Graziano, Benzene solubility in water: A reassessment, Chem. Phys. Lett. 429 (2006) 114–118. doi:10.1016/j.cplett.2006.08.006.

[62] C.E. Flores-Chaparro, L.F.C. Ruiz, M.C.A.-D. la Torre, J.R. Rangel-Mendez, Soluble hydrocarbons uptake by porous carbonaceous adsorbents at different water ionic strength and temperature: something to consider in oil spills, Environ. Sci. Pollut. Res. (2016) 1–11. doi:10.1007/s11356-016-6286-0.

[63] An Introduction to Graphene and Carbon Nanotubes, 2017. https://www.crcpress.com/An-Introduction-to-Graphene-and-Carbon-Nanotubes/Proctor-Armada-Vijayaraghavan/p/book/9781498751797 (accessed December 11, 2017).

[64] J.E. Proctor, D.M. Armada, A. Vijayaraghavan, An Introduction to Graphene and Carbon Nanotubes, CRC Press, 2017.

[65] C.-M. Chen, Surface Chemistry and Macroscopic Assembly of Graphene for Application in Energy Storage, Springer, 2015.

[66] G. Sheng, S. Zhu, S. Wang, Z. Wang, Removal of dyes by a novel fly ash–chitosan–graphene oxide composite adsorbent, RSC Adv. 6 (2016) 17987–17994. doi:10.1039/C5RA22091B.

[67] F. Guo, M. Creighton, Y. Chen, R. Hurt, I. Külaots, Porous structures in stacked, crumpled and pillared graphene-based 3D materials, Carbon. 66 (2014) 476–484. doi:10.1016/j.carbon.2013.09.024.

[68] Y. Chen, L. Chen, H. Bai, L. Li, Graphene oxide– chitosan composite hydrogels as broad- spectrum adsorbents for water purification, J. Mater. Chem. A. 1 (2013) 1992–2001. doi:10.1039/C2TA00406B.

[69] P.L.K. Fu, J.M. Symons, Removing Aquatic Organic Substances by Anion Exchange Resins, J. - Am. Water Works Assoc. 82 (n.d.) 70–77. doi:10.1002/j.1551-8833.1990.tb07039.x.

[70] S.D. Faust, O.M. Aly, Adsorption Processes for Water Treatment, Elsevier, 2013.

[71] M. Caetano, C. Valderrama, A. Farran, J.L. Cortina, Phenol removal from aqueous solution by adsorption and ion exchange mechanisms onto polymeric resins, J. Colloid Interface Sci. 338 (2009) 402–409. doi:10.1016/j.jcis.2009.06.062.

[72] V.B. Cashin, D.S. Eldridge, A. Yu, D. Zhao, Surface functionalization and manipulation of mesoporous silica adsorbents for improved removal of pollutants: a review, Environ. Sci. Water Res. Technol. 4 (2018) 110–128. doi:10.1039/C7EW00322F.

[73] S. Wang, Y. Peng, Natural zeolites as effective adsorbents in water and wastewater treatment, Chem. Eng. J. 156 (2010) 11–24. doi:10.1016/j.cej.2009.10.029.

[74] B. Volesky, Biosorption and me, Water Res. 41 (2007) 4017–4029. doi:10.1016/j.watres.2007.05.062.

[75] A. Ata, O.O. Nalcaci, B. Ovez, Macro algae Gracilaria verrucosa as a biosorbent: A study of sorption mechanisms, Algal Res. 1 (2012) 194–204. doi:10.1016/j.algal.2012.07.001.

[76] J.P. Cazón, M. Viera, S. Sala, E. Donati, Biochemical characterization of Macrocystis pyrifera and Undaria pinnatifida (Phaeophyceae) in relation to their potentiality as biosorbents, Phycologia. 53 (2014) 100–108. doi:10.2216/12-106.1.

[77] G.M. Gadd, Biosorption: critical review of scientific rationale, environmental importance and significance for pollution treatment, J. Chem. Technol. Biotechnol. 84 (2009) 13–28. doi:10.1002/jctb.1999.

[78] I. Moreno-Garrido, Microalgae immobilization: Current techniques and uses, Bioresour. Technol. 99 (2008) 3949–3964. doi:10.1016/j.biortech.2007.05.040.

[79] C.E. Flores-Chaparro, L.F. Chazaro Ruiz, M.C. Alfaro de la Torre, M.A. Huerta-Diaz, J.R. Rangel-Mendez, Biosorption removal of benzene and toluene by three dried macroalgae at different ionic strength and temperatures: Algae biochemical composition and kinetics, J. Environ. Manage. 193 (2017) 126–135. doi:10.1016/j.jenvman.2017.02.005.

[80] M.S.A. Hameed, Continuous removal and recovery of lead by alginate beads, free and alginate-immobilized Chlorella vulgaris, Afr. J. Biotechnol. 5 (2006). doi:10.4314/ajb.v5i19.55877.

[81] R. Gutiérrez Leyva, Uso de harinas de Macrocystis pyrifera ySargassum spp. en alimentos balanceados para el camarón Litopenaeus vannamei: efectos sobre el crecimiento y la digestibilidad in vivo., Thesis, Instituto Politécnico Nacional. Centro Interdisciplinario de Ciencias Marinas, 2006. http://www.repositoriodigital.ipn.mx/handle/123456789/14214 (accessed December 1, 2014).

[82] R.R.-R. María del Carmen Méndez-Trejo, Evaluación de la invasión de Acanthophora spicifera (Rhodophyta) sobre la epifauna en Bahía de La Paz; B.C.S., (2014) 433–456.

[83] M. Ghadiryanfar, K.A. Rosentrater, A. Keyhani, M. Omid, A review of macroalgae production, with potential applications in biofuels and bioenergy, Renew. Sustain. Energy Rev. 54 (2016) 473–481. doi:10.1016/j.rser.2015.10.022.

[84] A. Bhatnagar, M. Sillanpää, Applications of chitin- and chitosan-derivatives for the detoxification of water and wastewater — A short review, Adv. Colloid Interface Sci. 152 (2009) 26–38. doi:10.1016/j.cis.2009.09.003.

[85] G. Crini, P.-M. Badot, Application of chitosan, a natural aminopolysaccharide, for dye removal from aqueous solutions by adsorption processes using batch

studies: A review of recent literature, Prog. Polym. Sci. 33 (2008) 399–447. doi:10.1016/j.progpolymsci.2007.11.001.

[86] F. H. Isikgor, C. Remzi Becer, Lignocellulosic biomass: a sustainable platform for the production of bio-based chemicals and polymers, Polym. Chem. 6 (2015) 4497–4559. doi:10.1039/C5PY00263J.

[87] G. Crini, Non-conventional low-cost adsorbents for dye removal: A review, Bioresour. Technol. 97 (2006) 1061–1085. doi:10.1016/j.biortech.2005.05.001.

[88] S. De Gisi, G. Lofrano, M. Grassi, M. Notarnicola, Characteristics and adsorption capacities of low-cost sorbents for wastewater treatment: A review, Sustain. Mater. Technol. 9 (2016) 10–40. doi:10.1016/j.susmat.2016.06.002.

[89] V.K. Gupta, P.J.M. Carrott, M.M.L. Ribeiro Carrott, Suhas, Low-Cost Adsorbents: Growing Approach to Wastewater Treatment—a Review, Crit. Rev. Environ. Sci. Technol. 39 (2009) 783–842. doi:10.1080/10643380801977610.

[90] A.E. Navarro, J.C. Lazo, N.A. Cuizano, M.R. Sun-Kou, B.P. Llanos, Insights into Removal of Phenol from Aqueous Solutions by Low Cost Adsorbents: Clays Versus Algae, Sep. Sci. Technol. 44 (2009) 2491–2509. doi:10.1080/01496390903012197.

[91] C.-F. Chang, C.-Y. Chang, W. Höll, M. Ulmer, Y.-H. Chen, H.-J. Groß, Adsorption kinetics of polyethylene glycol from aqueous solution onto activated carbon, Water Res. 38 (2004) 2559–2570. doi:10.1016/j.watres.2004.03.001.

[92] Y.H. Khan, A. Islam, A. Sarwar, N. Gull, S.M. Khan, M.A. Munawar, S. Zia, A. Sabir, M. Shafiq, T. Jamil, Novel green nano composites films fabricated by indigenously synthesized graphene oxide and chitosan, Carbohydr. Polym. (n.d.). doi:10.1016/j.carbpol.2016.03.031.

[93] R.-Y. Tsai, P.-W. Chen, T.-Y. Kuo, C.-M. Lin, D.-M. Wang, T.-Y. Hsien, H.-J. Hsieh, Chitosan/pectin/gum Arabic polyelectrolyte complex: Process-dependent appearance, microstructure analysis and its application, Carbohydr. Polym. 101 (2014) 752–759. doi:10.1016/j.carbpol.2013.10.008.

[94] C.K.S. Pillai, W. Paul, C.P. Sharma, Chitin and chitosan polymers: Chemistry, solubility and fiber formation, Prog. Polym. Sci. 34 (2009) 641–678. doi:10.1016/j.progpolymsci.2009.04.001.

[95] A. Cabiac, E. Guillon, F. Chambon, C. Pinel, F. Rataboul, N. Essayem, Cellulose reactivity and glycosidic bond cleavage in aqueous phase by catalytic and non catalytic transformations, Appl. Catal. Gen. 402 (2011) 1–10. doi:10.1016/j.apcata.2011.05.029.

[96] L. Sun, H. Yu, B. Fugetsu, Graphene oxide adsorption enhanced by in situ reduction with sodium hydrosulfite to remove acridine orange from aqueous solution, J. Hazard. Mater. 203–204 (2012) 101–110. doi:10.1016/j.jhazmat.2011.11.097.

[97] T. Ghosh, K.-Y. Cho, K. Ullah, V. Nikam, C.-Y. Park, Z.-D. Meng, W.-C. Oh, High photonic effect of organic dye degradation by CdSe–graphene–TiO2 particles, J. Ind. Eng. Chem. 19 (2013) 797–805. doi:10.1016/j.jiec.2012.10.020.

[98] X. Liu, L. Pan, T. Lv, Z. Sun, C.Q. Sun, Visible light photocatalytic degradation of dyes by bismuth oxide-reduced graphene oxide composites prepared via microwave-assisted method, J. Colloid Interface Sci. 408 (2013) 145–150. doi:10.1016/j.jcis.2013.07.045.

[99] Y. Jiang, J.-L. Gong, G.-M. Zeng, X.-M. Ou, Y.-N. Chang, C.-H. Deng, J. Zhang, H.-Y. Liu, S.-Y. Huang, Magnetic chitosan–graphene oxide composite for anti-microbial and dye removal applications, Int. J. Biol. Macromol. 82 (2016) 702–710. doi:10.1016/j.ijbiomac.2015.11.021.

[100] D.A. Reddy, S. Lee, J. Choi, S. Park, R. Ma, H. Yang, T.K. Kim, Green synthesis of AgI-reduced graphene oxide nanocomposites: Toward enhanced visible-light photocatalytic activity for organic dye removal, Appl. Surf. Sci. 341 (2015) 175–184. doi:10.1016/j.apsusc.2015.03.019.

[101] D. Lu, Y. Zhang, S. Lin, L. Wang, C. Wang, Synthesis of magnetic ZnFe2O4/graphene composite and its application in photocatalytic degradation of dyes, J. Alloys Compd. 579 (2013) 336–342. doi:10.1016/j.jallcom.2013.06.098.

[102] S.B.C. Pergher, A. Corma, V. Fornes, Pillared layered materials: preparation and properties, Quím. Nova. 22 (1999) 693–709. doi:10.1590/S0100-40421999000500013.

[103] D. Ma, J. Lin, Y. Chen, W. Xue, L.-M. Zhang, In situ gelation and sustained release of an antitumor drug by graphene oxide nanosheets, Carbon. 50 (2012) 3001–3007. doi:10.1016/j.carbon.2012.02.083.

[104] A. Sahu, W.I. Choi, G. Tae, A stimuli-sensitive injectable graphene oxide composite hydrogel, Chem. Commun. 48 (2012) 5820–5822. doi:10.1039/C2CC31862H.

[105] Z.-Y. Sui, Y. Cui, J.-H. Zhu, B.-H. Han, Preparation of Three-Dimensional Graphene Oxide–Polyethylenimine Porous Materials as Dye and Gas Adsorbents, ACS Appl. Mater. Interfaces. 5 (2013) 9172–9179. doi:10.1021/am402661t.

[106] F. Li, X. Jiang, J. Zhao, S. Zhang, Graphene oxide: A promising nanomaterial for energy and environmental applications, Nano Energy. 16 (2015) 488–515. doi:10.1016/j.nanoen.2015.07.014.

[107] K. Christian Kemp, H. Seema, M. Saleh, N. H. Le, K. Mahesh, V. Chandra, K. S. Kim, Environmental applications using graphene composites: water remediation and gas adsorption, Nanoscale. 5 (2013) 3149–3171. doi:10.1039/C3NR33708A.

[108] T.A. Davis, B. Volesky, A. Mucci, A review of the biochemistry of heavy metal biosorption by brown algae, Water Res. 37 (2003) 4311–4330. doi:10.1016/S0043-1354(03)00293-8.

[109] A. Synytsya, J. Čopíková, W.J. Kim, Y.I. Park, Cell Wall Polysaccharides of Marine Algae, in: S.-K.K. Prof (Ed.), Springer Handb. Mar. Biotechnol., Springer Berlin Heidelberg, 2015: pp. 543–590. doi:10.1007/978-3-642-53971-8_22.

[110] D.S. Domozych, Algal Cell Walls, in: ELS, John Wiley & Sons, Ltd, 2011. http://onlinelibrary.wiley.com/doi/10.1002/9780470015902.a0000315.pub3/abstract (accessed December 12, 2015).

[111] Z.A. Popper, G. Michel, C. Hervé, D.S. Domozych, W.G.T. Willats, M.G. Tuohy, B. Kloareg, D.B. Stengel, Evolution and Diversity of Plant Cell Walls: From Algae to Flowering Plants, Annu. Rev. Plant Biol. 62 (2011) 567–590. doi:10.1146/annurev-arplant-042110-103809.

[112] D.S. Domozych, M. Ciancia, J.U. Fangel, M.D. Mikkelsen, P. Ulvskov, W.G.T. Willats, The Cell Walls of Green Algae: A Journey through Evolution and Diversity, Front. Plant Sci. 3 (2012). doi:10.3389/fpls.2012.00082.

[113] C. Rey-Castro, P. Lodeiro, R. Herrero, M.E. Sastre de Vicente, Acid−Base Properties of Brown Seaweed Biomass Considered As a Donnan Gel. A Model Reflecting Electrostatic Effects and Chemical Heterogeneity, Environ. Sci. Technol. 37 (2003) 5159–5167. doi:10.1021/es0343353.

[114] L. e. Cruz-Suárez, M. Tapia-Salazar, M. g. Nieto-López, C. Guajardo-Barbosa, D. Ricque-Marie, Comparison of Ulva clathrata and the kelps Macrocystis pyrifera and Ascophyllum nodosum as ingredients in shrimp feeds, Aquac. Nutr. 15 (2009) 421–430. doi:10.1111/j.1365-2095.2008.00607.x.

[115] Mohammadi M., Tajik H., Hajeb P., Nutritional composition of seaweeds from the Northern Persion Gulf., 12 (2013) 232–240.

[116] K.J. McDermid, B. Stuercke, Nutritional composition of edible Hawaiian seaweeds, J. Appl. Phycol. 15 (2003) 513–524. doi:10.1023/B:JAPH.0000004345.31686.7f.

[117] M. Weijerman, R. Most, K. Wong, S. Beavers, Attempt to Control the Invasive Red Alga Acanthophora spicifera (Rhodophyta: Ceramiales) in a Hawaiian Fishpond: An Assessment of Removal Techniques and Management Options, Pac. Sci. 62 (2008) 517–532. doi:10.2984/1534-6188(2008)62[517:ATCTIR]2.0.CO;2.

[118] L.E.A.-R. Raúl Aguilar-Rosas, Ulva fasciata Delile (Ulvaceae, Chlorophycota): a species newly introduced into Pacific Mexico, Bot. Mar. - BOT MAR. 48 (2005) 46–51. doi:10.1515/BOT.2005.005.

[119] M.K. Chung, M.T.K. Tsui, K.C. Cheung, N.F.Y. Tam, M.H. Wong, Removal of aqueous phenanthrene by brown seaweed Sargassum hemiphyllum: Sorption-kinetic and equilibrium studies, Sep. Purif. Technol. 54 (2007) 355–362. doi:10.1016/j.seppur.2006.10.008.

[120] J.P. Chen, L. Yang, Chemical Modification of Sargassum sp. for Prevention of Organic Leaching and Enhancement of Uptake during Metal Biosorption, Ind. Eng. Chem. Res. 44 (2005) 9931–9942. doi:10.1021/ie050678t.

[121] H.A. Arafat, M. Franz, N.G. Pinto, Effect of Salt on the Mechanism of Adsorption of Aromatics on Activated Carbon†, Langmuir. 15 (1999) 5997–6003. doi:10.1021/la9813331.

[122] D. Zhang, C. Ran, Y. Yang, Y. Ran, Biosorption of phenanthrene by pure algae and field-collected planktons and their fractions, Chemosphere. 93 (2013) 61–68. doi:10.1016/j.chemosphere.2013.04.068.

[123] N. Wibowo, L. Setyadhi, D. Wibowo, J. Setiawan, S. Ismadji, Adsorption of benzene and toluene from aqueous solutions onto activated carbon and its acid and heat treated forms: Influence of surface chemistry on adsorption, J. Hazard. Mater. 146 (2007) 237–242. doi:10.1016/j.jhazmat.2006.12.011.

[124] D.O. Cooney, Adsorption design for wastewater treatment, Lewis Publishers, Boca Raton, Fl., 1999.

[125] M.C. Rodriguez-Hernandez, C.E. Flores-Chaparro, J.R. Rangel-Mendez, Influence of dissolved organic matter and oil on the biosorption of BTEX by macroalgae in single and multi-solute systems, Environ. Sci. Pollut. Res. 24 (2017) 20922–20933. doi:10.1007/s11356-017-9672-3.

[126] Z. Aksu, Application of biosorption for the removal of organic pollutants: a review, Process Biochem. 40 (2005) 997–1026. doi:10.1016/j.procbio.2004.04.008.

[127] E. Rubín, P. Rodríguez, R. Herrero, M.E. Sastre de Vicente, Biosorption of phenolic compounds by the brown alga Sargassum muticum, J. Chem. Technol. Biotechnol. 81 (2006) 1093–1099. doi:10.1002/jctb.1430.

[128] A. Tiwari, R. Tiwari, A.K. Bajpai, Dynamic and Equilibrium Studies on Adsorption of Cu(II) Ions onto Biopolymeric Cross-Linked Pectin and Alginate Beads, J. Dispers. Sci. Technol. 30 (2009) 1208–1215. doi:10.1080/01932690802701838.

[129] Y. Liu, Y.-J. Liu, Biosorption isotherms, kinetics and thermodynamics, Sep. Purif. Technol. 61 (2008) 229–242. doi:10.1016/j.seppur.2007.10.002.

[130] I. Michalak, K. Chojnacka, A. Witek-Krowiak, State of the Art for the Biosorption Process—a Review, Appl. Biochem. Biotechnol. 170 (2013) 1389–1416. doi:10.1007/s12010-013-0269-0.

[131] A. Abdolali, W.S. Guo, H.H. Ngo, S.S. Chen, N.C. Nguyen, K.L. Tung, Typical lignocellulosic wastes and by-products for biosorption process in water and wastewater treatment: A critical review, Bioresour. Technol. 160 (2014) 57–66. doi:10.1016/j.biortech.2013.12.037.

[132] S. Tsuzuki, Interactions with Aromatic Rings, in: D.J. Wales (Ed.), Intermolecular Forces Clust. I, Springer-Verlag, Berlin/Heidelberg, 2005: pp. 149–193. http://www.springerlink.com/index/10.1007/b135618 (accessed May 25, 2015).

[133] D.A. Dougherty, Cation-π Interactions Involving Aromatic Amino Acids, J. Nutr. 137 (2007) 1504S-1508S.

[134] D. Da Silva Perez, R. Ruggiero, L.C. Morais, A.E.H. Machado, K. Mazeau, Theoretical and Experimental Studies on the Adsorption of Aromatic Compounds onto Cellulose, Langmuir. 20 (2004) 3151–3158. doi:10.1021/la0357817.

[135] C.I.A. Ferreira, V. Calisto, M. Otero, H. Nadais, V.I. Esteves, Fixed-bed adsorption of Tricaine Methanesulfonate onto pyrolysed paper mill sludge, Aquac. Eng. 77 (2017) 53–60. doi:10.1016/j.aquaeng.2017.02.006.

[136] M. Abolhassani, C.S. Griggs, L.A. Gurtowski, J.A. Mattei-Sosa, M. Nevins, V.F. Medina, T.A. Morgan, L.F. Greenlee, Scalable Chitosan-Graphene Oxide Membranes: The Effect of GO Size on Properties and Cross-Flow Filtration Performance, ACS Omega. 2 (2017) 8751–8759. doi:10.1021/acsomega.7b01266.

[137] N. Saravanan, R. Rajasekar, S. Mahalakshmi, T. Sathishkumar, K. Sasikumar, S. Sahoo, Graphene and modified graphene-based polymer nanocomposites – A review, J. Reinf. Plast. Compos. 33 (2014) 1158–1170. doi:10.1177/0731684414524847.

[138] M.T. Ale, J.D. Mikkelsen, A.S. Meyer, Designed optimization of a single-step extraction of fucose-containing sulfated polysaccharides from Sargassum sp., J. Appl. Phycol. 24 (2011) 715–723. doi:10.1007/s10811-011-9690-3.

[139] P. Hashemi, S. Bagheri, M.R. Fat'hi, Factorial design for optimization of experimental variables in preconcentration of copper by a chromotropic acid loaded Q-Sepharose adsorbent, Talanta. 68 (2005) 72–78. doi:10.1016/j.talanta.2005.04.058.

[140] N. Yıldız, H. Kapucu, A. Çalımlı, Response surface optimization of the phenol adsorption onto HDTMA-bentonite, Rev. Chem. Eng. 16 (2011) 55–70. doi:10.1515/REVCE.2000.16.1.55.

[141] R.H. Myers, D.C. Montgomery, C.M. Anderson-Cook, Response Surface Methodology: Process and Product Optimization Using Designed Experiments, John Wiley & Sons, 2016.

[142] R. Gottipati, S. Mishra, Process optimization of adsorption of Cr(VI) on activated carbons prepared from plant precursors by a two-level full factorial design, Chem. Eng. J. 160 (2010) 99–107. doi:10.1016/j.cej.2010.03.015.

[143] K. Gul, S. Sohni, M. Waqar, F. Ahmad, N.A.N. Norulaini, M.O. A. k., Functionalization of magnetic chitosan with graphene oxide for removal of cationic and anionic dyes from aqueous solution, Carbohydr. Polym. 152 (2016) 520–531. doi:10.1016/j.carbpol.2016.06.045.

[144] H. Yan, H. Yang, A. Li, R. Cheng, pH-tunable surface charge of chitosan/graphene oxide composite adsorbent for efficient removal of multiple pollutants from water, Chem. Eng. J. 284 (2016) 1397–1405. doi:10.1016/j.cej.2015.06.030.

[145] L. Fan, C. Luo, X. Li, F. Lu, H. Qiu, M. Sun, Fabrication of novel magnetic chitosan grafted with graphene oxide to enhance adsorption properties for methyl blue, J. Hazard. Mater. 215–216 (2012) 272–279. doi:10.1016/j.jhazmat.2012.02.068.

[146] Y. Sun, S. Yang, G. Zhao, Q. Wang, X. Wang, Adsorption of Polycyclic Aromatic Hydrocarbons on Graphene Oxides and Reduced Graphene Oxides, Chem. – Asian J. 8 (2013) 2755–2761. doi:10.1002/asia.201300496.

[147] W. Zeng, Y. Liu, X. Hu, S. Liu, G. Zeng, B. Zheng, L. Jiang, F. Guo, Y. Ding, Y. Xu, Decontamination of methylene blue from aqueous solution by magnetic chitosan lignosulfonate grafted with graphene oxide: effects of environmental

conditions and surfactant, RSC Adv. 6 (2016) 19298–19307. doi:10.1039/C5RA27657H.

[148] A. Zając, J. Hanuza, M. Wandas, L. Dymińska, Determination of N-acetylation degree in chitosan using Raman spectroscopy, Spectrochim. Acta. A. Mol. Biomol. Spectrosc. 134 (2015) 114–120. doi:10.1016/j.saa.2014.06.071.

[149] S. Kumari, P.K. Rath, Extraction and Characterization of Chitin and Chitosan from (Labeo rohit) Fish Scales, Procedia Mater. Sci. 6 (2014) 482–489. doi:10.1016/j.mspro.2014.07.062.

[150] F. Pendolino, N. Armata, Synthesis, Characterization and Models of Graphene Oxide, in: Graphene Oxide Environ. Remediat. Process, Springer, Cham, 2017: pp. 5–21. doi:10.1007/978-3-319-60429-9_2.

[151] R. Sips, Combined form of Langmuir and Freundlich equations, J. Chem. Phys. 16 (1948) 490–495.

[152] S.E. Agarry, O.O. Ogunleye, O.A. Aworanti, Biosorption equilibrium, kinetic and thermodynamic modelling of naphthalene removal from aqueous solution onto modified spent tea leaves, Environ. Technol. 34 (2013) 825–839. doi:10.1080/09593330.2012.720616.

[153] M.T. Raad, H. Behnejad, M.E. Jamal, Equilibrium and kinetic studies for the adsorption of benzene and toluene by graphene nanosheets: a comparison with carbon nanotubes, Surf. Interface Anal. 48 (2016) 117–125. doi:10.1002/sia.5877.

[154] H. Shi, W. Li, L. Zhong, C. Xu, Methylene Blue Adsorption from Aqueous Solution by Magnetic Cellulose/Graphene Oxide Composite: Equilibrium, Kinetics, and Thermodynamics, Ind. Eng. Chem. Res. 53 (2014) 1108–1118. doi:10.1021/ie4027154.

[155] A. Özer, D. Özer, A. Özer, The adsorption of copper(II) ions on to dehydrated wheat bran (DWB): determination of the equilibrium and thermodynamic parameters, Process Biochem. 39 (2004) 2183–2191. doi:10.1016/j.procbio.2003.11.008.

[156] T. Wu, X. Cai, S. Tan, H. Li, J. Liu, W. Yang, Adsorption characteristics of acrylonitrile, p-toluenesulfonic acid, 1-naphthalenesulfonic acid and methyl blue on graphene in aqueous solutions, Chem. Eng. J. 173 (2011) 144–149. doi:10.1016/j.cej.2011.07.050.

[157] H. Bi, X. Xie, K. Yin, Y. Zhou, S. Wan, L. He, F. Xu, F. Banhart, L. Sun, R.S. Ruoff, Spongy Graphene as a Highly Efficient and Recyclable Sorbent for Oils and Organic Solvents, Adv. Funct. Mater. 22 (n.d.) 4421–4425. doi:10.1002/adfm.201200888.

[158] A. Azizi, A. Torabian, E. Moniri, A.H. Hassani, H.A. Panahi, Adsorption performance of modified graphene oxide nanoparticles for the removal of toluene, ethylbenzene, and xylenes from aqueous solution, Desalination Water Treat. 57 (2016) 28806–28821. doi:10.1080/19443994.2016.1193769.

[159] M. Yusuf, F.M. Elfghi, S.A. Zaidi, E.C. Abdullah, M.A. Khan, Applications of graphene and its derivatives as an adsorbent for heavy metal and dye removal: a

systematic and comprehensive overview, RSC Adv. 5 (2015) 50392–50420. doi:10.1039/C5RA07223A.

[160] D.O. Njobuenwu, S.A. Amadi, P.C. Ukpaka, Dissolution Rate of BTEX Contaminants in Water, Can. J. Chem. Eng. 83 (2005) 985–989. doi:10.1002/cjce.5450830608.

[161] US EPA, Basic Information about Benzene in Drinking Water, (2013). http://water.epa.gov/drink/contaminants/basicinformation/benzene.cfm (accessed January 21, 2014).

[162] A. Lillicrap, M. Schaanning, A. Macken, Assessment of the Direct Effects of Biogenic and Petrogenic Activated Carbon on Benthic Organisms, Environ. Sci. Technol. 49 (2015) 3705–3710. doi:10.1021/es506113j.

[163] C.R. Holkar, A.J. Jadhav, D.V. Pinjari, N.M. Mahamuni, A.B. Pandit, A critical review on textile wastewater treatments: Possible approaches, J. Environ. Manage. 182 (2016) 351–366. doi:10.1016/j.jenvman.2016.07.090.

[164] S. Valili, G. Siavalas, H.K. Karapanagioti, I.D. Manariotis, K. Christanis, Phenanthrene removal from aqueous solutions using well-characterized, raw, chemically treated, and charred malt spent rootlets, a food industry by-product, J. Environ. Manage. 128 (2013) 252–258. doi:10.1016/j.jenvman.2013.04.057.

[165] B. Henriques, L.S. Rocha, C.B. Lopes, P. Figueira, A.C. Duarte, C. Vale, M.A. Pardal, E. Pereira, A macroalgae-based biotechnology for water remediation: Simultaneous removal of Cd, Pb and Hg by living Ulva lactuca, J. Environ. Manage. 191 (2017) 275–289. doi:10.1016/j.jenvman.2017.01.035.

[166] D. Zhang, Y. Ran, X. Cao, J. Mao, J. Cui, K. Schmidt-Rohr, Biosorption of nonylphenol by pure algae, field-collected planktons and their fractions, Environ. Pollut. 198 (2015) 61–69. doi:10.1016/j.envpol.2014.12.020.

[167] F.J. Millero, Chemical Oceanography, Third Edition, 3rd ed., CRC Press, Boca Raton, Fl., 2005.

[168] S. Brunauer, P.H. Emmett, E. Teller, Adsorption of Gases in Multimolecular Layers, J. Am. Chem. Soc. 60 (1938) 309–319. doi:10.1021/ja01269a023.

[169] J. Jagiello, Stable Numerical Solution of the Adsorption Integral Equation Using Splines, Langmuir. 10 (1994) 2778–2785. doi:10.1021/la00020a045.

[170] T.J. Bandosz, J. Jagiello, C. Contescu, J.A. Schwarz, Characterization of the surfaces of activated carbons in terms of their acidity constant distributions, Carbon. 31 (1993) 1193–1202. doi:10.1016/0008-6223(93)90072-I.

[171] E. Marinho-Soriano, P.C. Fonseca, M.A.A. Carneiro, W.S.C. Moreira, Seasonal variation in the chemical composition of two tropical seaweeds, Bioresour. Technol. 97 (2006) 2402–2406. doi:10.1016/j.biortech.2005.10.014.

[172] AOAC, ed., Official Methods of Analysis of the AOAC International, The Association, Washington, D.C., USA, 2006.

[173] A. Peña-Rodríguez, T.P. Mawhinney, D. Ricque-Marie, L.E. Cruz-Suárez, Chemical composition of cultivated seaweed Ulva clathrata (Roth) C. Agardh, Food Chem. 129 (2011) 491–498. doi:10.1016/j.foodchem.2011.04.104.

[174] P.J. Van Soest, J.B. Robertson, B.A. Lewis, Methods for Dietary Fiber, Neutral Detergent Fiber, and Nonstarch Polysaccharides in Relation to Animal Nutrition, J. Dairy Sci. 74 (1991) 3583–3597. doi:10.3168/jds.S0022-0302(91)78551-2.

[175] C. Bertagnolli, M.G.C. da Silva, E. Guibal, Chromium biosorption using the residue of alginate extraction from Sargassum filipendula, Chem. Eng. J. 237 (2014) 362–371. doi:10.1016/j.cej.2013.10.024.

[176] Shell Chemicals, Safety Data Sheet - Benzene, (2012).

[177] W.-H. Xie, W.-Y. Shiu, D. Mackay, A review of the effect of salts on the solubility of organic compounds in seawater, Mar. Environ. Res. 44 (1997) 429–444. doi:10.1016/S0141-1136(97)00017-2.

[178] H. Benbouzid, S. Le Floch, L. Stephan, R. Olier, M. Privat, Combined effects of salinity and temperature on the solubility of organic compounds, J. Chem. Thermodyn. 48 (2012) 54–64. doi:10.1016/j.jct.2011.11.020.

[179] I. Langmuir, The constitution and fundamental properties of solids and liquids. Part I. Solids., J. Am. Chem. Soc. 38 (1916) 2221–2295. doi:10.1021/ja02268a002.

[180] H. Freundlich, Über die Adsorption in Lösungen, W. Engelmann, 1906.

[181] S. Kraan, Algal Polysaccharides, Novel Applications and Outlook, (2012). doi:10.5772/51572.

[182] J. Pérez, J. Muñoz-Dorado, T. de la Rubia, J. Martínez, Biodegradation and biological treatments of cellulose, hemicellulose and lignin: an overview, Int. Microbiol. 5 (2002) 53–63. doi:10.1007/s10123-002-0062-3.

[183] G. Ravishanker, P.K. Mehrotra, M. Mezei, D.L. Beveridge, Aqueous hydration of benzene, J. Am. Chem. Soc. 106 (1984) 4102–4108. doi:10.1021/ja00327a006.

[184] K.E. Borchani, C. Carrot, M. Jaziri, Untreated and alkali treated fibers from Alfa stem: effect of alkali treatment on structural, morphological and thermal features, Cellulose. 22 (2015) 1577–1589. doi:10.1007/s10570-015-0583-5.

[185] N. Koutahzadeh, E. Daneshvar, M. Kousha, M.S. Sohrabi, A. Bhatnagar, Biosorption of hexavalent chromium from aqueous solution by six brown macroalgae, Desalination Water Treat. 51 (2013) 6021–6030. doi:10.1080/19443994.2013.764353.

[186] H.-X. Zou, N. Li, L.-H. Wang, P. Yu, X.-F. Yan, Equilibrium and Kinetic Studies of Cd2+ Biosorption by the Brown Algae Sargassum fusiforme, PLoS ONE. 9 (2014) e95242. doi:10.1371/journal.pone.0095242.

[187] S.-K. Kim, Springer Handbook of Marine Biotechnology, Springer, 2015.

[188] R. Tuvikene, Kalle Truss, M. Vaher, T. Kailor, G. Matin, P. Kersen, Extraction and quantification of hybrid carrageenans from the biomass of the red algae

Furcellaria lumbricalis and Coccotylus truncatus, Proc Est. Acad Sci Chem. 55 (2006) 40–53.

[189] J. Schijf, A.M. Ebling, Investigation of the Ionic Strength Dependence of Ulva lactuca Acid Functional Group pKas by Manual Alkalimetric Titrations, Environ. Sci. Technol. 44 (2010) 1644–1649. doi:10.1021/es9029667.

[190] N.A. Cuizano, B.P. Llanos, L. Chang, A.E. Navarro, Equilibrio ácido-base de algas marinas del litoral peruano elucida su alta afinidad por contaminantes ambientales, Rev. Soc. Quím. Perú. 73 (2007) 85–93.

[191] E.C. de Lima, J.C. Masini, Acid base characterization of the surface of mixed species of algae Spirulin by potentiometric titration and discrete site distribution model, Quím. Nova. 22 (1999) 679–683. doi:10.1590/S0100-40421999000500011.

[192] V. Murphy, H. Hughes, P. McLoughlin, Cu(II) binding by dried biomass of red, green and brown macroalgae, Water Res. 41 (2007) 731–740. doi:10.1016/j.watres.2006.11.032.

[193] D.J. Lane, M. Zevenhoven, P.J. Ashman, P.J. van Eyk, M. Hupa, R. de Nys, D.M. Lewis, Algal Biomass: Occurrence of the Main Inorganic Elements and Simulation of Ash Interactions with Bed Material, Energy Fuels. 28 (2014) 4622–4632. doi:10.1021/ef500989n.

[194] K.Y. Foo, B.H. Hameed, Insights into the modeling of adsorption isotherm systems, Chem. Eng. J. 156 (2010) 2–10. doi:10.1016/j.cej.2009.09.013.

[195] F. Yang, H. Liu, J. Qu, J. Paul Chen, Preparation and characterization of chitosan encapsulated Sargassum sp. biosorbent for nickel ions sorption, Bioresour. Technol. 102 (2011) 2821–2828. doi:10.1016/j.biortech.2010.10.038.

[196] D. Pal, Adsorption of Polycyclic Aromatic Hydrocarbons using Agricultural Wastes-Effect of Lignin Content, (2012).

[197] P.X. Sheng, Y.-P. Ting, J.P. Chen, L. Hong, Sorption of lead, copper, cadmium, zinc, and nickel by marine algal biomass: characterization of biosorptive capacity and investigation of mechanisms, J. Colloid Interface Sci. 275 (2004) 131–141. doi:10.1016/j.jcis.2004.01.036.

[198] Z. Aksu, E. Balibek, Effect of salinity on metal-complex dye biosorption by Rhizopus arrhizus, J. Environ. Manage. 91 (2010) 1546–1555. doi:10.1016/j.jenvman.2010.02.026.

[199] H. Hindarso, S. Ismadji, F. Wicaksana, Mudjijati, N. Indraswati, Adsorption of Benzene and Toluene from Aqueous Solution onto Granular Activated Carbon, J. Chem. Eng. Data. 46 (2001) 788–791. doi:10.1021/je000176g.

[200] R. Heede, N. Oreskes, Potential emissions of CO2 and methane from proved reserves of fossil fuels: An alternative analysis, Glob. Environ. Change. 36 (2016) 12–20. doi:10.1016/j.gloenvcha.2015.10.005.

[201] D.M. Pampanin, M.O. Sydnes, Polycyclic Aromatic Hydrocarbons a Constituent of Petroleum: Presence and Influence in the Aquatic Environment, (2013). doi:10.5772/48176.

[202] N. Wang, Y. Zhang, F. Zhu, J. Li, S. Liu, P. Na, Adsorption of soluble oil from water to graphene, Environ. Sci. Pollut. Res. 21 (2014) 6495–6505. doi:10.1007/s11356-014-2504-9.

[203] R.L. Ziolli, W.F. Jardim, Photocatalytic decomposition of seawater-soluble crude-oil fractions using high surface area colloid nanoparticles of TiO2, J. Photochem. Photobiol. Chem. 147 (2002) 205–212. doi:10.1016/S1010-6030(01)00600-1.

[204] M.O. Caetano, I.A.H. Schneider, L.P. Gomes, A.G. Kieling, L.A.S. Miranda, A compact remediation system for the treatment of groundwater contaminated with BTEX and TPH, Environ. Technol. 38 (2017) 1408–1420. doi:10.1080/09593330.2016.1231222.

[205] M. Rathod, K. Mody, S. Basha, Efficient removal of phosphate from aqueous solutions by red seaweed, Kappaphycus alverezii, J. Clean. Prod. 84 (2014) 484–493. doi:10.1016/j.jclepro.2014.03.064.

[206] P.S. Vankar, R. Sarswat, A.K. Dwivedi, R.S. Sahu, An assessment and characterization for biosorption efficiency of natural dye waste, J. Clean. Prod. 60 (2013) 65–70. doi:10.1016/j.jclepro.2011.09.021.

[207] R. Angelova, E. Baldikova, K. Pospiskova, Z. Maderova, M. Safarikova, I. Safarik, Magnetically modified Sargassum horneri biomass as an adsorbent for organic dye removal, J. Clean. Prod. 137 (2016) 189–194. doi:10.1016/j.jclepro.2016.07.068.

[208] H. Zhao, H. Yan, S. Dong, Y. Zhang, B. Sun, C. Zhang, Y. Ai, B. Chen, Q. Liu, T. Sui, S. Qin, Thermogravimetry study of the pyrolytic characteristics and kinetics of macro-algae Macrocystis pyrifera residue, J. Therm. Anal. Calorim. 111 (2011) 1685–1690. doi:10.1007/s10973-011-2102-8.

[209] J.L. Davila-Rodriguez, V.A. Escobar-Barrios, K. Shirai, J.R. Rangel-Mendez, Synthesis of a chitin-based biocomposite for water treatment: Optimization for fluoride removal, J. Fluor. Chem. 130 (2009) 718–726. doi:10.1016/j.jfluchem.2009.05.012.

[210] W.S. Wan Ngah, L.C. Teong, M.A.K.M. Hanafiah, Adsorption of dyes and heavy metal ions by chitosan composites: A review, Carbohydr. Polym. 83 (2011) 1446–1456. doi:10.1016/j.carbpol.2010.11.004.

[211] S. Motlagh, P. Ravines, Q. Ma, F. Jaksch, Identification of Gum Arabic sing PAGE and IEF A2, in: Gums Stabilisers Food Ind. 10, Woodhead Publishing, 2000: pp. 53–58. http://www.sciencedirect.com/science/article/pii/B9781855737884500095 (accessed March 12, 2016).

[212] P. Sriamornsak, Application of pectin in oral drug delivery, Expert Opin. Drug Deliv. 8 (2011) 1009–1023. doi:10.1517/17425247.2011.584867.

[213] E. Eroglu, S.M. Smith, C.L. Raston, Application of Various Immobilization Techniques for Algal Bioprocesses, in: N.R. Moheimani, M.P. McHenry, K. de Boer,

P.A. Bahri (Eds.), Biomass Biofuels Microalgae, Springer International Publishing, 2015: pp. 19–44. doi:10.1007/978-3-319-16640-7_2.

[214] P.E.D.-F. A. Pérez-Escobedo, Fluoride adsorption capacity of composites based on chitosan zeolite-algae, Rev. Mex. Ing. Quím. 15 (2016) 139–147.

[215] K. Ravikumar, B. Deebika, K. Balu, Decolourization of aqueous dye solutions by a novel adsorbent: Application of statistical designs and surface plots for the optimization and regression analysis, J. Hazard. Mater. 122 (2005) 75–83. doi:10.1016/j.jhazmat.2005.03.008.

[216] J. Antony, Design of Experiments for Engineers and Scientists, Elsevier, 2014.

[217] C. Lastoskie, K.E. Gubbins, N. Quirke, Pore size distribution analysis of microporous carbons: a density functional theory approach, J. Phys. Chem. 97 (1993) 4786–4796. doi:10.1021/j100120a035.

[218] H. Qiu, L. Lv, B. Pan, Q. Zhang, W. Zhang, Q. Zhang, Critical review in adsorption kinetic models, J. Zhejiang Univ. Sci. A. 10 (2009) 716–724. doi:10.1631/jzus.A0820524.

[219] I. Tsibranska, E. Hristova, Comparison of different kinetic models for adsorption of heavy metals onto activated carbon from apricot stones, Bulg. Chem. Commun. 43 (2011) 370–377.

[220] L. Santos, A. Pinto, O. Filipe, Â. Cunha, E.B.H. Santos, A. Almeida, Insights on the Optical Properties of Estuarine DOM – Hydrological and Biological Influences, PLOS ONE. 11 (2016) e0154519. doi:10.1371/journal.pone.0154519.

[221] M. Marudova, A.J. MacDougall, S.G. Ring, Pectin–chitosan interactions and gel formation, Carbohydr. Res. 339 (2004) 1933–1939. doi:10.1016/j.carres.2004.05.017.

[222] N. Terinte, R. Ibbett, K. Schuster, Overview on native cellulose and microcrystalline cellulose I structure studied by X-ray diffraction (WAXD): Comparison between measurement techniques, Lenzing. Berichte. 89 (2011).

[223] X. Yang, Y. Tu, L. Li, S. Shang, X. Tao, Well-Dispersed Chitosan/Graphene Oxide Nanocomposites, ACS Appl. Mater. Interfaces. 2 (2010) 1707–1713. doi:10.1021/am100222m.

[224] M. Rinaudo, Chitin and chitosan: Properties and applications, Prog. Polym. Sci. 31 (2006) 603–632. doi:10.1016/j.progpolymsci.2006.06.001.

[225] G.Z. Kyzas, D.N. Bikiaris, Recent Modifications of Chitosan for Adsorption Applications: A Critical and Systematic Review, Mar. Drugs. 13 (2015) 312–337. doi:10.3390/md13010312.

[226] J. Cho, M.-C. Heuzey, A. Bégin, P.J. Carreau, Physical Gelation of Chitosan in the Presence of β-Glycerophosphate: The Effect of Temperature, Biomacromolecules. 6 (2005) 3267–3275. doi:10.1021/bm050313s.

[227] A. Balaria, S. Schiewer, Assessment of biosorption mechanism for Pb binding by citrus pectin, Sep. Purif. Technol. 63 (2008) 577–581. doi:10.1016/j.seppur.2008.06.023.

[228] S. Pandey, A. Mishra, P. Raval, H. Patel, A. Gupta, D. Shah, Chitosan–pectin polyelectrolyte complex as a carrier for colon targeted drug delivery, J. Young Pharm. 5 (2013) 160–166. doi:10.1016/j.jyp.2013.11.002.

[229] G.P. Jeppu, T.P. Clement, A modified Langmuir-Freundlich isotherm model for simulating pH-dependent adsorption effects, J. Contam. Hydrol. 129–130 (2012) 46–53. doi:10.1016/j.jconhyd.2011.12.001.

[230] Y. Shimizu, K. Kono, I.S. Kim, T. Takagishi, Effects of added metal ions on the interaction of chitin and partially deacetylated chitin with an azo dye carrying hydroxyl groups, J. Appl. Polym. Sci. 55 (1995) 255–261. doi:10.1002/app.1995.070550208.

[231] S. Schiewer, M.H. Wong, Ionic strength effects in biosorption of metals by marine algae, Chemosphere. 41 (2000) 271–282. doi:10.1016/S0045-6535(99)00421-X.

[232] K.D. Yao, H. Tu, F. Cheng, J.W. Zhang, J. Liu, pH-sensitivity of the swelling of a chitosan-pectin polyelectrolyte complex, Angew. Makromol. Chem. 245 (1997) 63–72. doi:10.1002/apmc.1997.052450106.

[233] A. Sluiter, B. Hames, R.O. Ruiz, C. Scarlata, J. Sluiter, D. Templeton, Determination of structural carbohydrates and lignin in biomass, ResearchGate. 2011 (2004) 1–14.

[234] J.R. Rangel-Mendez, R. Monroy-Zepeda, E. Leyva-Ramos, P.E. Diaz-Flores, K. Shirai, Chitosan selectivity for removing cadmium (II), copper (II), and lead (II) from aqueous phase: pH and organic matter effect, J. Hazard. Mater. 162 (2009) 503–511. doi:10.1016/j.jhazmat.2008.05.073.

[235] K. Chon, K. Chon, J. Cho, Characterization of size fractionated dissolved organic matter from river water and wastewater effluent using preparative high performance size exclusion chromatography, Org. Geochem. 103 (2017) 105–112. doi:10.1016/j.orggeochem.2016.11.003.

[236] L. Bandura, D. Kołodyńska, W. Franus, Adsorption of BTX from aqueous solutions by Na-P1 zeolite obtained from fly ash, Process Saf. Environ. Prot. 109 (2017) 214–223. doi:10.1016/j.psep.2017.03.036.

[237] M. Mohamed, S. Ouki, Removal Mechanisms of Toluene from Aqueous Solutions by Chitin and Chitosan, Ind. Eng. Chem. Res. 50 (2011) 9557–9563. doi:10.1021/ie200110t.

[238] F. Simantiraki, C.G. Kollias, D. Maratos, J. Hahladakis, E. Gidarakos, Qualitative determination and application of sewage sludge and municipal solid waste compost for BTEX removal from groundwater, J. Environ. Chem. Eng. 1 (2013) 9–17. doi:10.1016/j.jece.2013.02.002.

[239] S.M. Yakout, Removal of the hazardous, volatile, and organic compound benzene from aqueous solution using phosphoric acid activated carbon from rice husk, Chem. Cent. J. 8 (2014) 52. doi:10.1186/s13065-014-0052-5.

[240] J. Ma, Y. Yang, X. Jiang, Z. Xie, X. Li, C. Chen, H. Chen, Impacts of inorganic anions and natural organic matter on thermally activated persulfate oxidation of BTEX in water, Chemosphere. 190 (2018) 296–306. doi:10.1016/j.chemosphere.2017.09.148.

[241] C.F. Bustillo-Lecompte, D. Kakar, M. Mehrvar, Photochemical treatment of benzene, toluene, ethylbenzene, and xylenes (BTEX) in aqueous solutions using advanced oxidation processes: Towards a cleaner production in the petroleum refining and petrochemical industries, J. Clean. Prod. 186 (2018) 609–617. doi:10.1016/j.jclepro.2018.03.135.

[242] Y. Xue, S. Lu, X. Fu, V.K. Sharma, I. Mendoza-Sanchez, Z. Qiu, Q. Sui, Simultaneous removal of benzene, toluene, ethylbenzene and xylene (BTEX) by CaO2 based Fenton system: Enhanced degradation by chelating agents, Chem. Eng. J. 331 (2018) 255–264. doi:10.1016/j.cej.2017.08.099.

[243] S. Jiménez, M.M. Micó, M. Arnaldos, F. Medina, S. Contreras, State of the art of produced water treatment, Chemosphere. 192 (2018) 186–208. doi:10.1016/j.chemosphere.2017.10.139.

[244] Y. Wang, J. Zhao, Advances in Energy, Environment and Materials Science: Proceedings of the International Conference on Energy, Environment and Materials Science (EEMS 2015), Guanghzou, P.R. China, August 25-26, 2015, CRC Press, 2016.

[245] E.S.W. Kong, Nanomaterials, Polymers and Devices: Materials Functionalization and Device Fabrication, John Wiley & Sons, 2015.

[246] W.S. Hummers, R.E. Offeman, Preparation of Graphitic Oxide, J. Am. Chem. Soc. 80 (1958) 1339–1339. doi:10.1021/ja01539a017.

[247] L. Zhang, H. Luo, P. Liu, W. Fang, J. Geng, A novel modified graphene oxide/chitosan composite used as an adsorbent for Cr(VI) in aqueous solutions, Int. J. Biol. Macromol. 87 (2016) 586–596. doi:10.1016/j.ijbiomac.2016.03.027.

[248] M. Espinal-Ruiz, F. Parada-Alfonso, L.-P. Restrepo-Sánchez, C.-E. Narváez-Cuenca, D. Julian McClements, Impact of dietary fibers [methyl cellulose, chitosan, and pectin] on digestion of lipids under simulated gastrointestinal conditions, Food Funct. 5 (2014) 3083–3095. doi:10.1039/C4FO00615A.

[249] B. Konkena, S. Vasudevan, Understanding Aqueous Dispersibility of Graphene Oxide and Reduced Graphene Oxide through pKa Measurements, J. Phys. Chem. Lett. 3 (2012) 867–872. doi:10.1021/jz300236w.

[250] C.A. Hunter, J.K.M. Sanders, The nature of .pi.-.pi. interactions, J. Am. Chem. Soc. 112 (1990) 5525–5534. doi:10.1021/ja00170a016.

[251] W.H. Bragg, W.L. Bragg, The reflection of X-rays by crystals, Proc R Soc Lond A. 88 (1913) 428–438. doi:10.1098/rspa.1913.0040.

[252] K. Krishnamoorthy, M. Veerapandian, R. Mohan, S.-J. Kim, Investigation of Raman and photoluminescence studies of reduced graphene oxide sheets, Appl. Phys. A. 106 (2012) 501–506. doi:10.1007/s00339-011-6720-6.

[253] M.S. Dresselhaus, A. Jorio, M. Hofmann, G. Dresselhaus, R. Saito, Perspectives on Carbon Nanotubes and Graphene Raman Spectroscopy, Nano Lett. 10 (2010) 751–758. doi:10.1021/nl904286r.

[254] S. Nethaji, A. Sivasamy, A.B. Mandal, Adsorption isotherms, kinetics and mechanism for the adsorption of cationic and anionic dyes onto carbonaceous particles prepared from <Emphasis Type="Italic">Juglans regia</Emphasis> shell biomass, Int. J. Environ. Sci. Technol. 10 (2013) 231–242. doi:10.1007/s13762-012-0112-0.

[255] M.A. Acheampong, K. Pakshirajan, A.P. Annachhatre, P.N.L. Lens, Removal of Cu(II) by biosorption onto coconut shell in fixed-bed column systems, J. Ind. Eng. Chem. 19 (2013) 841–848. doi:10.1016/j.jiec.2012.10.029.

[256] S. Ghorai, K.K. Pant, Equilibrium, kinetics and breakthrough studies for adsorption of fluoride on activated alumina, Sep. Purif. Technol. 42 (2005) 265–271. doi:10.1016/j.seppur.2004.09.001.

[257] H.C. Thomas, Heterogeneous Ion Exchange in a Flowing System, J. Am. Chem. Soc. 66 (1944) 1664–1666. doi:10.1021/ja01238a017.

[258] R.M. Clark, Evaluating the cost and performance of field-scale granular activated carbon systems, Environ. Sci. Technol. 21 (1987) 573–580. doi:10.1021/es00160a008.

[259] Y.H. Yoon, J.H. Nelson, Application of Gas Adsorption Kinetics — II. A Theoretical Model for Respirator Cartridge Service Life and Its Practical Applications, Am. Ind. Hyg. Assoc. J. 45 (1984) 517–524. doi:10.1080/15298668491400205.

[260] G. Yan, T. Viraraghavan, M. Chen, A New Model for Heavy Metal Removal in a Biosorption Column, Adsorpt. Sci. Technol. 19 (2001) 25–43. doi:10.1260/0263617011493953.

[261] J. Crittenden, Montgomery Watson Harza, Water treatment principles and design, J. Wiley, Hoboken, N.J., 2005.

[262] A.A. Azzaz, S. Jellali, R. Souissi, K. Ergaieg, L. Bousselmi, Alkaline-treated sawdust as an effective material for cationic dye removal from textile effluents under dynamic conditions: breakthrough curve prediction and mechanism exploration, Environ. Sci. Pollut. Res. 24 (2017) 18240–18256. doi:10.1007/s11356-017-9388-4.

[263] M.A. Ferro-García, F. Carrasco-Marín, J. Rivera-Utrilla, E. Utrera-Hidalgo, C. Moreno-Castilla, The use of activated carbon columns for the removal of ortho-phosphate ions from aqueous solutions, Carbon. 28 (1990) 91–95. doi:10.1016/0008-6223(90)90098-J.

[264] Rowe R. Kerry, Mukunoki Toshifumi, Sangam Henri P., Benzene, Toluene, Ethylbenzene, m&p-Xylene, o-Xylene Diffusion and Sorption for a Geosynthetic Clay

Liner at Two Temperatures, J. Geotech. Geoenvironmental Eng. 131 (2005) 1211–1221. doi:10.1061/(ASCE)1090-0241(2005)131:10(1211).

APPENDIX A

Table A.1. Full factorial experimental design matrix [a].

No. Experiment	Factor 1 Chitosan (g)	Factor 2 Pectin (g)	Factor 3 Algae biomass (g)	Response Benzene removal (mg/g)
1	3	2	0	58.59
2	3	2	5.4	51.71
3	3	0	0	50.92
4	3	0	5.4	47.31
5 [CP]	4	1	2.7	45.34
6 [CP]	4	1	2.7	44.18
7	5	0	5.4	22.83
8	5	2	0	47.76
9	5	0	0	46.74
10	5	2	5.4	27.88

[a] The factors and combinations listed in this table are in chitosan preferred order.

[CP] Center point

Table A.2. Analysis of variance for the factorial model describing the adsorptive capacity (q_e) with the estimate effect and coefficients.

Source	Sum of squares	d.f.[a]	Mean square	F–ratio	p [b]
Model	1008.02	3	336.01	31.73	0.0011
A – Ch	501.57	1	501.57	47.37	0.0010
C – Ma	368.08	1	368.08	34.76	0.0020
AC	138.37	1	138.37	13.07	0.0153

[a] d.f.: degree of freedom.

[a] p: probability for F–ratio test

Table A.3. Analysis of variance for a response surface quadratic model for biosorption of benzene.

Source	Sum of Squares	DF	Mean Square	F Value	Prob > F PS$_{tatistics}$
Model	654.53	5	130.91	136.50	< 0.0001
A	65.87	1	65.87	68.69	< 0.0001
B	1.73	1	1.73	1.80	0.2214
A^2	157.36	1	157.37	164.09	< 0.0001
B^2	149.14	1	149.14	155.51	< 0.0001
AB	91.87	1	91.9	95.80	< 0.0001
Residual	6.71	7	0.967		
Lack of Fit	5.43	3	1.81	5.67	0.0635
Pure Error	1.28	4	0.32		
Correlation Total	661.27	12			